Processes and factors controlling and affecting the retreat of mangrove shorelines in South Vietnam

Dissertation

zur Erlangung des Doktorgrades

der Mathematisch-Naturwissenschaftlichen Fakultät

der Christian-Albrechts-Universität zu Kiel

Vorgelegt von

Nguyen Cong Thanh

Kiel 2012

Referent: **Professor Dr. Karl Stattegger**

Koreferent: **Professor Dr. Athanasios Vafeidis**

Tag der mündlichen Prüfung: **04.02.2013**

Zum Druck genehmigt: **04.02.2013**

gez. Prof. Dr. Wolfgang J. Duschl, Dekan

Ich versichere an Eides statt, dass:

1) Ich bis zum heutigen Tage weder an der Christian-Albrechts-Universität zu Kiel noch an einer anderen Hochschule ein Promotionsverfahren endgültig nicht bestanden habe oder mich in einem entsprechenden Verfahren befinde oder befunden habe.
2) Ich die Inanspruchnahme fremder Hilfen aufgeführt habe, sowie, dass ich die wörtlich oder inhaltlich aus anderen Quellen entnommenen Stellen als solche gekennzeichnet habe.
3) Die Arbeit unter Einhaltung der Regeln guter wissenschaftlicher Praxis der Deutschen Forschungsgemeinschaft entstanden ist.

Kiel, 20 December 2012 Unterschrift:

Acknowledgements

This thesis is carried out within the project "SEdiment DYnamics in MANgrove areas, second phase (SEDYMAN-II)", which was funded by the Deutsche Forschungsgemeinschaft (DFG). I greatly thank for this financial support. I would like to thank the Ministry of Science and Technology (MOST), Vietnam, for funding the project "Dynamics of the mangrove belt of the Saigon - Dong Nai estuary and the eastern coast of the Mekong Delta", which partly supported my field activities in Vietnam.

I am greatly thankful to Professor Karl Stattegger for accepting the supervision and his support during my study.

I would like to thank Professor Athanasios Vafeidis for being the co-supervisor of my thesis.

I am particularly thankful to Professor La Thi Cang for the valuable contributions in my study and the intensive cooperation between our institutes.

I am deeply grateful to Klaus Schwarzer, who initiates the SEDYMAN-II and leads the project running perfectly. Thanks to your efforts and guidance during my graduate study

Thanks to Klaus Ricklefs, who gave great support in technical questions and discussions.

Professor La Thi Cang and Dr. Le Xuan Thuyen extensively supported my field activities in Vietnam. I would like to thank you for all their arrangements.

During the field work, my colleagues from the University of Sciences, Ho Chi Minh City, gave great support. I am particular grateful to Dang Truong An, Dr. Vo Luong Hong Phuoc, and Bui Ngoc Chung for their work in the field. I will not forget the great times during our field campaigns.

I also like to thank the soldiers at the Hai Doi 2 army station in Can Gio for their kindness and the protection we got during our field activities in Can Gio. Special thanks go to the captains Khai and An for their good job in driving our research boat and making it possible to perform valuable measurements.

I received many help from my working group "Sedimentogy, Coastal and Continental Shelf Research". I am thankful for the assistance. Especially, I am grateful to my best friends Daniel Unverricht and Christoph Heinrich for their support in communication with German authorities during my time here in Kiel. Daniel, Christoph, I hardly survived here without your support!

Then, I would like to thank all of my Vietnamese friends in Kiel, who share their experiences and helped me to solve many little difficulties in Germany.

I am very much thankful to my mother in law, my mom, and especially my wife, who take care of my children throughout my long time in Kiel. I apologize my long absence to them, especially to my little son and daughter.

I would like to thank many people more, but unfortunately, I could not name everybody here. Thanks to everybody!

Kiel, 20 December 2012

Nguyen Cong Thanh

Summary

Mangrove environments are considered as a very valuable ecological resource and important element for stabilizing shorelines and reducing coastal erosion. However, coastal mangroves have been lost rapidly in many countries due to human impacts and natural forcing. Changes in mangrove vegetations or losses of mangroves accelerate coastal erosion. Only few investigations have been done to determine coastal retreat or shoreline change along mangrove coasts. Some previous studies have addressed hydrological factors like tide and wave action controlling this erosion. However, the relations between mangrove shoreline erosion and hydrodynamic factors could not be shown clearly.

The methods to determine shoreline change or retreat along mangrove coasts are mainly based on the analyses of historical maps, aerial photographs, and/or the application of remote sensing techniques. These methods are valuable to assess coastal erosion in large spatial and long-term temporal scales up to decades. They are not useful for understanding erosion with regard to hydrological forcing factors, which fluctuate on short-term time scales like days, fortnights, and seasons. Moreover, field observations combining hydrological parameters (water level fluctuation, tide, waves, and currents) with shoreline erosion are sparse. The lack of those data relate mainly from difficulties to measure these parameters in the field. As a result, coastal erosion along mangrove coast are not been fully explained yet. Some important questions remain unanswered:

(1) How do tides, waves, and tidal currents cause coastal erosion and among those factors which is the dominant parameter?

(2) How do seasonal-based water level fluctuations along the coast of the whole Mekong Delta (Vung Tau to Ca Mau) influence mangrove coasts erosion?

(3) What is the influence of short-term events (tropical storm and tsunami) on the erosion of mangrove coasts?

(4) How do soil properties and structure of the vegetation control the stability of mangrove coasts?

Several field experiments along different locations along the Mekong Delta have been carried-out to collect appropriate data to fill these gaps in knowledge.

Two investigation sites (Can Gio and Bo De), where the shorelines are formed by eroding cliffs, were chosen for this study. At both sites, living and truncated mangroves are present.

The cliff retreat was measured during a whole spring-neap tidal cycle (14 days) and as well for a whole year with irregular intervals between weeks and months. Sediment samples were taken from the cliff and the adjacent tidal flat; measurements of shear strengths were carried out on the surface of the active cliffs to characterize relevant soil properties. Water level and wave- and current parameters were measured in front of both cliffs to get the hydrodynamic input. Additionally, to assess the general tide and flow regimes affecting cliff retreat, tide and current data were collected in the Nga Bay estuary (Can Gio region) and along the coast of the Mekong River Delta.

Both sites are strongly influenced by a mixed, mainly semi-diurnal tide with a maximum tidal range of more than 4 m. During the NE monsoon (November to March) the areas are exposed to higher inundations due to higher water levels and influence of stronger waves. Hourly water levels, which have been recorded for a period of 19-years at seven tide gauges along the Mekong Delta, were analyzed. The maximum and minimum values of mean higher high water (MHHW) occur in November and in June/July respectively with a seasonal difference in its height of about 45 cm on average.

The short-term rate of cliff retreat based-on a two weeks period with daily measurements in Can Gio, amounts to 0.42 cm/day on average, which is related to tidal inundation and wave action. The cliff is retreating under low wave energy input with simultaneously high inundation. During neap tide, the cliff retreat is faster than during spring tide, while during spring tide, high wave energy input does not always cause the erosion immediately but with a delay of about one day. For the cliff in Nga Bay estuary, it could be calculated that a retreat of 1 cm cliff coast needs a wave energy input of app. 857 J/m^2.

The estimated annual rate of cliff retreat in Can Gio based on 14 measurements during a whole year amounts to 1.54 cm/day or 4.79 m/year. This value is about 3.6 times higher than the value (0.42 cm/day) derived from the short-term dataset, obtained during the SW monsoon with minor wave attack. This difference suggests that the cliff retreat during the NE monsoon is higher because of higher tidal inundation and stronger wave energy input.

The short-term of cliff retreat in Bo De, based-on a 14-day period, amounts to an average rate of approximately 2.38 cm/day. This retreat is strongly related to wave action. The peaks of cliff retreat correlate to peaks of maximum wave energy input. Due to the longer period of inundation during neap tide, the cliff retreat is faster than during spring tide. On average, a retreat of 1 cm cliff shoreline in Bo De needs wave energy input of about 1105 J/m^2.

The cliff retreat in Bo De is strongly related to wave impact while the recession of the less wave exposed site in Can Gio is more controlled by the duration of inundation. Remarkably,

at both sites the cliff retreat during neap tide is faster than during spring tide. As waves can only act at cliffs when at least the base of cliff is inundated, the tide plays a more dominant role for erosion than wave energy input.

On the tidal flats in front of the both cliffs, sediment accumulation was not observed. Tidal currents in the main channels of close the study sites show velocities more than 1 m/s. They are ebb dominant. These strong currents prevent the eroded sediment to be deposited close to the cliffs. Therefore, the ebb dominant current flow is a third important factor effecting cliff retreat by exporting sediment.

The two sites also differ from each other in their shear strength values, which are higher in Bo De (0.1923 kg/cm^2) compared to Can Gio (0.1273 kg/cm^2). To remove 1 cm of cliff shoreline, the necessary wave energy input in Bo De (1105 J/m^2) is about 1.3 times higher than in Can Gio (857 J/m^2). These results suggest that besides hydrodynamic parameters, soil properties are relevant for cliff retreat. High consolidated sediment (high shear strength) reduce erosion speed.

In Bo De, where the shoreline is striking north-east, the coastline is attacked by southwest wind-induced waves but as well swell conditions. The latter do not appear in Can Gio. The shoreline in Bo De was also affected by a tropical depression/storm (the Chan-hom 2009), which was formed at about 300 km offshore moving northwards. These waves, which are induced by the afternoon onshore winds and or the southwest monsoon, and the tropical storm supports the explanation of shoreline retreat at both sites even during low hydrodynamic conditions season.

Besides regular conditions, the impact of a storm event could be measured as well. During the short-term measuring campaigns, in Bo De, the coastline was attacked by southwest wind-induced waves but as well by swells from the tropical depression/storm Chan-hom (2009), causing strong erosion.

There are three kinds of mangrove cliff retreat: ‘surface erosion’, ‘notched (or scoured) erosion’, and ‘slope failure erosion’. Surface erosion, in which the cliff surface is eroded uniformly from top to bottom, is typically seen at locations without mangrove trees or less densely trees on top. Notched erosion is usually observed at places where the mangrove root systems is distributed densely down to the middle part of the cliff. Due to the binding sediment of the roots, the higher part of the cliff, which is also less exposed to tide and wave actions, is eroded more slowly than the lower part; therefore a notch hole is formed. Slope failure erosion is simply a result of notched erosion. These types of erosion also imply that densely mangrove distribution can reduce the erosion.

The above results lead to the following conclusions: (1) Tide, wave, and tidal current are primary factors driving the mangrove shoreline retreat. Among these factors, the tide, especially tidal inundation plays a key role in controlling mangrove shoreline retreat. (2) Mangrove shorelines are usually retreating stronger during neap tide than during spring tide. (3) Soil composition of mangrove shoreline can effect erosion in reducing the speed of retreat. (4) Mangrove shoreline retreat is a natural phenomenon, site specific and non-uniform in time and space.

Zusammenfassung

Mangroven sind eine wichtige ökologische Ressource und ein wesentliches Element, um Küstenerosion zu vermindern. Dennoch sind in vielen Ländern Mangroven sowohl aufgrund anthropogener Einflüsse als auch durch natürliche Prozesse zurückgegangen. Sowohl Veränderungen in der Vegetationsstruktur als auch der Verlust der Mangroven führen zu vermehrter Küstenerosion. Bisher gibt es wenig wissenschaftliche Untersuchungen, die sich mit dem Rückgang von Mangrovenküsten beschäftigen. In einigen Studien sind hydrologische Faktoren wie Tide und Strömungen als die Erosion kontrollierendes Element untersucht worden; ein direkter Einfluss konnte aber bis heute nicht aufgezeigt werden.

Die bisherigen Untersuchung des Rückganges von Mangrovenküsten basieren im Wesentlichen auf dem Vergleich entweder historischen Kartenmateriales oder Luftbild- oder Sattelittenbildaufnahmen. Diese Methoden sind gut geeignet, um Aussagen über große Gebiet und lange Zeiträume zu erhalten. Sie eignen sich aber nicht für die Untersuchung von Prozessen, die auf kurzen Zeitskalen wie Tagen, Wochen oder saisonalen Zeiträumen stattfinden. Geländeuntersuchungen, die den direkten Einfluss von hydrologischen Parametern (Wasserstandsschwankungen, Tide, Wellen, Strömungen) auf die Küstenerosion zum Gegenstand haben, sind bisher kaum durchgeführt worden. Das Fehlen dieser Daten beruhte bisher auf den schwierigen Zugangsmöglichkeiten im Gelände. Aus diesem Grund können die den Mangrovenküstenrückgang steuernden Prozesse immer noch nicht erklärt werden. Die nachfolgenden Fragen gilt es zu beantworten:

(1) Wie steuern Tide, Wellen und Tideströmungen die Küstenerosion und welcher dieser Parameter dominiert?

(2) Wie steuern saisonale Wasserstandsfluktuationen entlang des Mekongdeltas (von Vung Tau bis Ca Mau) die Erosion der Mangrovenküste?

(3) Wie wirkt sich der Einfluss von kurzzeitigen Ereignissen (Tropenstürme, Tsunamis) auf die Erosion von Mangrovenküsten aus?

(4) Wie beeinflussen Bodeneigenschaften und Mangrovenstruktur die Stabilität von Mangrovenküsten?

Zur Beantwortung dieser Fragen sind für empirische Untersuchungen entlang des Mekongdeltas die beiden Lokalitäten Can Gio und Bo De, an denen die Küste durch aktive Mangrovenkliffs dominiert wird, ausgewählt worden. In beiden Gebieten gibt es sowohl lebende als auch abgestorbene Mangrovenvegetation. Der Rückgang der Kliffküsten wurde

sowohl für gesamte Springtidezyklen als auch für Zeiträume bis zum einem Jahr erfasst. Es wurden dafür Sedimentproben sowohl vom Kliff als auch von den vorgelagerten Wattflächen entnommen und analysiert. Zur weiteren Bestimmung der Bodeneigenschaften erfolgten Scherfestigkeitsmessungen an der Kliffwand. Unmittelbar vor den Kliffküsten wurden Wellen- Strömungs- und Tideparameter gemessen. Um den großräumigen Einfluss des Tideregimes zu erfassen, erfolgten weiterhin Tide- und Strömungsmessungen im Nga Bay Ästuar und entlang des Mekong Deltas.

Es wurden stündliche Werte über einen 19-jährigen Zeitraum von 7 Stationen entlang des Mekong Deltas ausgewertet. Beide Arbeitsgebiete sind durch eine semi-diurnale Tide mit einem Tidehub bis zu 4 m charakterisiert. Während des NE-Monsuns (November bis März) ist das mittlere Tidehochwasser generell bis zu 45 cm höher; gleichzeitig wird die Küste durch eine höhere Wellenenergie beeinflusst. Die höchsten Wasserstände treten im November auf, die geringsten im Juni/Juli.

Für das Arbeitsgebiet Nga Bay Ästuar beträgt der kurzfristige Küstenrückgang basierend auf 2-wöchigen Messungen im Mittel 0,42 cm/Tag. Der Rückgang wird maßgeblich durch die Überflutungsdauer des Klifffußes und den gleichzeitigen Welleneinfluss gesteuert. Da während der Nipptide die Überflutungsdauer des Klifffußes höher ist als während der Springtide, ist während der Nipptide der Kliffrückgang höher. Für das Kliff im Nga Bay Ästuar ist eine Energie von 857 J/m² erforderlich um einen Kliffrückgang von 1 cm zu erzeugen.

Der Kliffrückgang im Nga Bay Ästuar beträgt basierend auf 14 Messungen über ein gesamtes Jahr 1,54 cm/Tag bzw. 4,79 cm/Jahr. Dieser Wert ist um das 3,6 fache höher als die Messwerte aus den Messungen im gleichen Gebiet während des SW-Monsuns. Aus dieser Differenz kann geschlossen werden, dass es während des NE-Monsuns zu wesentlich höheren Kliffrückgangsraten kommt.

Der Kliffrückgang in Bo De beträgt für einen 14-tägigen Messzeitraum 2,38 cm / Tag. Dieser Rückgang basiert im Wesentlich auf dem Einfluss von Wellen, wobei die maximalen, täglichen Rückgangswerte mit dem maximalen Energieeintrag durch Welleneinfluss korrelieren. Analog zu Can Gio ist durch die längere Überflutungsdauer während der Nipptide der Küstenrückgang während dieser Periode höher als während der Springtide. Im Mittel ist für einen Kliffrückgang von 1 cm eine Energie von 1105 J/m^2 notwendig. Gegenüber Can Gio spielt für den Kliffrückgang in Bo De der Welleneinfluss eine größere Rolle. Dennoch ist für beide Kliffabschnitte die Überflutungsdauer der maßgebliche Faktor.

Vor beiden Kliffabschnitten wurde auf den vorgelagerten Wattflächen keine Akkumulation von Lockermaterial beobachtet. In den vorgelagerten Tiderinnen erreicht die ebbdominierte

Strömung Werte bis zu 1 m/s. Aufgrund dieser hohen Strömungen kommt es nicht zur Akkumulation von erodiertem Sediment auf den Wattflächen.

Beide Gebiete unterscheiden sich weiterhin in der Scherfestigkeit der Kliffsedimente. Mit einem Wert von 0.1923 kg/cm^2 in Bo De gegenüber 0.1273 kg/cm^2 für Can Gio ist Bo De wesentlich erosionsresistenter. Um 1 cm Kliff zu erodieren sind in Bo 1105 J/m² notwendig, in Can Gio sin es lediglich 857 J/m^2. Damit kommt auch den Bodeneigenschaften eine maßgebliche Rolle für die Geschwindigkeit des Kliffrückgangs zu.

Während der Messphase in Bo De trat der Tropensturm Chan-hom auf. Auch wenn das Sturmzentrum 300 km entfernt lag, führten die durch diesen Sturm induzierten Wellen dennoch kurzfristig zu einem höheren Kliffrückgang.

Es gibt 3 Arten des Rückganges von Mangrovenkliffküsten: Oberflächenerosion, Bildung von Hohlkehlen und Rutschungen. Die Oberflächenerosion tritt dort auf, wo es entweder keine Mangroven gibt oder die Vegetation nur spärlich ausgebildet ist. Hohlkehlen bilden sich in der Regel unterhalb des Wurzelbereiches aus. Der obere, durchwurzelte Bereich wird zunächst durch die Bindung des Wurzelgeflechtes weniger erodiert, als der darunterliegende Bereich. Ist die Hohlkehle aber sehr weit fortgeschritten, so bricht der obere Bereich nach und es kommt kurzfristig zu sehr hohen Erosionsraten.

Zusammenfassend ergeben sich folgende Schlüsse: (1) Tide, wellen und welleninduzierte Strömungen sind die maßgeblichen Faktoren für den Rückgang von Mangrovenkliffs, wobei die Überflutungsdauer die maßgebliche Rolle spielt. (2) Währen der Nipptide kommt es gegenüber der Springtide zu höheren Rückgangsraten. (3) Die Scherfestigkeit des Mangrovenbodens beeinflusst den Kliffrückgang. (4) Der Rückgang von Mangroven-Kliffküsten ist ein natürliches Phänomen und variiert lokal in Zeit und Raum.

Table of contents

List of figures

List of tables

1. INTRODUCTION

Mangroves mainly grow along sheltered coastlines, estuaries, lagoons, and deltaic shorelines, limited to the intertidal environment of tropical and subtropical areas (Woodroffe, 1992). Notable extensions to higher latitude in both the Northern and Southern hemispheres are up to 32°20'N (in Japan and Bermuda) and 38°45'S (east coast of South Africa, New Zealand, and Australia) (Spalding et al., 1997; FAO, 2007). Regarding the worldwide distribution of mangroves, tropical areas are dominant and the latitudinal limits are related to major ocean currents and the 20 °C seawater isotherm in winter (Alongi, 2002). Mangroves are highly adaptable to daily effects by tidal changes, temperature, and salinity (Alongi, 2008). Because of their high salt tolerance, mangrove communities are the most popular habitats along tropical coasts.

Mangrove forests are among the most productive ecosystem that supplies high services, products, biodiversities, etc. This ecosystem is important for the economy and livelihoods, especially in developing countries (Alongi, 2002). Mangrove forests are also favorable places for birds, mammals, fish, shellfish, etc. (Kathiresan and Bingham, 2001). The green belts of mangrove forests are as well known as an element, which function to protect coastal areas. High density mangroves increase the friction factor and therefore help to reduce current flow, enhance sedimentation and stabilize the shorelines (Furukawa et al., 1997). The vegetation in mangrove forests can also reduce wave energy and mitigate catastrophic damages caused by extreme events such as tropical storms or tsunamis (Mazda et al., 1997; Massel and Brinkman, 1998; Dahdouh-Guebas et al., 2005; Kathiresan and Rajendran, 2005; Vo, 2006; Vo and Massel, 2006).

Due to increasing anthropogenic stresses, sea level rise and climate change, mangrove ecosystems are threatened greatly (Duke et al., 2007; Gilman et al., 2008). Loss of mangroves is appearing worldwide, especially in developing countries, where mangroves occupy about 90% of the global mangroves resources; the loss rates are increasing quickly (Duke et al., 2007). From 1980 to 2005 the world wide distribution of mangroves have been decreased annually from about 0.66 to 1.04%, respectively from 187,940 km^2 in 1980 to 152,310 km^2 in 2005 (FAO, 2007). Depending on the method and the technique, which are used to estimate the area covered by mangroves, the values are different. The most reliable estimation of global mangrove distribution in 2000 was 157,050 km^2 (FAO, 2007); this value is about 12.3% higher than 137,760 km^2, which is the value estimated by Giri et al. (2011). Although the spatial area covered by mangroves estimated by FAO (2007) might be smaller than the true value, the world wide area of mangrove environments is being lost alarmingly.

If this rate of mangrove loss cannot be altered, our next generations will no longer see one of the most useful and wonderful ecosystem in the next hundred years (Duke et al., 2007).

Mangrove destructions are forced by human impacts as well as by natural factors. However, human activities are causing mangrove loss, which is faster than the loss due to natural impacts. The study of Blasco and Aizpuru (2002) in Myanmar showed that in protected areas, the loss of mangrove is less than in unprotected areas. The conversions of mangroves for urbanization, industry, aquaculture, and agriculture are the main causes of mangrove destructions, in which shrimp farming is a primary cause in Southeast Asia, especially in Thailand and Vietnam (Alongi et al., 1999; Thu and Populus, 2007).

Losses of mangroves are largely due to human activities; however, mangroves can also be damaged by extreme events such as storms, cyclones, tsunamis, and lightning or even by normal tide and wave actions (Semeniuk, 1980; Smith et al., 1994; Winterwerp et al., 2005; Yanagisawa et al., 2009). During the period of the tropical storm Durian in December 2006, which was moving along the coast of Southern Vietnam, huge mangrove areas were completely devastated (own observation). The evolution of mangroves is recognized to follow accumulation of fine-grained sediment (Woodroffe, 1992); however, mangrove trees can die due to both, either high sedimentation rate or a lack of sediment supply (Semeniuk, 1980; Hong and San, 1993; Ellison, 1999).

As mangroves are occupying the coastal regions, they are directly subject to sea level changes. Under the influence of sea level rise and climate change, mangrove shoreline development and mangrove ecosystems are vulnerable, as these impacts would cause higher inundation and increase in wave energy, disrupting mangroves (Woodroffe, 1990; Ellison, 1993; Gilman et al., 2006). Gilman et al. (2006) proposed three general scenarios for mangrove response to sea level rise relative to mangrove surface:

(a) No change in sea level: mangrove margins remain in the same position,

(b) Relative sea level drop: mangroves migrate to seaward,

(c) Relative sea level rise: mangrove margins retreat landward.

One of the highlights of climate change is the increasing intensity and frequency of tropical storms due to the increase of the tropical sea surface temperature (Emanuel, 1987, 2005). The consequence of sea level rise associated with the effects of climate change is putting mangrove ecosystem at risk (Ellison, 1993).

Besides the destructions of coastal mangrove forests or changes in mangrove vegetations, reduction of sediment supply to the coast supports additionally rapid coastal erosion (Mazda et al., 2002; Winterwerp et al., 2005; Thampanya et al., 2006; Le et al., 2007).

About 1% of the global mangrove forests are located in Vietnam of which most are located in the Mekong Delta (Southern Vietnam) and in the Red River Delta (Northern Vietnam) (FAO, 2007). In the Mekong Delta the spatial distribution of mangroves is bigger than in the Red River Delta (Hong and San, 1993; Giri et al., 2011).

During the Vietnam War (1962-1971), herbicides were heavily sprayed by the U.S. Army on the mangrove forests of Southern Vietnam, especially in Can Gio and the Mekong Delta. About 36% of the whole mangrove forest was destroyed (NAS, 1974). Since 1978, mangroves have been replanted successfully in Can Gio and several regions in the Mekong Delta. In some areas they started to develop naturally after the efforts of reforestation (Hong and San, 1993; Tuan et al., 2002). However, many mangroves in Vietnam have been lost due to the impact of developing purposes, particularly for shrimp farming (Seto and Fragkias, 2007; Thu and Populus, 2007).

The loss of mangrove forest in Vietnam increased annually from 0.1% to 3.0% during 1980-2005. Although the loss rates tend to decrease in the period from 2000 to 2005, the area of mangrove forest decreased from 269,150 ha (in 1980) to 157,000 ha (in 2005). It is equivalent to about 42% of the total mangroves in Vietnam that have disappeared from 1980 to 2005 (FAO, 2007). The detailed study about mangrove changes in Tra Vinh province of Thu and Populus (2007) shows that the mangroves of this region were lost by about 51% during the period 1965-2001.

The Mekong Delta is suffering from increasing trends of temperature, southward moving tracks of tropical storms and sea level rise (MONRE, 2009). Moreover, the Mekong Delta is also one of those deltas that are sinking rapidly (Syvitski et al., 2009). If the scenario of sea level rise with a rate of about 100 cm/century happens, 32.8% of the Mekong Delta region will be flooded (MONRE, 2009). Along the east coast of South Vietnam, mangroves have been lost rapidly and coastal erosion occurs almost everywhere. The shorelines have been retreated, for examples, up to 50 m/year in some places in Can Gio (Mazda et al., 2002), and up to 30-40 m/year in Ganh Hao (Tran et al., 2004). More than 600 ha of mangrove environments have been lost at the coast from Bo De to Rach Goc (350 km) during the period 1982-1983 (Hong and San, 1993) (see the locations of these regions in Figure 4.1).

Because of the extremely important functions of mangrove ecosystems, these environments have been studied widely by many disciplines using different approaches. Many efforts for

conservation and reforestation of the mangrove ecosystems have been done; however, they are threatened strongly by anthropogenic and natural stresses.

Previous studies have shown clearly that mangrove shorelines are usually retreating and changing. However, the relationship between erosion and the processes controlling this erosion has received less attention and is still poorly understood. A better understanding of the response of mangrove coastlines to adverse effects is necessary to manage and protect these coastal areas as valuable ecosystem in a sustainable way.

2. STATE OF THE ART

Mangrove belts are well approved as a factor that can reduce wave energy and current velocity by their root systems, trunks, and canopies and therefore help to minimize coastal erosion (Furukawa and Wolanski, 1996; Mazda et al., 1997; Mazda et al., 2006; Vo, 2006; Vo and Massel, 2006). This does not mean that there has been no erosion along mangrove coasts. Many mangrove shorelines have been eroded or changed in different areas all over the world, for instance, in southwest and northwest Malaysia (Carter, 1959; bin Hassan, 1993), north-west Australia (Semeniuk, 1980), Gulf of Papua New Guinea (Walsh and Nittrouer, 2004), Thailand (Winterwerp et al., 2005; Thampanya et al., 2006) or southern Vietnam (Hong and San, 1993; Mazda et al., 2002; Tran et al., 2004; Vo and Massel, 2006), natural erosion occurred. Coastal mangroves usually undergo erosion or retreat (Woodroffe, 1992), but in recent time, this erosion has been strongly increased by anthropogenic impact.

Semeniuk (1980) classified three types of erosion of mangrove dominated coasts: sheet erosion, cliff erosion and tidal-creek erosion. The retreat of mangrove dominated shoreline usually occurs as cliff erosion and sheet erosion (Woodroffe, 1992) (Figure 3.1). Rapid mangrove shoreline retreat with the rate of up to 90m/year happens only as cliff erosion (Semeniuk, 1980).

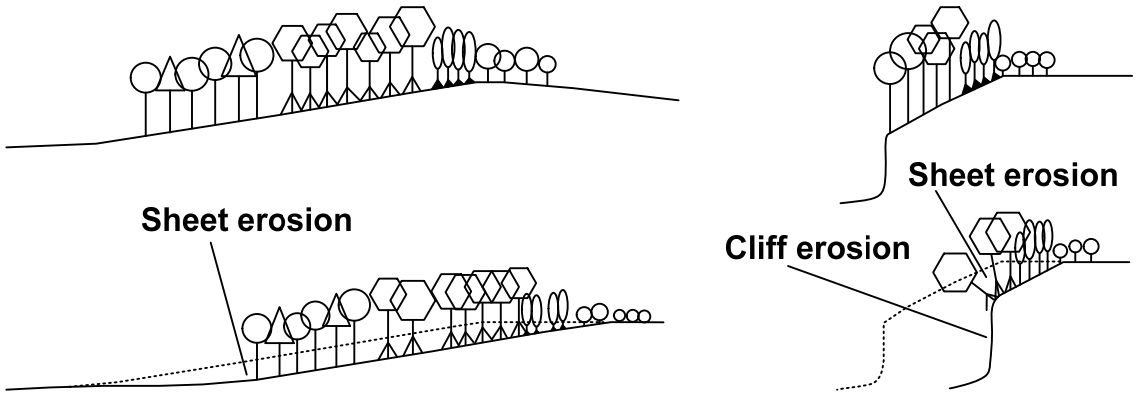

Figure 3.1. Two types of mangrove shoreline erosion: sheet erosion and cliff erosion according to the classification of Semeniuk (1980) (Woodroffe, 1992).

Mangrove cliffs are an indicator for fast erosion processes. They are usually created due to the cohesive forces of the minerals building up the mangrove soil combined with the binding of mangrove root systems (Semeniuk, 1980). These cliffs are often found at scalloped shorelines or estuaries where at the top of the cliff is occupied by living or dead mangroves (Semeniuk, 1980). The height of mangrove cliffs are typically about 1-2 m up to 6 m locally in King Sound, Australia (Semeniuk, 1980), or about 0.4 to 2.3 m in South Vietnam.

In general, there are several kinds of coastal cliff (e.g. sea cliff, salt marsh cliff, and mangrove cliff) depending on their geological built up and environmental impact factors. Sea cliffs are the most popular types of coastline. They occupy about 80% of the world ocean coasts (Emery and Kuhn, 1982). Sea cliffs are very different from mangrove cliffs because of their soil compositions and cliff heights. They are eroding episodically due to storm events (Carter and Guy Jr, 1988; Sterr, 1989).

Mangrove cliffs are similar to salt-marsh cliff concerning their evolution (Allen, 1989; Allen and French, 1989; Feagin et al., 2009). However, the differences between mangrove cliffs and salt marsh cliffs are the geographical areas, as mangroves appear only in the tropics and subtropics, and the vegetation itself. Mangroves form big trees up to 30 m in height (Ross, 1974) with an extensive root system while salt marshes are composed of a much smaller plants (Davidson-Arnott et al., 2002). Although coastal erosion or retreat of mangrove areas is due to complex interaction of different processes, the erosion or retreat is mainly caused by tide and wave actions (Semeniuk, 1980, 1981; Mazda et al., 2002; Winterwerp et al., 2005; Vo and Massel, 2006).

Semeniuk (1980, 1981) calculated the mangrove cliff erosion from direct measurements using fixed datum points and the analysis of coastline changes from historical aerial photographs. His studies showed that the rates of cliff erosion were significantly different from region to region and typically about 2 m/year and locally up to 90 m/year. He also indentified that mangrove cliff erosion in King Sound, north-west Australia is strongly due to tidal scouring by strong currents; waves are only a minor important factor. However, field data for illustrating the relations between mangrove cliff erosion and tidal current and wave actions were not shown in this study.

Mazda et al. (2002) defined that coastal erosion needs two conditions related to the flow regime including strong tidal current and one-way sediment transport due to the asymmetry of tidal currents. Their study was based on long-term coastline changes from the analysis of historical maps and measurements of coastal currents at one location for the duration of about 36 hours. Finally, they used a numerical model to explain how strong currents can be formed around a river mouth in mangrove swamps. The study of Mazda et al. (2002) showed that the coastline in the mangrove area of Can Gio in South Vietnam has been retreated in some areas up to 50 m/year. Their work pointed out that the mechanisms of long-term coastal erosion in Can Gio are caused by strong tidal currents with velocities higher than 70 cm/s and changes in mangrove vegetation. This study only focused on one hydrodynamic factor, the strong tidal current that could cause the mangrove shoreline erosion in the long-term. The role of wave and tidal inundation for shoreline erosion was not considered.

Also in Can Gio, but only in a small area, Vo and Massel (2006) show, by repeated measurements of topographical changes along one transect, that the mangrove shoreline retreats of about 3 m/year. However, their work mainly focused on the interaction and the influence of waves current and suspended matters in the mangrove swamp. The relation between shoreline retreat and wave and tidal currents were not analyzed in their study.

Winterwerp et al. (2005) described for the Bang Khum Thien coast in Thailand five governing processes that can cause erosion of a muddy mangrove coast: subsidence, erosion by larger waves, erosion by smaller waves (even capillary waves), storm events, transport by alongshore currents. Unfortunately, their study does not show any field data to prove how these factors are controlling the erosion of mangrove coastline.

Mangroves are living in tide-dominated areas (Woodroffe, 1995); therefore, mangrove coasts are almost daily inundated and affected by tidal processes. The influences of tidal processes on coastal erosion in mangrove coasts have been investigated or considered only with respect to tidal currents (Semeniuk, 1980; Mazda et al., 2002; Vo and Massel, 2006). Semi-annual or seasonal variations of sea level due to tides or tides associated with the monsoonal winds in a mangrove swamp have been mentioned in some studies (Mazda et al., 2002; Vo and Massel, 2006), but the important influence of tides on inundation of mangrove coast was rarely analyzed. Moreover, the role of sea level changes due to tide and tidal inundation regarding coastal erosion of mangrove coasts have not been considered in previous studies. In addition, the relationship between erosion and soil properties of mangrove shorelines (e.g. shear strength and grain size distribution) has not been considered yet. Quantitative studies on mangrove erosion or retreat due to the wave and tide are limited.

The methods for estimating or measuring mangrove coastline changes or recessions are usually based on the analysis of historical maps, satellite images, and aerial photographs (Semeniuk, 1980, 1981; bin Hassan, 1993; Spalding et al., 1997; Blasco and Aizpuru, 2002; Mazda et al., 2002; Walsh and Nittrouer, 2004; Thampanya et al., 2006; Giri et al., 2011). Therefore, the resolutions and precisions in time and space are low. Moreover, mangrove shoreline erosion has not been measured frequently in shorter time scales like in daily or fortnightly tidal cycles, monthly or semiannually.

3. OBJECTIVES

Due to missing field data about mangrove coastal erosion, the following important questions remain unanswered so far.

- How do hydrodynamic influences from water level variations (tides), wave energy inputs and tidal currents cause coastal erosion?
- What is the dominant hydrodynamic factor of the influences mentioned above?
- What is the amount of wave energy input, which is needed to erode a mangrove shoreline?
- How do seasonal-based water level fluctuations along the coast of the whole Mekong Delta (Vung Tau to Ca Mau) influence mangrove coasts erosion?
- What is the influence of short-term events (tropical storm and tsunami) on the erosion of mangrove coasts?
- How do soil properties, structure of the vegetation, seasonal variations of wind velocity, and short- and long term sea level changes affect the coastal erosion?

The main goal of this study is to answer these questions by carrying-out *in-situ* field measurement in different areas along the open coast of the Mekong Delta.

As mangrove shoreline erosion usually occurs as rapid cliff erosion (Semeniuk, 1980), this study will focus mainly on this issue. The field studies are designed to measure all related hydrodynamic and sediment dynamic parameters as well as meteorological data at two specific mangrove coasts in Southern Vietnam. Two investigation areas, Bo De and Can Gio (Figure 4.1) were chosen, which differ in the distribution of mangrove species, soil components, and their exposure to meteorological- and hydrological impacts. Tides strongly influence both sites. The cliffs are inundated only during high tide. Therefore, the field measurements have been designed as follow:

- Investigation of tidal aspects along the whole easterly coast of Southern Vietnam from Vung Tau to Ca Mau Cape to gather information about the influence of tides and to assess tidal impacts on the mangrove coast (e.g. tidal inundation or seasonal variation of tidal levels).
- Analysis of the hydrodynamic processes (e.g. tide, wave, and tidal flow regime), which control and influence the mangrove cliff retreat, especially under short-term conditions (e.g. daily tidal cycle during the fortnight period). Based on these datasets, it is attempted to identify how these hydrodynamics parameters play roles in cliff recession, how the tidal regimes drives the erosion, and what kind of waves usually act on the cliffs.

- Measurement and analysis of the seasonal variation of the mangrove cliff retreat.
- Measurement and analysis of soil properties (e.g. grain size distribution, shear strength and root penetration) at the two specific investigation sites to ascertain its role regarding to the velocity of the mangrove cliff retreat.
- Investigation of tidal current influences of adjacent estuaries around the study sites to address their role in mangrove shoreline retreat.

Beside the above main objectivities, it was the aim to collect the meteorological data (such as wind, rainfall, tropical storm/depression tracks) as close to the sites as possible, to evaluate the influence of meteorological factors on mangrove shoreline erosion.

It was assumed that, there is a gradient in tidal range variations along the app. 350 km long outer coast of the Mekong Delta from Vung Tau to Ca Mau. Therefore, tidal data have to be analyzed from different stations along the whole coastline. As there are irregular tide and water level fluctuations during a nodal cycle (a 18.6 years period) (Clifford and Gary, 1973), data of that period need to be taken into account as well. It was not possible to collect these data during the time of the research period presented here. The raw data of water level fluctuations for a nodal cycle were collected by the Southern Region Hydro-Meteorological Center (SRHMC). They were available for this study.

4. INVESTIGATION AREAS

4.1. Study sites

Two sites were chosen in the North and the South of the Mekong Delta. One site is located on the western bank of the Nga Bay river mouth, the east side of Can Gio; the other site on the northern bank of the Bo De tide dominated channel (Figure 4.1). The sites are different each other. While the site in Can Gio is sheltered from waves approaching from offshore, Bo De is located at the outer open coast. Along both sites, mangroves exist and the shorelines are formed by cliffs, which are under retreat (Figure 4.2). In the past, these sites were accumulation areas because old mangrove stumps are found at about 80-100 cm below the present mangrove surface (Figure 4.3).

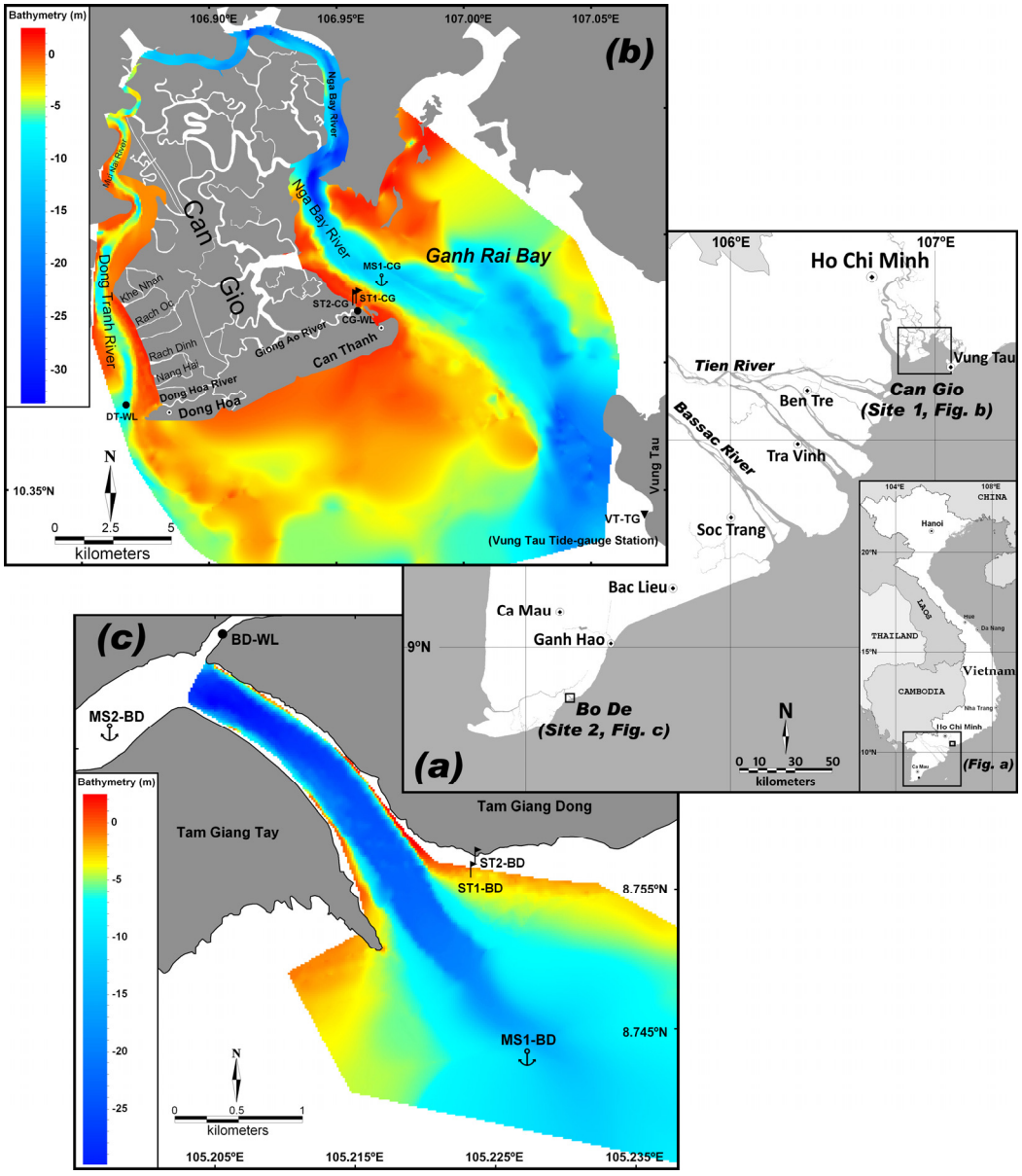

Figure 4.1. Location of the study areas (Fig. a) and bathymetric maps of the regions of Can Gio Ho Chi Minh City district (Site 1, Fig. b) and Bo De, Ca Mau City district (Site 2, Fig. c) based on own data.

Figure 4.2. Mangrove cliff shorelines in Can Gio (left) and Bo De (right). On average, cliff height in Can Gio is 1.8 m, in Bo De it is about 0.7 m.

Figure 4.3. Old dead mangrove stump (marked by white dotted line) in Can Gio (left), which is located approximately 0.8 m below the present mangrove surface and an old mangrove surface layer (the dark layer) in Bo De (right), which is situated about 1 m below the present mangrove surface.

Figure 4.4 (left) Mangrove species (mainly Rhizophora sp. and *Phoenix sp.) existing on the top of cliff in Can Gio. (right) Truncated mangrove trees (Ceriops sp.) presenting on top of cliff in Bo De.*

In Can Gio, densely young mangrove trees with mixed species (mainly *Rhizophora sp.* and *Phoenix sp.*) are living on top of the cliff. The cliff height varies from about 1.3 to 2.3 m (1.8

m on average). At the site in Bo De, on top of the cliff are the truncated mangrove trees (mainly *Ceriops sp.*). The mangrove forest is about 15 m behind the edge of the cliff shoreline. The cliff heights in Bo De range from about 0.4 m to 1.0 m (0.7 m on average).

The site in Can Gio was an ideal site for the investigation about coastal erosion. On the west side of Can Gio accumulation is observed along the banks of the estuary except the area around the Nang Hai Creek (Figure 4.1b) where the erosion rate of the mangrove shoreline is about 3 m/year (Vo and Massel, 2006). On the eastern side of Can Gio the mangrove, shoreline forms a cliff, which is under erosion (Figure 4.4). Moreover, in terms of logistics, Can Gio site is not far away from Ho Chi Minh City and easy to revisit. Therefore, repeated field surveys have been performed more often. Bo De site is far away from Ho Chi Minh City and not easy to visit. Therefore, most of the field activity was carried-out at the site in Can Gio. Bo De was chosen not only as a reference site to compare short-term shoreline retreat under different environmental conditions but also because it is exposed to wave energy input from the open coast during the monsoon. In the recent past, strong erosion could be seen at this site by the collapsed of the old Bo De lighthouse (Figure 4.4).

4.2. Climate conditions

The climate of the study area is influenced by the Northeast (NE) monsoon creating the dry season and the Southwest (SW) monsoon, which creates the rainy season. The distributions of wind speeds and directions at two coastal locations (Vung Tau and Bac Lieu, Figure 4.1a) show that the study areas are affected by East (E) or NE wind from November to March and SW wind from May until October (Figure 4.5). April and October are transitional months of the monsoon. The strongest wind speeds of the NE and SW monsoons prevail from January-February and in August, respectively. The SW wind direction is dominant during the SW monsoon at both stations. At Vung Tau the east wind direction is dominant during the NE-monsoon period while the ENE wind is dominant at Bac Lieu. During stormy conditions, wind speeds can reach up to 23 m/s (9 Beaufort, at Vung Tau), which happened on 5 Dec 2012 during the storm Durian 2006 (see this storm in Table 4.1). Maximum wind speed with a dominant range of 5 Beaufort (8 - 10.7 m/s) was observed during NE monsoon as well as during SW monsoon for both sites (Vung Tau and Bac Lieu).

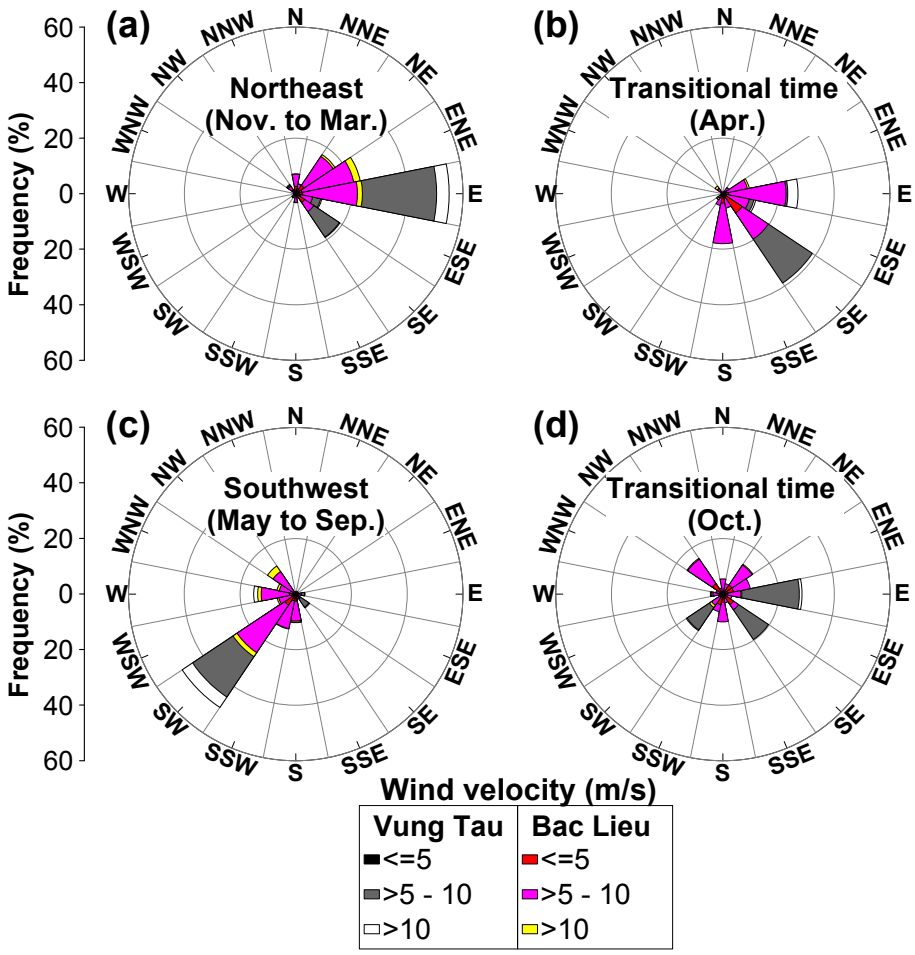

Figure 4.5. Daily maxima of wind velocities for the period 1999-2008 at Vung Tau and Bac Lieu. (a) NE monsoon: November to March; (b) transitional period: April; (c) SW monsoon: May until September. (d) transitional period: October (Data source: Southern Regional Hydro-Meteorological Center – SRHMC, Vietnam).

The rainfall data at four stations (Ca Mau, Soc Trang, Ben Tre, and Can Gio; Figure 4.1a, Figure 4.6) shows that the rainy season lasts from May to November and the dry season normally from December to May, respectively. In Ben Tre and Can Gio, the rainfall in October is higher than during other months. In Soc Trang, the rainiest month is August. In Ca Mau the strongest rainfall is recorded for July. There is an annual rainfall gradient from north-east to south-west with increasing rainfall towards the spit of the Mekong Delta at Ca Mau. February is the driest month along the whole Mekong Delta with no rain during this month from 2004 to 2007. In general, the highest rainfall is recorded for Ca Mau while Can Gio shows the lowest rainfalls. The mean annual rainfall in Ca Mau is about 2 times higher compared to Can Gio.

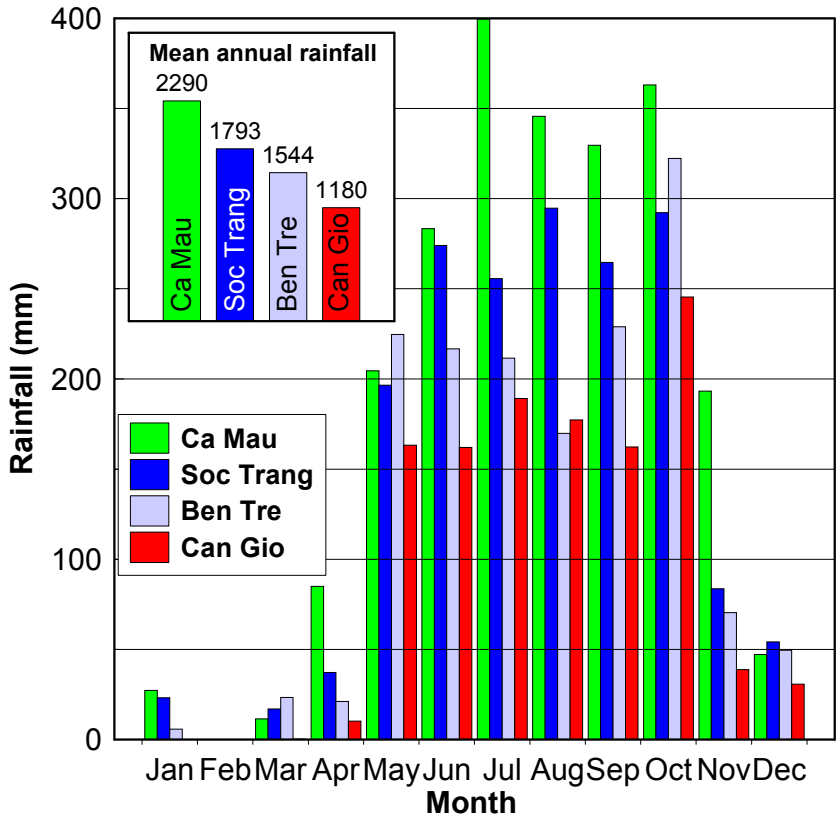

Figure 4.6. Mean monthly rainfall and mean annual rainfall in the Mekong Delta and Can Gio for the period 2004-2007, for explanation see text (Data source: SRHMC, Vietnam).

The study area is characterized by tropical climate with only small temperature changes within the year. For the period 1999-2001, monthly mean air temperatures at three stations in South Vietnam (Vung Tau, Soc Trang, and Ca Mau) vary from about 25.4-25.7 °C to 28.3-29.1 °C with January as the 'coldest' month, while April and/or May are the hottest periods (Figure 4.7a).

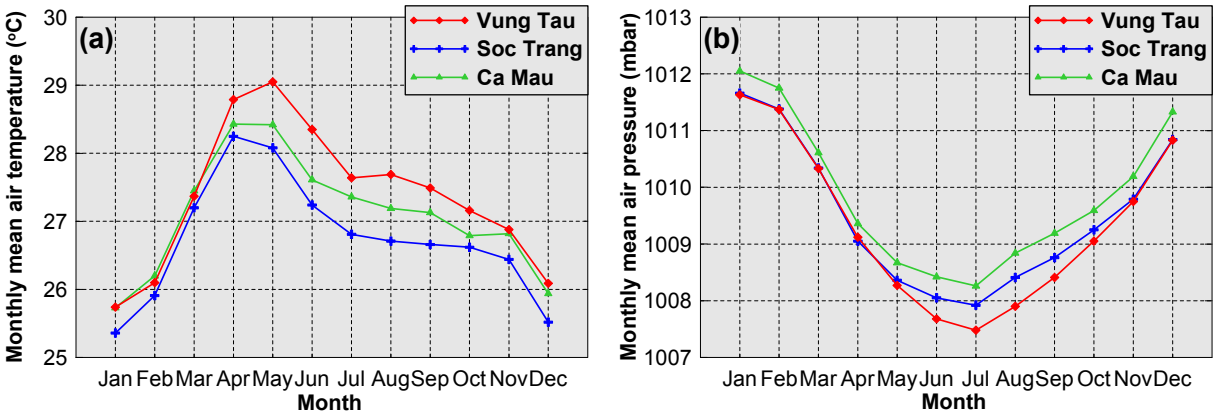

Figure 4.7. Monthly mean values of air temperature and air pressure for the period 1991-2000 at the Vung Tau, Soc Trang, and Ca Mau stations. Data source: Nguyen (2007b).

At three locations (Vung Tau, Soc Trang, and Ca Mau), the mean values of air pressure fluctuate between 1008 and 1012 mbar. It implies that seasonal variations of air pressure of

the study area are low. However, the air pressure in summer is lower than during winter (Figure 4.7b). Gagliano and McIntire (1968) provide also for the past similar variations of the mean air pressure at Sai Gon (Ho Chi Minh City) and Phnom Penh. These stations are located marginal to the study area and indicate no high variation of the air pressure over the recent past.

Tropical storms/depressions rarely occur in South Vietnam. During the period 1945-2010, about 36 tropical storms/depressions struck or affected the coast of South Vietnam (from Binh Thuan to Ca Mau area, see Figure 4.8, data source: UNISYS). On average, there are about 0.55 tropical storms/depressions per year and they usually occur from November to December with November as the stormiest month (Table 4.1, Table 4.2). Among these tropical storms/depressions only eight remarkable tropical storms, or about 0.14 storms per year including #28 (Lucky, 1962), #22 (Thelma, 1973), #27 (1991), #34 (1994), #37 (1996), #30 (Linda, 1997), #29 (2004), and #24 (Durian, 2006) hit the investigation areas. These eight storms happened from late October to early December and strongly influenced the study area from Vung Tau to Ca Mau. The number of tropical storms tends to increase since 1991. From 1945 to 1991, only two tropical storms attacked the area, while from 1991 to 2010, six storms crossed that area with an occurrence frequency of about 1 - 6 years.

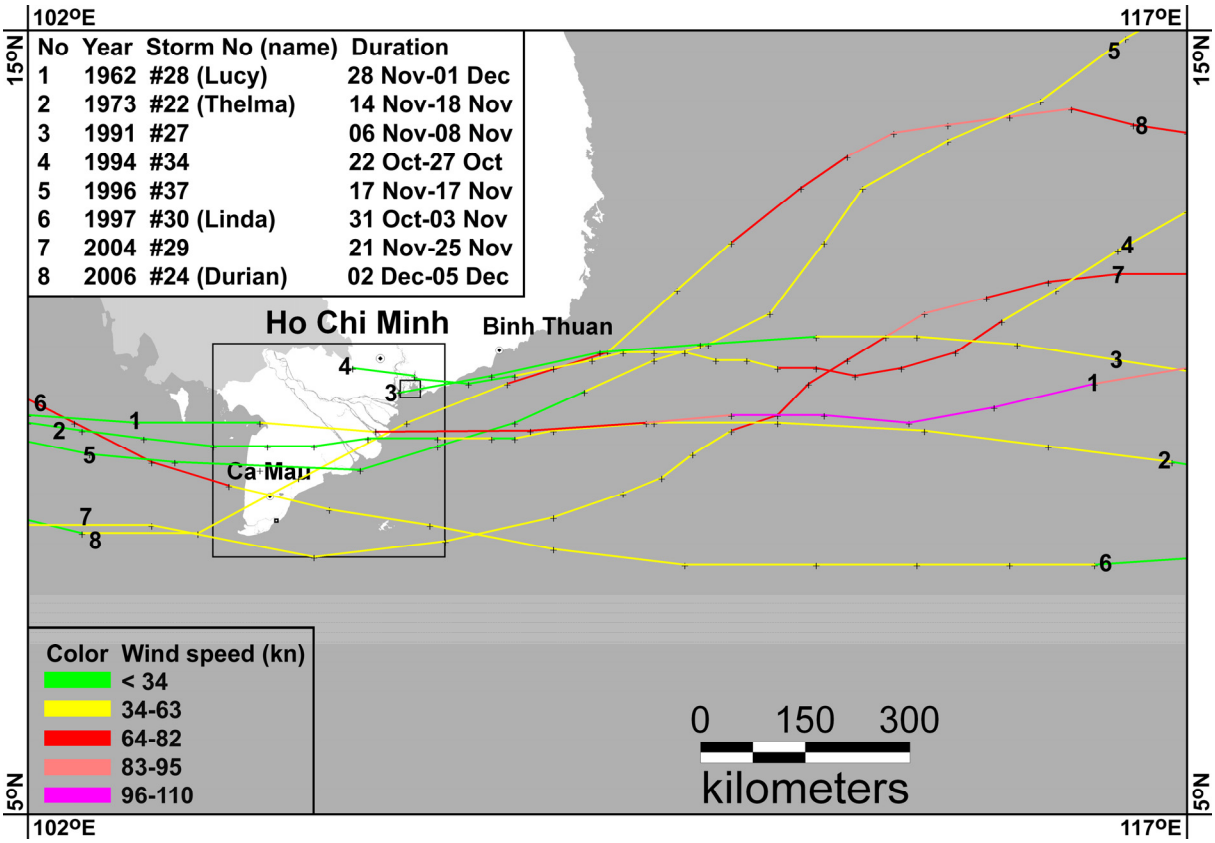

Figure 4.8. Tropical storms, which stroke the study area during the period 1945-2010 (see Table 4.2). Data source UNISYS webpage.

Table 4.1. Tropical storms/depressions that affected the area between Binh Thuan and Ca Mau during the period 1945-2010. Data source: UNISYS[1] webpage.

No	Year	Storm No. name	Wind speed (knots)	Start			End		
		(Name)		dd/mm hh	Lat	Long	dd/mm hh	Lat	Long
1	1949	#18	25-30	03/11 00	11.2	116.1	04/11 18	9.5	107.3
2	1954	#19	35-50	30/11 12	10.6	115.2	01/12 06	10.8	110.9
3	1961	#4	25-50	09/04 18	9.3	109.6	10/04 12	9.9	106.8
4	1962	#39	NA	18/11 12	11.5	114.0	20/11 00	11.0	109.0
5	**1962**	**#28 (Lucy)**	**20-100**	**28/11 12**	**10.7**	**117.0**	**01/12 06**	**10.1**	**102.0**
6	1965	#3	25-45	14/02 18	6.8	109.7	17/02 06	9.3	102.1
7	1965	#35	30-40	18/12 06	7.8	110.2	20/12 06	7.2	102.3
8	1968	#20	30-55	18/10 12	11.6	112.3	20/10 06	12.0	106.7
9	1968	#25	20-60	20/11 18	10.3	116.7	24/11 00	11.6	108.0
10	1968	#26	20-70	25/11 18	9.0	116.5	28/11 00	9.4	108.4
11	1970	#19	25-60	27/10 06	11.8	115.5	29/10 06	10.7	106.5
12	1970	#22	25-50	14/11 12	15.6	116.3	17/11 06	9.4	107.9
13	1972	#19	25-80	30/11 00	7.4	115.4	03/12 06	8.4	102.3
14	**1973**	**#22 (Thelma)**	**25-55**	**14/11 06**	**9.5**	**116.8**	**18/11 00**	**10.0**	**102.0**
15	1973	#35	20-40	22/12 06	10.0	115.9	24/12 12	8.8	107.0
16	1983	#16	20-40	15/10 06	9.3	116.9	18/10 00	13.6	102.2
17	1985	#25	20-45	19/11 18	6.8	108.1	26/11 00	13.5	108.3
18	1985	#26	25-60	16/12 06	7.6	114.6	22/12 00	6.1	105.9
19	1988	#25	35-65	04/11 18	9.6	116.6	06/11 18	10.9	108.2
20	**1991**	**#27**	**25-35**	**06/11 18**	**10.8**	**116.1**	**08/11 12**	**10.4**	**106.8**
21	1992	#30	25-55	12/11 06	10.2	116.9	15/11 00	7.9	102.1
22	1993	#36	25-40	12/12 00	10.6	117.0	15/12 12	7.3	102.0
23	**1994**	**#34**	**15-65**	**22/10 06**	**12.7**	**117.0**	**27/10 00**	**10.7**	**106.2**
24	**1996**	**#37**	**25-40**	**13/11 18**	**14.9**	**116.2**	**17/11 06**	**9.6**	**102.8**
25	**1997**	**#30 (Linda)**	**30-65**	**31/10 12**	**8.2**	**115.8**	**03/11 00**	**10.0**	**102.6**
26	1998	#21	20-50.	10/11 18	9.4	115.6	15/11 00	10.3	107.5
27	1998	#25	20-35	08/12 12	7.6	113.9	11/12 18	8.4	102.7
28	1999	#31	15-30	29/11 18	10.8	116.5	03/12 12	7.8	102.8
29	2000	#33	20-35	03/12 06	11.3	116.0	08/12 00	8.6	106.3
30	2004	#5	25-30	14/05 00	9.2	113.8	18/05 12	11.0	110.9
31	**2004**	**#29**	**40-90**	**21/11 06**	**11.9**	**116.1**	**25/11 00**	**8.7**	**103.6**
32	2004	#25	25-45	17/12 18	9.5	116.4	21/12 06	7.9	106.3
33	**2006**	**#24 (Durian)**	**25-90**	**02/12 00**	**13.7**	**117.0**	**05/12 18**	**8.6**	**102.7**
34	2009	#2	20-75	02/05 18	9.9	111.2	07/05 00	15.3	117.5
35	2009	TD 1	25-30	18/01 18	8.2	110.6	19/01 18	9.4	108.3
36	2009	TD19	20-25	12/12 12	9.9	112.1	13/12 06	10.2	110.4

Start and End times are considered when the tropical storm/depression passes the latitudes 117°E and 102°E, respectively. Storms are numbered according to tropical storms/depressions, which occurred in the West Pacific. Rows in bold format show the noticeable tropical storm that stroke directly the study area (see also Figure 4.8).

[1]**The data downloaded at the website: http://weather.unisys.com/hurricane/w_pacific/index.html**

Table 4.2. Monthly occurrence of the tropical depressions/storms that affected the area between Binh Thuan and Ca Mau during the period 1945-2010.

Month	Jan	Feb	Mar	Apr	May	Jun	Jul	Aug	Sep	Oct	Nov	Dec	SUM
Number of depression/storm	1	1	0	1	2	0	0	0	0	5	15.5	10.5	36
Frequency distribution (%)	2.8	2.8	0.0	2.8	5.6	0.0	0.0	0.0	0.0	13.9	43.1	29.2	100

4.3. Oceanographic conditions

The study area is strongly affected by hydrodynamic processes reflecting the circulations of the South China Sea and the Gulf of Thailand (Gagliano and McIntire, 1968).

From Vung Tau to Cape Ca Mau the area is strongly influenced by complex tidal processes, which are the primary factor controlling the hydrodynamics of the coastal waters. The tides are classified as mixed tide, mainly semi-diurnal with a tidal range partly exceeding 4 m. Tidal variations and characteristics will be shown in detail in Chapter 6 (Results).

The area is strongly affected by seasonal coastal currents, which are mainly induced by the monsoon (Gagliano and McIntire, 1968). These current directions are reversing due to the monsoonal seasons. During the NE monsoon, the coastal currents are directly towards southwest whereas northeasterly direction is dominant during the SW monsoon (Wyrtki, 1961; Gagliano and McIntire, 1968; Shaw and Chao, 1994).

Along this coast, currents are strongly affected by tide as well. Tidal currents mostly flow parallel to the coast. Asymmetry of current velocities between ebb and flood usually observed. At the Dinh An river mouth, Nguyen and Duong (2006) showed a dataset of current velocities, which were measured at near the bottom during the period from 8 March to 14 March 1997 in spring tide. This dataset illustrates that tidal current directions at this station are reversed from W to E, in which W direction represents for flood current and E direction for ebb current. Maxima current velocity of about 1.5 m/s happened during flood and 0.75 m/s during ebb. On the delta slope near the Hon Khoai Island (app. 20 km offshore from Ca Mau Cape), Unverricht et al (2012) presented current velocity, which were collected between 30 and 31 March 2008 during spring tide, at two mooring stations located at the mean water depth of 12 m and 26 m. The velocity data shows ebb current is dominant at both mooring stations. At near the bottom, maximum of ebb current velocity is of app. 0.6 cm/s, while maximum of flood is about 0.4 m/s. The currents flow to WSW direction during flood and to ENE during ebb.

The wave regime of along the coast from Vung Tau to Ca Mau is supposed to be directly induced by the wind of the monsoons; changes in wave directions and wave height follow variations in the wind directions of the monsoonal seasons (Gagliano and McIntire, 1968; Hoang and Nguyen, 2006; Tamura et al., 2010; Albers and von Lieberman, 2011).

In the delta shelf, Hoang and Nguyen (2006) and Albers and Lieberman (2011) showed long-term wave data at Bach Ho (app. 180 km offshore from the coast of Can Gio) and Con Dao (app. 140 km offshore from Bo De). At Bach Ho, during winter, most of waves approach from

NE, whereas, during summer waves approach dominantly from SW (Hoang and Nguyen, 2006). During winter, maximum wave height could reach a value of 7.0 m, while a maximum wave height of 5.0 m was observed during summer. At Con Dao station, waves mainly approach from NE during winter (NE monsoon) and from SW-W during summer (SW monsoon) (Albers and von Lieberman, 2011). Significant wave heights of more than 3 m could be seen in both NE and SW monsoons.

In the coastal zone, at outer of the Dinh An river mouth, near the coast of Tra Vinh, Nguyen and Duong (2006) showed a significant wave height of up to 1.55 m in between 4 October 1997 and 11 October 1997. Also in Tra Vinh, Tamura et al (2010) observed near shore breaking waves in Tra Vinh with heights of about 0.5 m in autumn and of 0.5 - 1 m in spring. At about 300m from the sea dike of Vinh Tan (near Bac Lieu), Albers and Lieberman (2011) showed maximum significant wave heights of 0.25 m (during 3 - 5 October 2009) and 0.55 m (during 21- 28 January 2010).

Mean surface salinity and mean water temperature along the delta front is not significantly different between summer and winter. The mean salinity of 32-33 ppt (parts per thousand) is normally recorded in the winter and more than 33 ppt in the summer (Gagliano and McIntire, 1968). At the Mekong river mouths, the salinities are reduced to 1-10 ppt from the averaged of 22-26 ppt due to high fresh water discharge and rainfall in the summer (Hong and San, 1993). Highest and lowest mean monthly water temperatures are about 25 °C (in winter) and 29 °C (in summer), respectively (Mikhailov and Arakelyants, 2010).

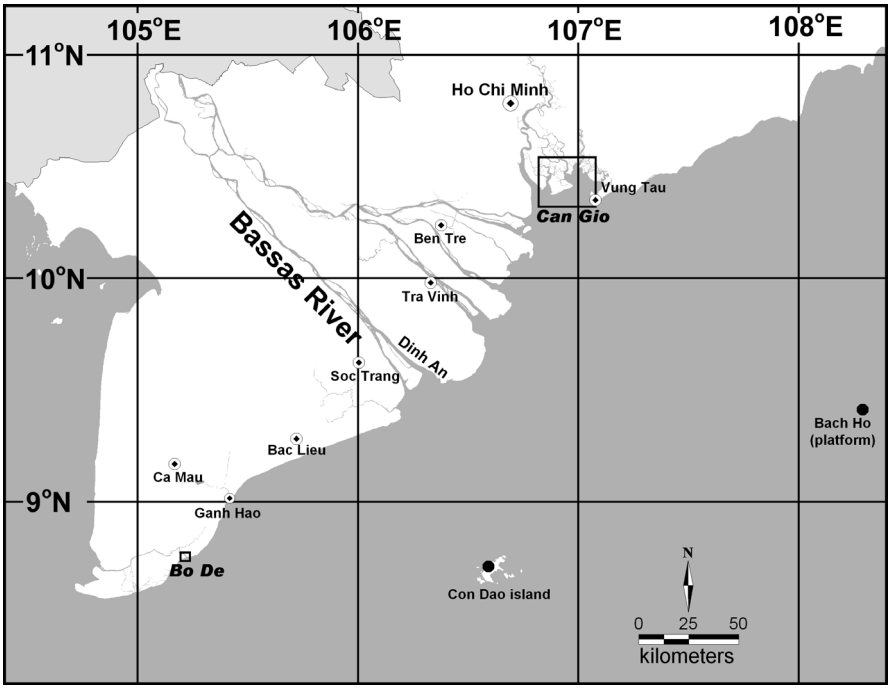

Figure 4.9. Map showing the study areas including two stations in the delta shelf (Bach Ho platform and Con Dao Island) where long-term wave data are available.

4.4. Mangrove species distribution

During the Vietnam War, about 36% (109,939 ha) of the total mangrove forests in South Vietnam have been died after they were heavily sprayed with herbicides by the U.S. Army in the period 1962-1971 (NAS, 1974). Since 1978 mangroves, mainly *Rhizophora apiculata*, have been replanted successfully, especially in Can Gio. After the efforts of reforestation some of them have been developed naturally (Hong and San, 1993; Tuan et al., 2002). However, since 1983 the mangroves of Vietnam have been cleared mainly for shrimp farming and cooking fuel (Hong and San, 1993).

Hong (1984, 1991; cited in Hong and San, 1993) separated mangroves of Vietnam in four zones (Zone 1, Zone 2, Zone 3, and Zone 4) due to the differences in geographical and climatic conditions as well as the distribution and development of mangroves. The study sites are located in the Zone 4, which is the largest spatial area of mangroves in Vietnam. This zone is divided into four subzones. The study sites in Can Gio and Bo De are located in the first subzone (subzone 4a) and third subzone (subzone 4c) (Figure 4.10). According to the Forest Inventory and Planning Institute (FIPI, 1983; cited in Hong and San, 1993) the total mangrove area in the fourth zone amounts to 191,810 ha, which accounts for about 76% of the total amount of mangroves in Vietnam (252,500 ha). Replanted mangroves occupy approximately about 22% of the total amount of mangroves of the Zone 4.

The study site in Can Gio belongs to the well known mangrove forest in Vietnam (the Can Gio Mangrove Biosphere Reserve), which is recognized as an international biosphere reserve by UNESCO since 2000. Therefore, this area is the most protected mangrove forest in Vietnam. The Can Gio Mangrove Biosphere Reserve has a total area of 75,740 ha and is divided into three zones: the core zone (4,721 ha), the buffer zone (37,339 ha), and the transition zone (29,310 ha). The total area of mangrove forest is about 30,385 ha including replanted forest, which accounts for about 58% of the total mangrove forest of the Can Gio Mangrove Biosphere Reserve (Tuan et al., 2002). Depending on tidal inundation, mangrove species distribute at different elevation (Figure 4.11). The pioneer species *Sonneratia alba* and *Avicenna alba* are located at the lower levels. The next higher elevations are occupied by *Rhizophora sp.*, followed by *Xylocarpus granatum, Bruguiera gymnorrhiza, Lumnitera littoralis and Excoecaria agallocha*. *Phoenix species dominate* at the highest elevation (Vu Van Cuong, 1964; cited in Tuan et al., 2002). Although the classification of Vu Van Cuong was done before the deforestation during the Vietnam War and the distribution of recent reforested mangrove communities might be different, his classification basically agrees with the recent classification by van Loon et al. (2007). The hydrological classification of

mangrove communities is a good indicator to estimate the elevation as well as tidal inundation in case when topographical data are not available.

Can Gio is located in the 'transition zone' where the human activities are partly allowed if these effects are not harmful to the Biosphere Reserve (Tuan et al., 2002). Therefore, the mangroves at this study site were partly cleared for shrimp farming. Nowadays only young mixed mangroves communities (mainly *Rhizophora sp.* and *Phoenix sp.*) are living along the shoreline. Due to the shoreline retreat, the pioneer communities such as *Sonneratia alba or Avicennia alba* are not found in the lower parts of tidal flat (Figure 4.2).

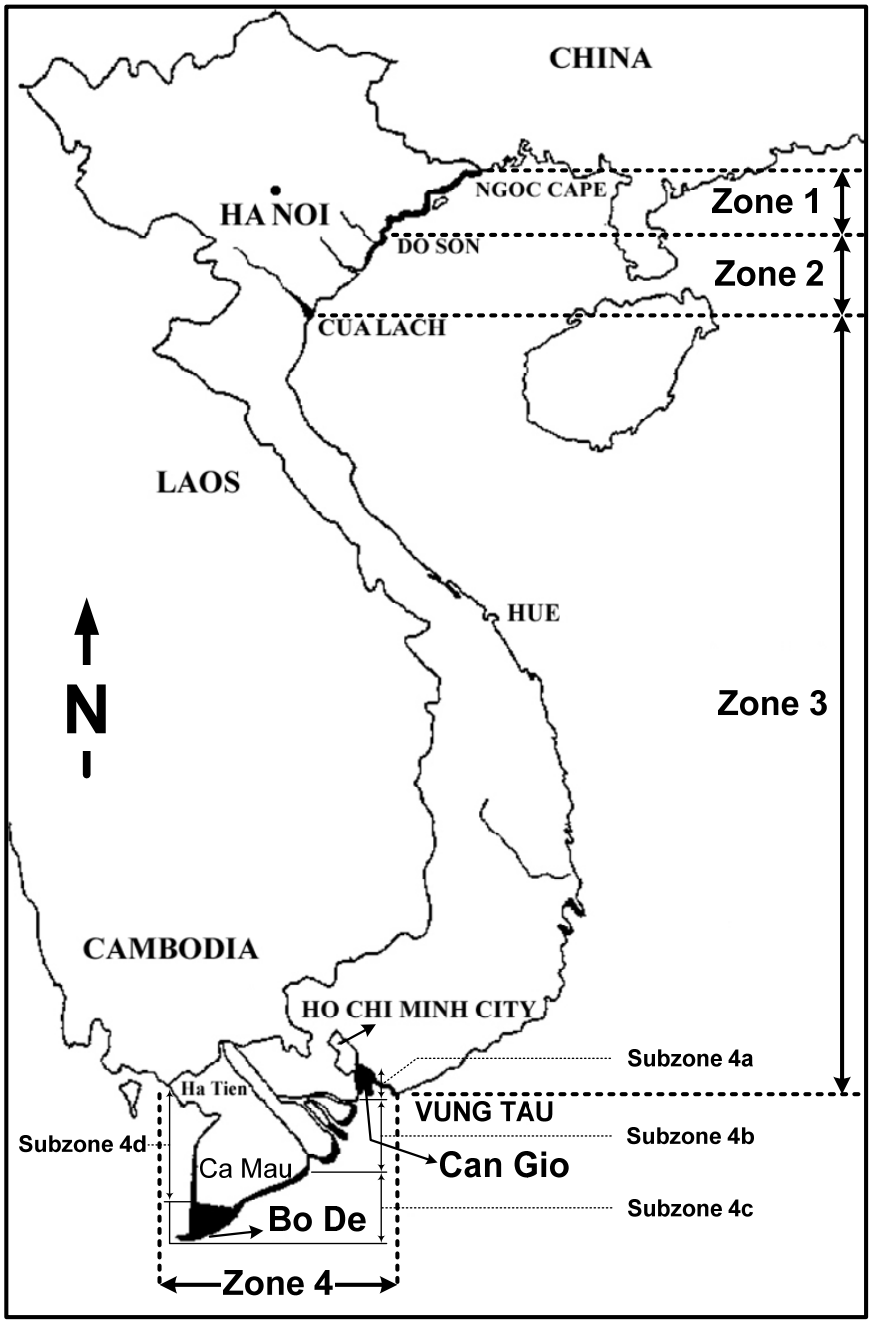

Figure 4.10. Distribution of mangroves (black coloring) in Vietnam (FAO, 1993; Hong and San, 1993).

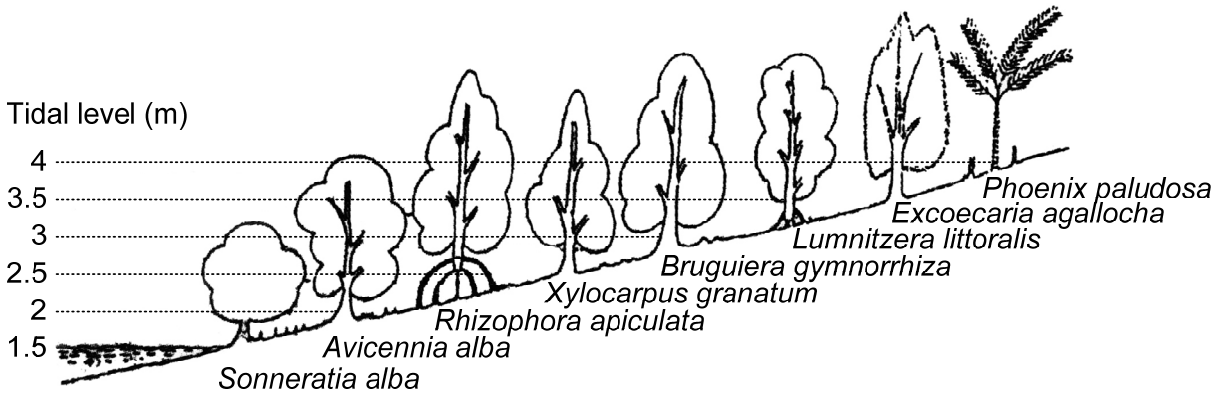

Figure 4.11. Distribution of mangrove communities in Can Gio due to tidal levels (Vu Van Cuong, 1964; cited in Tuan et al., 2002).

Although the mangrove forests at Ca Mau Peninsula were destroyed by about 52% of the total area of mangrove forest by the herbicides during period from 1962-1971, the study site in Bo De seemed to be not influenced by the defoliant action (NAS, 1974; Ross, 1974) (Figure 4.12). Before the Vietnam War, the mangrove forests in this area were mainly *Rhizophora apiculata* with some *Bruguiera parviflora* with heights up to 30 m (Ross, 1974). In areas where accumulation prevailed, *Avicennia alba* and *Excoecaria agallocha* were pioneer communities, followed by *Rhizophora apiculata* and *Bruguiera parviflora* (Ross, 1974). After the deforestation by herbicides, here the mangrove forests seemed to have been recovered faster compared to the recovering process in Can Gio (formerly named Rung Sat). This was due to the high abundance of seeds and seedlings in this area (Ross, 1974). The classification of Hong and San (1993) shows that the mangrove communities in the Ca Mau Peninsula is similar to those described by Ross (1974), and the distribution of mangrove trees in elevations follows tidal levels (Figure 4.13).

In comparison to the Can Gio study site, the mangrove community around the Ca Mau peninsula, including the Bo De study site, is different. Recently, at Bo De site, the pioneer communities such as *Avicennia sp.* are not found due to strong erosion in lower elevation on the tidal flat. Truncated mangrove trees (mainly Ceriops sp) occupy in higher elevations on tidal flat. The natural mangrove forest with mainly *Ceriops sp.* and *Exoecaria agallocha* are located about 15 m from the shoreline (Figure 4.2).

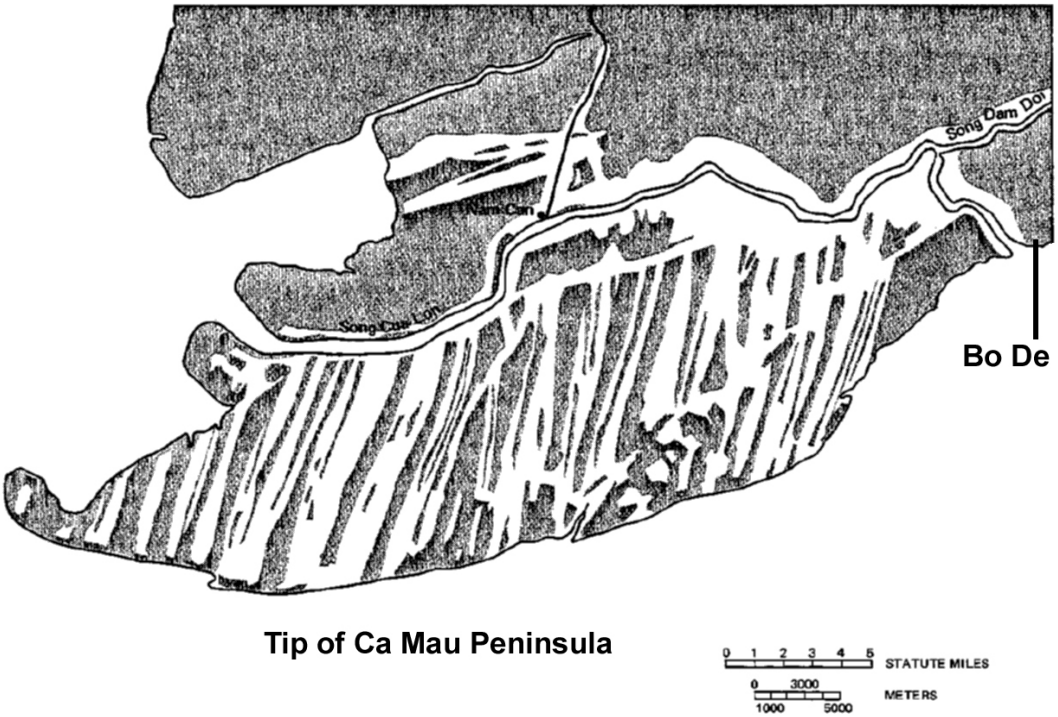

Figure 4.12. Status of the mangroves in the Ca Mau Peninsula in 1972 after having been sprayed by herbicides. White stripes indicate the bare land of cleared mangroves (NAS, 1974).

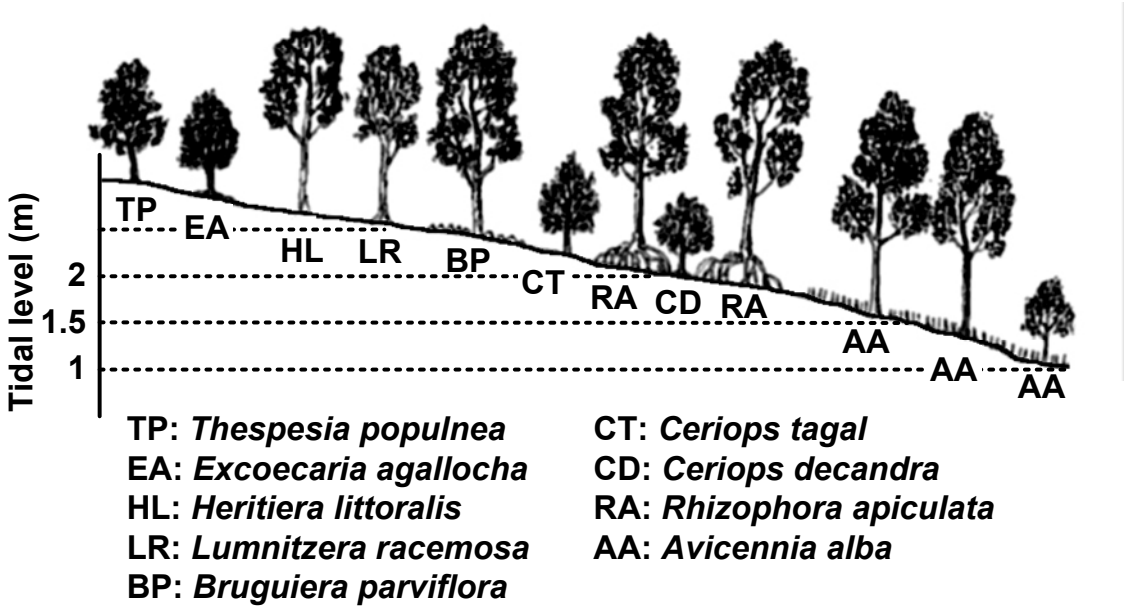

Figure 4.13. Distribution of mangrove communities in the Ca Mau Peninsula due to tidal levels (Hong and San, 1993).

4.5. Geomorphological and geological conditions

The study site Can Gio is located in on the marginal tidal basin close to the Mekong Delta (Figure 4.14). It is controlled by the Sai Gon and Dong Nai Rivers. Bo De is located of the marginal plain of the Mekong River Delta (Gagliano and McIntire, 1968).

The Can Gio region was formed at least 800 years before today (Schwarzer et al., 2007). This area has been formed by sediment from the river system of the Sai Gon and Dong Nai Rivers, some sediment from the Vaico (or Vam Co) River (Gagliano and McIntire, 1968) and from offshore (Figure 4.14). Surface sediment in Can Gio is mainly Holocene sediments (Huynh and Nguyen, 2003). The topography in Can Gio is relative flat with altitudes of about 0 to 1.5 m, except at Giong Chua Hill, which has a maximum altitude of 10.1 m (Tuan et al., 2002).

The study site in Bo De is located on the east side of the Ca Mau Peninsula, at the eastern coast of the Mekong River Delta that was formed during the last 8 ka (Nguyen et al., 2000; Ta et al., 2002b; Tamura et al., 2009; Proske et al., 2010). Since about 3 ka, the Ca Mau Peninsula has been formed due to the spreading of the Mekong River Delta in southwestern direction (Ta et al., 2005). The propagation rate was about 26m/year (Xue et al., 2010). The coastal plain extends in a low elevated area of about 1 - 2 m above mean sea level and huge area is covered by mangroves (Ta et al., 2005). During the Late Holocene, the evolution of the delta has changed from a tide-dominated to a mixed wave-influenced tide-dominated delta (Ta et al., 2002a; Ta et al., 2002b).

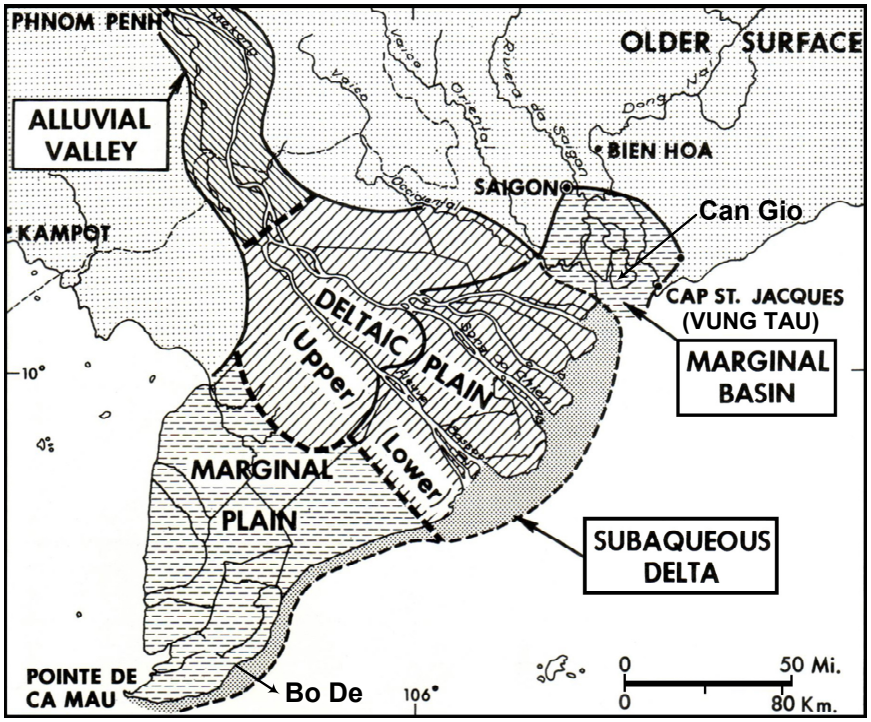

Figure 4.14. Major physiographic units of the Mekong River Delta (Gagliano and McIntire, 1968).

5. METHODS

5.1. General introduction

By previous studies, it has been identified that coastal erosion along mangrove coasts is commonly due to tidal and wave actions. However, field observations about these governing factors, namely the tide, waves and currents together with shoreline erosion are sparse. This lack of precise and detailed measurements together with the impacting factors is a major reason why the mechanism of mangrove shoreline erosion has not been convincingly explained yet. Among the driving factors, the relevance of each factor for mangrove shoreline erosion also has not been assessed yet. The main cause of the lack of field data might be due to the difficulties to measure these parameters in-situ as Robinson (1977) or Sunamura (1982) noted in their studies.

In order to understand the processes controlling mangrove cliff retreat, the study was designed to collect simultaneously data of cliff retreat, wave energy input, tidal fluctuations and current velocities. Measurements of the cliff retreat in short-term time scale were carried-out almost every day when the cliff was exposed during low tides. The measuring strategy was the same for both study sites with the periods of continuous data collection for at least 14 days to capture a whole neap-spring tidal cycle.

To ascertain the seasonal variation of cliff retreat, long-term measurements of the cliff retreat were carried-out for the site in Can Gio for about one year with revisiting the area about few weeks.

Besides the major field surveys, to measure the cliff retreat and related parameters (e.g. tide, wave), the investigations of tide regimes (e.g. tide and tidal current) were also carried-out at the river mouths around the main study sites to understand the driving forces of the entire coastal area. In addition, bathymetric data around the study sites were taken to get information about the morphology surrounding the study areas.

5.2. Study design for measuring cliff retreat and related parameters

5.2.1. Measurement of cliff retreat

Along the mangrove cliff shorelines in Can Gio and Bo De, sections of 125 m in length in Can Gio and 110 m in length in Bo De were chosen for investigating the cliff retreat (Figure 4.1b, c; Figure 5.1a1, b1). The cliff retreat was measured using erosion pins, which were made from iron sticks with a length of 50 cm and diameter of 6 mm. This method is similar to that applied by Hooke (1979) who measured the river bank erosion using steel stick, 6.35 mm in

diameter and 40-80 cm in length. Depending on the height of the cliff, three or four erosion pins were put in a profile from the top to the bottom of the cliff. In Can Gio, 21 of such profiles (four stations at each profile) were installed, and 10 of those profiles (three stations at each profile) in Bo De (Figure 5.1a1, a3, b1, b3).

The cliff retreat value was determined by measuring the free length of the erosion pin which was inserted perpendicularly into the active cliff surface. Each measurement, the erosion pin was knocked again into the cliff with 3 cm remaining outside (47 cm inside the cliff, Figure 5.1a3, b3). In cases that the erosion pins were lost due to fast erosion, it is assumed that the erosion rate will be at least 47 cm. Benchmarks were put on top of the cliff about 2 m inside the forest at each cliff retreat profile (Figure 5.1a3). This was done to estimate the cliff retreat with higher accuracy in case of fast erosion. When all erosion pins at a profile were lost, the length from the benchmark to the edge of the active cliff was measured and used as the representative retreat of that profile.

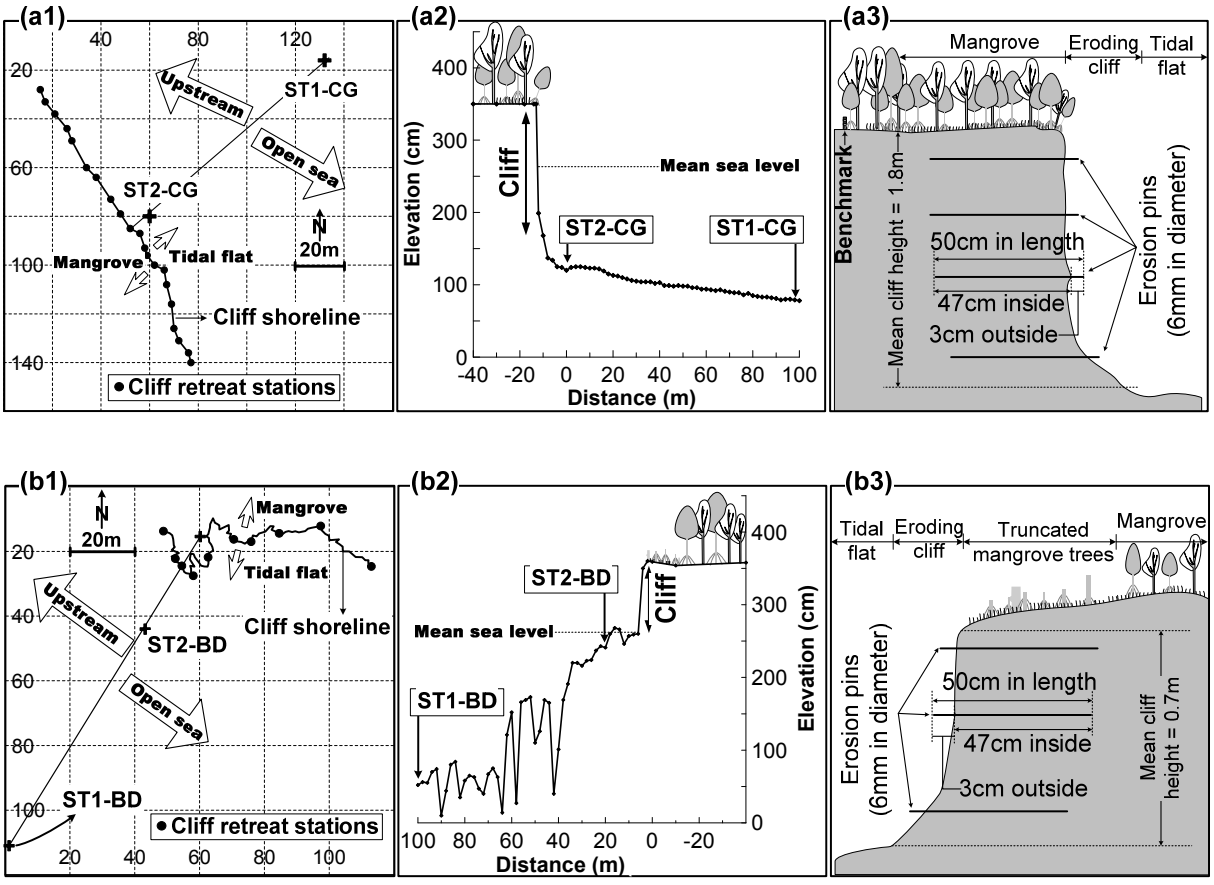

Figure 5.1. Design of field measurements at Can Gio (a) and Bo De (b). The maps of the mangrove cliff shorelines (a1 and b1), the position of the measurement stations on the tidal flats in front of the mangrove cliffs (a1-2 and b1-2), and the position of the deployed erosion pins in the cliff profiles (a3 and b3). The zero elevations in figure 5.1a2, b2 refer to the zero level at the Vung Tau tide gauge station (Figure 4.1).

5.2.2. Soil properties

To characterize the soil properties of the mangrove cliff section, sediment samples were taken. Additionally, the shear strengths were measured close to the position of the erosion pins at the beginning of the field campaign.

The shear strength of the cliff soil was measured using a 'Pocket Van Tester' device (Eijkelkamp Agrisearch Equipment). With the Pocket Van Tester, the force required to break the soil from the cliff surface at a special point was measured. From this result, the shear strength of this point was calculated using the following equation:

Shear strength (kg/cm^2) = 0.10963 kg/cm^2 * x

Where x is the value which is shown on the instrument (Eijkelkamp, 2005).

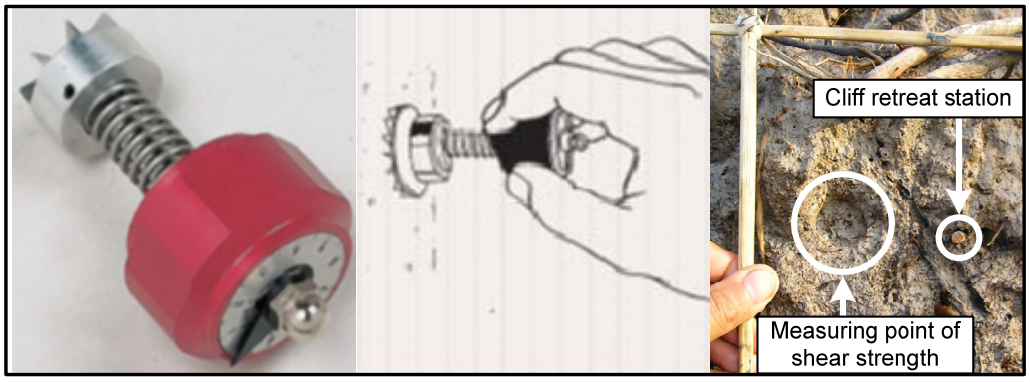

Figure 5.2. Pocket vane tester (left: Eijkelkamp Agrisearch Equipment) and the application in the field (right). The right figure shows the hole after the pocket tester has been applied on the mangrove cliff surface. A sediment sample was taken at this hole to analyze the grain size distribution later on.

Sediment samples taken from the cliff close to every position of shear strengths measurement (see also in Figure 5.2) were analyzed for grain size using the Malvern Lasersizer. Before the measurement, organic matter and carbonate were removed by adding 10 ml of hydrochloric acid (HCl) and by heating this sample by 60 °C for four hours. After rinsing the sediment sample to remove the residuals of the HCl-acid, 10 ml of Hydrogen oxygen (H_2O_2) was added (removes the organic matter) and heated for 24 hours. Afterwards the sediment samples were rinsed again to remove the residuals of H_2O_2. Finally, the grain size parameters were calculated using the GRADISTAT-software (Blott and Pye, 2001).

5.2.3. Hydrodynamics and suspended matter measurements

To gather information about the hydrodynamics acting at the study sites in Can Gio and Bo De, data acquisitions of hydrological parameters were carried out. Water level as well wave

and current characteristics were measured in a distance of 10 to 20 m in front of the mangrove cliff. Parallel to these recordings the same parameters were measured approximately 100 m offshore on the open tidal flats (ST1-CG, ST2-CG for the site in Can Gio and ST1-BD, ST2-BD for the site in Bo De, Figure 5.1a1, a2, b1, b2). This graduated setup allows the estimation to which extend waves and currents are altered on the way from the open mud flats to the cliff and by the cliff itself. In addition to the hydrological measurements also suspended matter concentration was quantified at all sites to estimate the response of sediment stability and mobility to hydrodynamic forcing.

Directional wave and current parameters are measured using shallow water directional wave current recorders (Midas DWR, VALEPORT Co., LTD) (abbreviation DWR will be used in the further text). These instruments are equipped with a precise piezo-resistive pressure sensor, a 2-axis electromagnetic current sensor, and a fluxgate compass, as well as auxiliary sensors for temperature, conductivity, and turbidity (optical backscattering). In the field, the DWRs are buried in the sediment so that the sensors have a height of only 10 cm above the bed (Figure 5.3). They are operated in 30 minutes intervals, with 4 Hz sampling rate, and 4096 samples per bursts tantamount to a burst duration of 17.06 minutes. To calculate statistical wave parameters like wave height, wave period or wave direction, the instrument's inherent or the post processing capabilities of the DWR are used. Both are based on long-established principles of Linear Wave Theory (find citation).

Figure 5.3. In-situ deployment of a CTD (Conductivity Temperature Depth) and a DWR (Directional Wave and current Recorder) (delete Midas).

Tidal water level fluctuations are measured by self recording CTDs (conductivity, temperature and pressure) probes. The CTDs are always installed close to the DWRs (Figure 5.3). The sampling interval is 1 minute. The post processing of the water level is shown in

Chapter 5.5.2. After wave and water level data were obtained, total wave energy input and duration of cliff inundation were calculated from these datasets. This calculation is shown in Chapter 5.5.3.

Turbidity is measured by optical backscatter sensors (OBS) (Seapoint Sensors Inc., 2000). Each DWR is equipped with one of these sensors. For turbidity measurements in different heights above the seabed, three OBS arrays were installed. To convert the raw data from this sensor, a calibration is necessary (see Chapter 5.5.4).

5.3. Collecting tide and tidal current data around the study sites

Tides are a striking attribute of the Mekong Delta coast. Therefore, a detailed knowledge of general and site specific tidal action in terms of water level fluctuations and currents is essential for studies of coastal evolution. However, especially data for the study areas are rather sparse or completely missing. For this reason own short term measurements over at least one neap-spring tidal cycle have been carried out in the investigation areas Can Gio and Dong Tranh, as well as in Bo De and Rach Goc (Figure 5.4, Table 5.1).

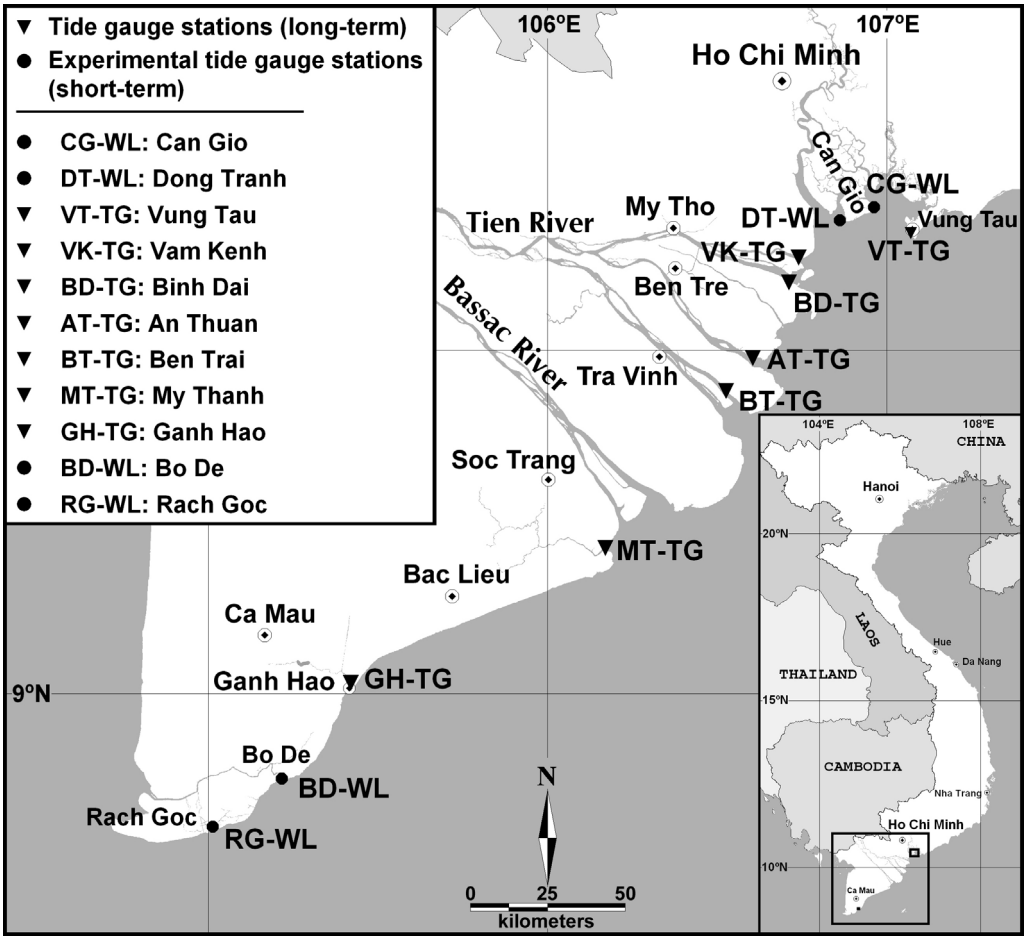

Figure 5.4. Map showing the tide gauge stations surrounding the study sites in Can Gio and Bo De, along the coast from Vung Tau to Rach Goc.

Table 5.1. The locations of the water level and tide gauge stations along the Sai Gon and Dong Nai Rivers estuaries and along the Mekong Delta.

Station	Lat. (°N)	Long. (°E)	Name, location at the river (or mouth), province (City)
CG-WL	10.421062	106.959984	Can Gio, Giong Ao River, Can Gio, HCM City
DT-WL	10.382335	106.867417	Dong Tranh, Dong Tranh river mouth, Can Gio, HCMC
VT-TG	**10.340000**	**107.071000**	**Vung Tau, Vung Tau City**
VK-TG	**10.269889**	**106.740194**	**Vam Kenh, Cua Tieu river mouth, Tien Giang**
BD-TG	**10.197028**	**106.711222**	**Binh Dai, Cua Dai river mouth, Ben Tre**
AT-TG	**9.966667**	**106.605222**	**An Thuan, Ham Luong river mouth, Ben Tre**
BT-TG	**9.880889**	**106.529000**	**Ben Trai, Co Chien river mouth, Ben Tre**
MT-TG	**9.424778**	**106.170917**	**My Thanh, Tran De river mouth, Soc Trang**
GH-TG	**9.031444**	**105.419500**	**Ganh Hao, Ganh Hao river mouth, Bac Lieu**
BD-WL	8.773134	105.205543	Bo De, at the creek near the mouth of the Bo De tidal channel, Ca Mau
RG-WL	8.613813	105.012604	Rach Goc, Rach Goc river mouth, Ca Mau

Note: The stations in bold with the suffix '-TG' are the national stations where long-term hourly water levels are available. The other stations are short-term experimental stations where water levels were measured using the CTD (the locations are shown in Figure 5.4).

To get insight into the general tidal behavior along the coast of South Vietnam, long term water level recordings from the tide gauge station from Vung Tau (VT-TG), Vam Kenh (VK-TG), Binh Dai (BD-TG), An Thuan (AT-TG), Ben Trai (BT-TG), and Ganh Hao (GH-TG) (see Table 5.1, Figure 5.4) were investigated. The raw data have been collected by the Southern Regional Hydro-Meteorological Center (SRHMC) and had to be bought by the Vietnamese part of the SEDYMAN project. The datasets, which almost continuously cover a period of more than 19 subsequent years with a temporal resolution of one hour, were analyzed in terms of typical tidal characteristics (component analyse), annual water level fluctuations and relative sea level rise. The comparison of these results with the data of the short-term measurements was used to estimate the magnitude of annual water level variations and relative sea level rise at the four study sites.

To identify tidal regimes along this coast, harmonic analyses of tides were performed using the program T_Tide (Pawlowicz et al., 2002). The results of these analyses were also used to evaluate dominant contributions of tidal constituents on the water level.

Current velocities around the study sites were collected in the main channels of the river mouth in Can Gio and Bo De. In Can Gio area current velocities were collected in both river mouths, Dong Tranh and Nga Bay River (DT-WL and MS1-CG stations, Figure 4.1b). In Bo De, current velocities were recorded at two locations in the inner and outer part of the Bo De tidal channel (MS1-BD and MS2-BD stations, Figure 4.1c).

In the Dong Tranh river mouth (DT-WL, Figure 4.1b) a steal pipe was erected in the deepest part of the channel at a mean water depth of about 8.7 m (Figure 5.5, right picture). Here currents were measured using a Directional Electro-magnetic Current Meter (Mash Mc Birney, Seapac 2100, Woods Hole Co., LTD). The instrument was mounted about 1.5 m

above the sea bed (see Figure 5.5). Data were collected in a 10 min burst mode with 32 samples per burst, and a 5-second sampling rate. These 32 samples are averaged and represent the current velocity for a 10 min interval.

This "mid-estuary measurement station" was also equipped with a self-recording CTD to collect water level, temperature and salinity data (Figure 5.5). Sampling interval was two minutes.

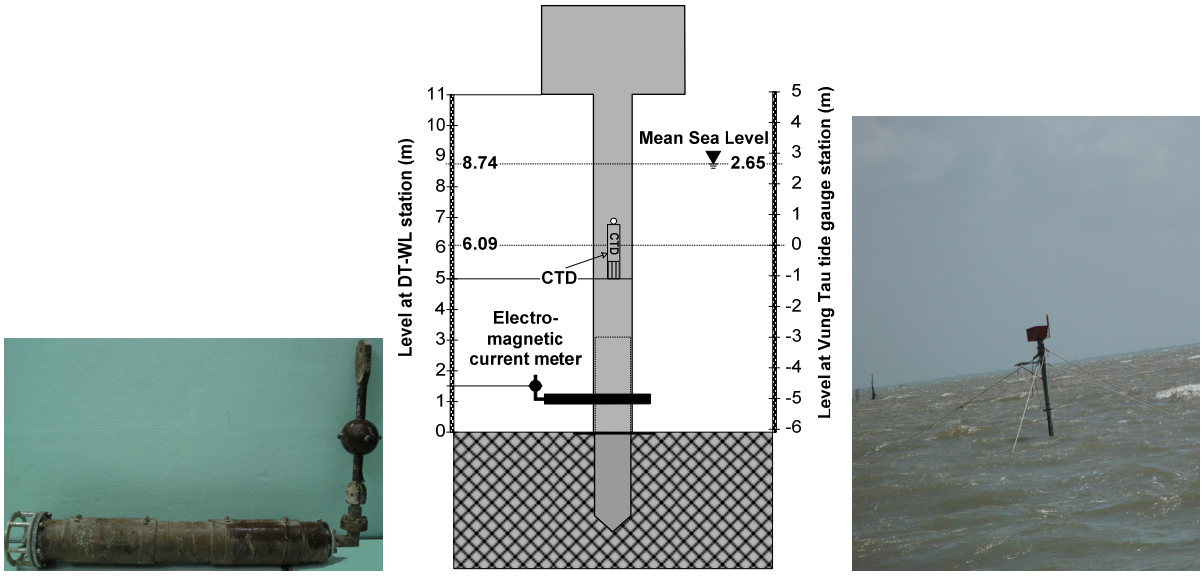

Figure 5.5. From left to right: an electro-magnetic current meter (Mash Mc Birney, Seapac 2100, Woods Hole Co., LTD); design of instrumentation at the Dong Tranh river mouth station (DT-WL station, see Figure 4.1b); picture of this station in the field.

In the main channels of the Nga Bay river mouth and Bo De tidal channel mouth, the data of current velocities were collected at the mooring stations an ADCP (Acoustic Doppler Current Profiler, WHSW600, Teledyne RD Instruments). The instrument was mounted down-looking on a catamaran that was held beside the anchored fishing boat (Figure 5.6).

Figure 5.6. Pictures showing the ADCP (Acoustic Doppler Current Profiler, WHSW600, Teledyne RD Instruments), which was mounted on the catamaran, before and after lowering to the water.

5.4. Bathymetry and topography measurements

The bathymetry around the study areas was measured using a single beam echo sounder (Lowrance LC X-15, dual-frequencies at 50 kHz and 200 kHz). In deeper water, fishing boats were used and for measurement in very shallow water and tidal flats the instrument was mounted on a rubber boat. The bathymetric data were corrected for tides using own water level recordings from nearby pressure gauge station (self recording CTDs).

The topographies of the higher elevated tidal flats were measured by land based leveling. The interval between two consecutive points was usually 2 m. In areas with a small scale topography area, this interval was reduced to 1 m.

The zero levels of the bathymetries and the topographies at the study areas were referenced to the zero level of the Vung Tau tide gauge station.

5.5. Data processing

5.5.1. Computing tidal characteristics

The semi-diurnal tides of a mixed tidal system are characterized by different water levels of the two high waters and the two low waters that develop during a tidal day of 24.84 hours. The four extremes of the semi-diurnal tidal evolution are called higher high water (HHW), lower high water (LHW), higher low water (HLW) and lower low water (LLW) (see Figure 5.7). There is also only one pair of high-low water, which is not coupled with the other high-low water. Normally these ‘single’ pairs of high-low water occur periodically twice in a synodic month during neap tide with the mean period of about 14 days (Figure 5.7b). Therefore, for calculating the tidal range (TR), the ‘single’ pairs of high-low water are indentified from the set of high low waters. These single pairs of high-low water are treated independently (see Figure 5.5c).

Tidal ranges are calculated following the definitions below (see also in Figure 5.7):

(1) For coupled two pairs of high-low water: **Tidal range** = HHW - LLW (see NOOA definition, Figure 5.7a, c and Table 5. 2)

(2) For the ‘single’ high-low water: **Tidal range** = HW - LW (see Figure 5.7c)

To indentify which pair of high-low waters is the single of high-low water, a simple algorithm was applied from the set of low waters. There are only two cases to find the single low water from a set of low waters (Figure 5.8).

Case 1 (Figure 5.8a1, a2):

If ($LW_{i-1} < LW_i \leq LW_{i+1}$) then LW_i is single low water;

Case 2 (Figure 5.8b1, b2):

If ($LW_{i-1} > LW_i \geq LW_{i+1}$) then LW_{i+1} is single low water;

Where LW_i is a set of low waters; i=1, 2, …n; n is number of low waters.

Examples to indentify single pairs of high-low water are shown in Figure 5.7b and Figure 5.8.

A FORTRAN script was written to compute the above tidal characteristics parameters.

Table 5. 2. Definitions of tide (NOAA, 2000, 2003).

Name	Abbreviation	Description
High Water	**HW**	(or high tide) This is the maximum water level during a rising tide.
Higher High Water	**HHW**	The highest high water between two high waters of a tidal day.
Low Water	**LW**	(or low tide) this is the minimum water level during a falling tide.
Lower Low Water	**LLW**	The highest low water between two high waters of a tidal day.
Mean high water	**MHW**	An arithmetic mean of all high waters.
Mean Higher High Water	**MHHW**	An arithmetic mean of higher high waters.
Mean Lower Water	**MLW**	An arithmetic mean of all low waters.
Mean Higher High Water	**MHHW**	An arithmetic mean of lower low waters.
Mean Sea Level	**MSL**	An arithmetic mean of all observed water levels.
mean Diurnal High Water Inequality	**DHQ**	**DHQ = MHHW – MHW.** This is a half mean difference in heights between two consecutive high waters at each tidal day.
mean Diurnal Low Water Inequality	**DLQ**	**DLQ = MLW – MLLW.** This is also a half mean difference in heights between two consecutive low waters at each tidal day.
tidal period	**NA**	A difference in times between two consecutive high waters.
duration of ebb	**NA**	A difference in times between two consecutive high water and low water.
duration of flood	**NA**	A difference in times between two consecutive low water and high water.
tidal range of ebb	**NA**	A difference in heights between two consecutive high water and low water.
tidal range of flood	**NA**	A difference in heights between two consecutive low water and high water.

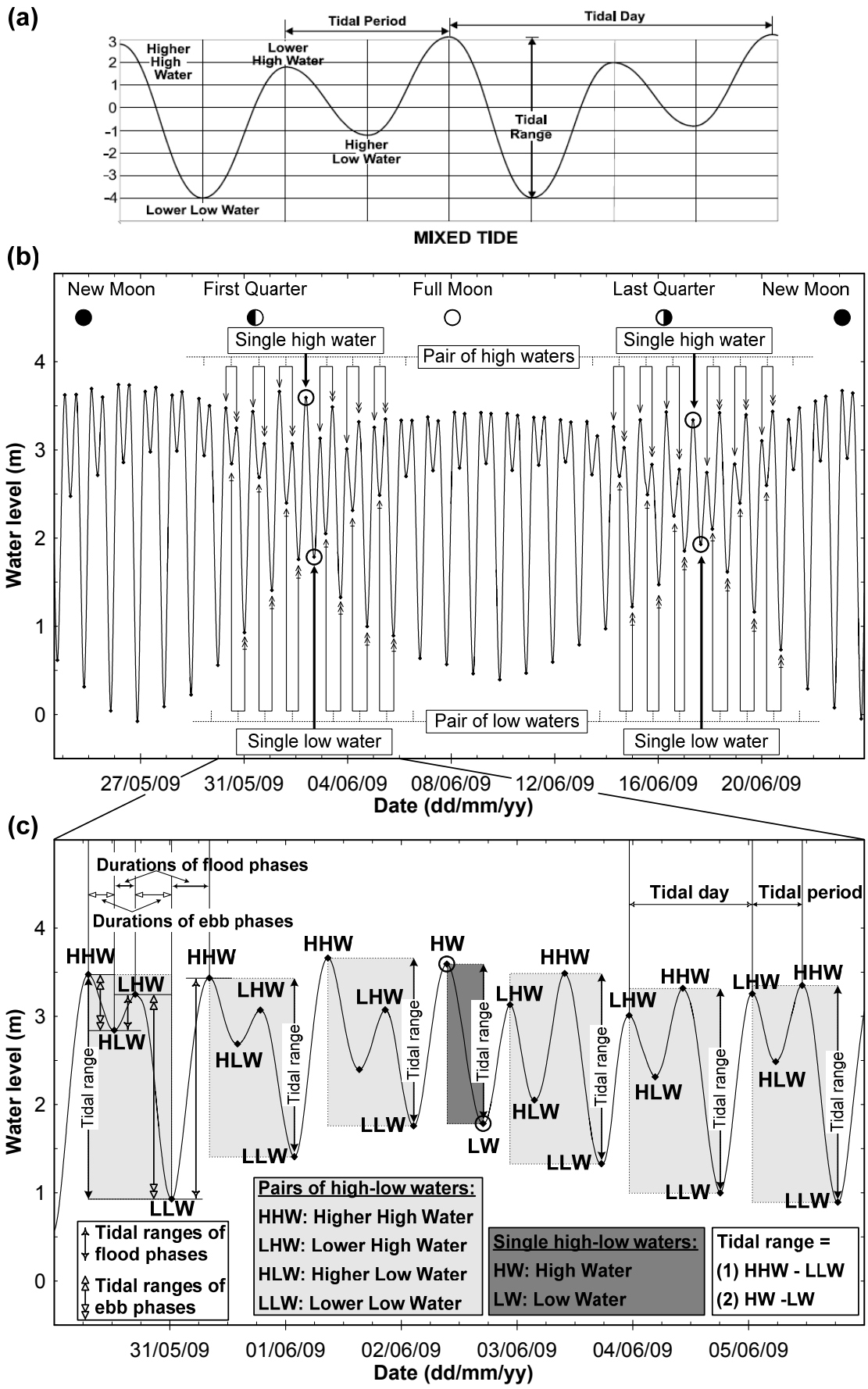

Figure 5.7. (a) Tidal range of mixed tide (NOAA, 2003); (b) Typical water level variations of a mixed tide (mainly semi-diurnal) at Vung Tau tide gauge station (VT-TG, for location see Figure 5.4) for the spring and neap tidal cycles; (c) Adapting definitions for the tide (NOAA, 2000, 2003) at the study site.

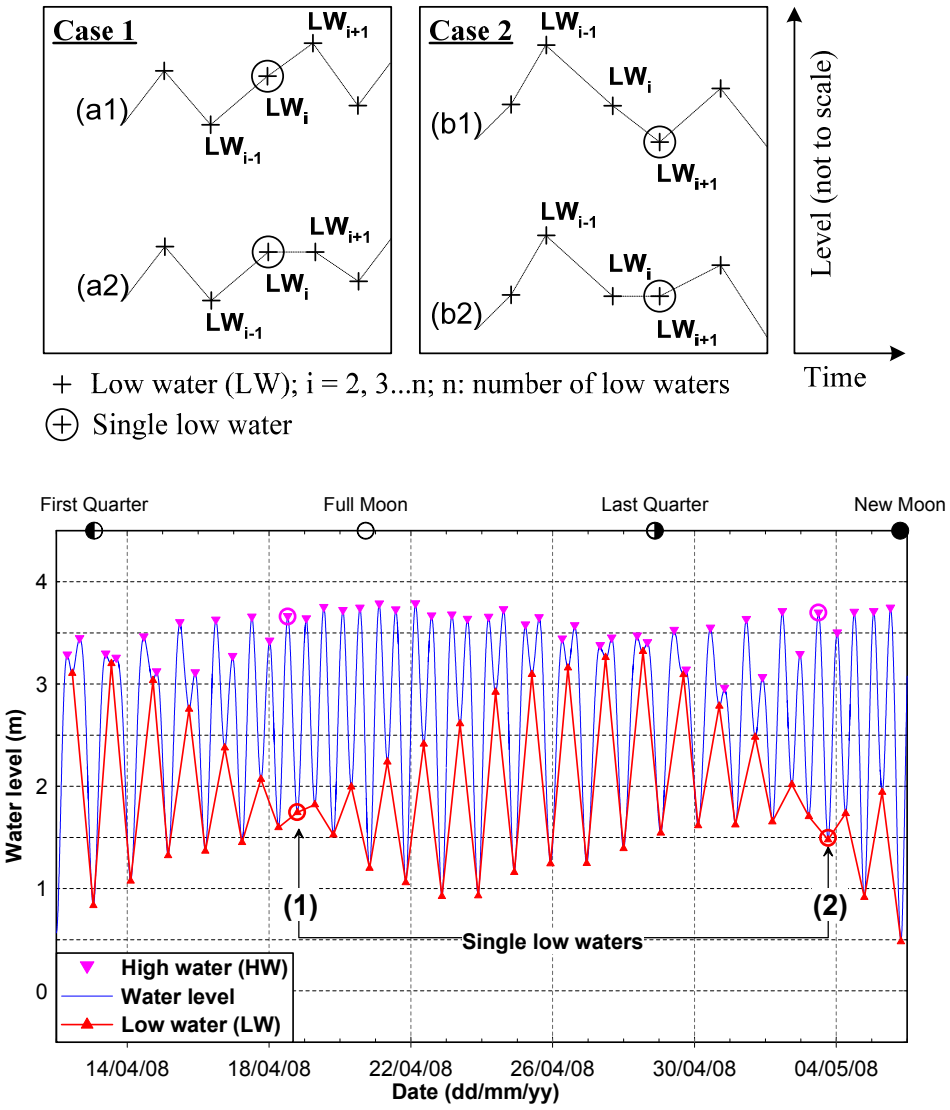

Figure 5.8. Sketch of detecting single low waters (see text) from the envelop of low water (upper fig.) and an example to find these single low waters from low water level dataset (lower fig.).

5.5.2. Post processing the CTD data and smoothing the water level

The own water level measurements are based on pressure recordings of autonomous CTD probes. Hence, to get precise levels, in a first step the data have to be corrected for air pressure fluctuations and density differences of the surrounding water.

The pressure gauges carry out only single point measurements in intervals of one or two minutes. As a consequence of this relatively rough sample rate the datasets are relatively noisy, because higher frequent signals e.g. from wind waves directly are included. For the quantitative frequency analysis of the tidal signal as well as for the computation of tidal characteristics like tidal range or tidal period the erratic high frequent signal components should be eliminated by smoothing procedures. For this purpose, a Butterworth band-pass filter was applied to the dataset. The script with the algorithm proposed by (Russel, 2004)

for n^{th}-order Butterworth band-pass filter was written in Fortran. The cutoff periods (or frequencies) were chosen from the list of 146 tidal constituents and their frequencies given by (Foreman, 2004). The shortest period is always 2.052 hours (the period of the ST35 tidal constituent). The longest period is based on the length of water level record. This period is not longer than the record length. For example, if the record length is 43 days, the longest period for band-pass filter is 31.81 days (or 763.487 hours, which is the period of the MM tidal constituent). Therefore, the components that have periods larger than 763.487 hours (or 31.81 days) and smaller than 2.052 hours will be removed from the water level datasets.

Filtering with 2^{nd} - 9^{th} order Butterworth band-passes was applied to every dataset. To assess the quality in terms of continuity and resolution of the smoothed time series the differences between the unsmoothed and smoothed data were calculated to find the appropriate order of filter. An example for such procedures is shown in Figure 5.9. The figure shows an 18 hours clipping from a 13 days water level recording in the Nga Bay river mouth (CG-WL, Figure 4.1b). Sampling interval was 1 min. In this case, the Butterworth filter passed only signals with periods ranging from 0.0855 to 1.2114 days. Best smoothing is achieved if mean and standard deviation of the differences between the smoothed and unsmoothed signals are lowest. In this case, this is true for the 4^{th} - 6^{th} order Butterworth filter (Figure 5.9b).

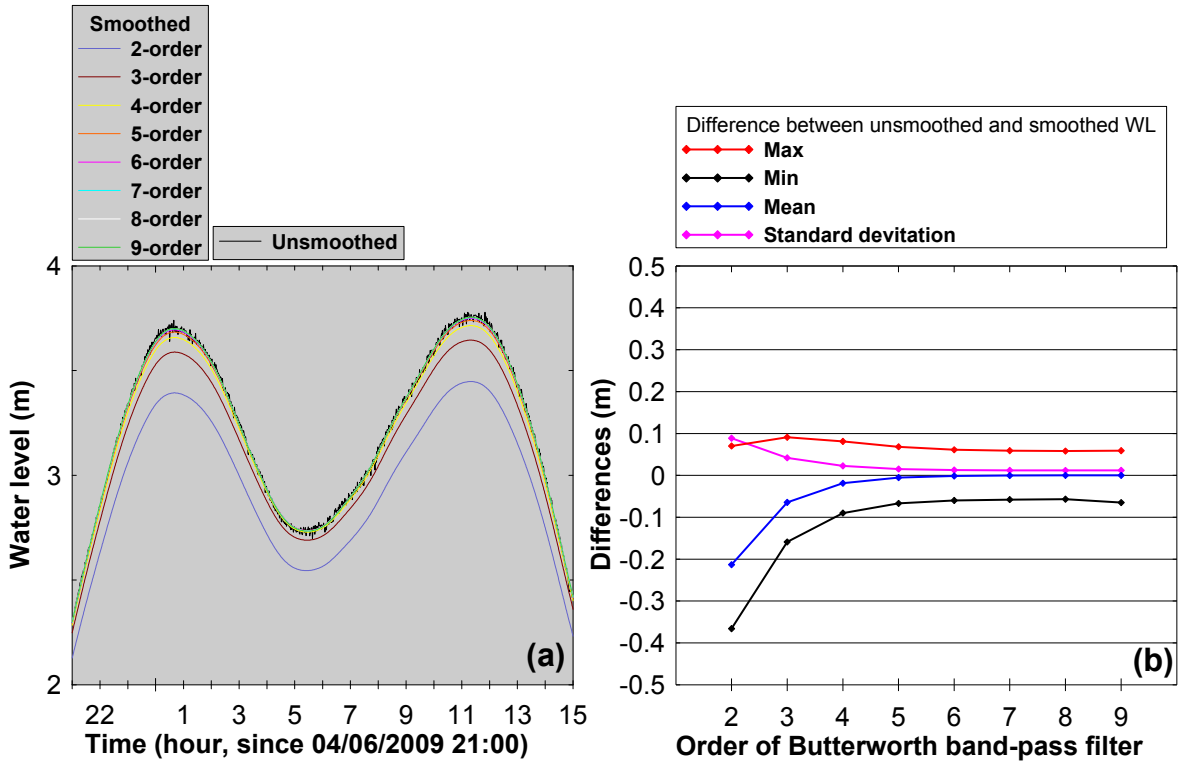

Figure 5.9. (a) Comparison of the raw water level signal (the black line with spikes) with the Butterworth 2^{nd}order to 9^{th}order band-pass filter smoothed water level time series. (b) Statistics of the difference between the unsmoothed and smoothed water levels using the Butterworth band-pass filters with nine different orders (for detailed explanation, see text).

5.5.3. Calculations of tidal inundation duration and total wave energy input

The duration of the cliff inundation and the wave energy impact to the cliff are an important factor for mangrove cliff retreat and have to be assessed. Therefore, duration of tidal inundation and total wave energy input were also calculated from the data obtained from water level and wave height.

It is assumed that the action of tide and wave does not affect the mangrove cliff retreat when the water level is below the cliff base level. Duration of tidal inundation and total wave energy input to the cliff were only calculated during the time of inundation of cliff base (Figure 5.10).

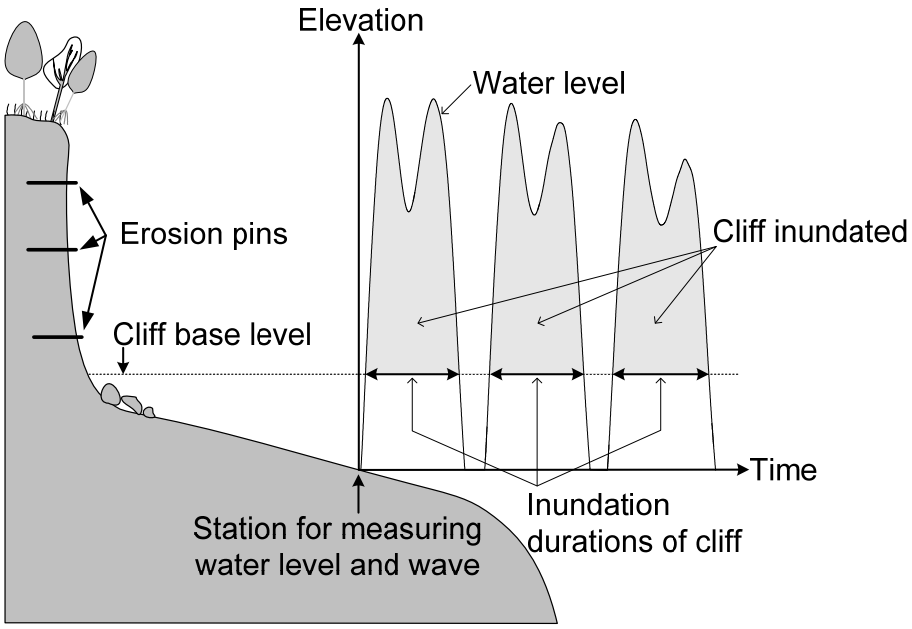

Figure 5.10. Sketch illustrating how to calculate duration of cliff inundation.

The duration of tidal inundations is that period when the water level is higher than the cliff base level.

The total wave energy input is calculated as the amount of wave energy (arithmetic sum) for that time when the base of the cliff inundated. The wave energy (E) is a function of significant wave height (Komar, 1976):

$$E = \frac{1}{16}\rho g H_s^2$$

Where, E is mean wave energy (J/m^2), ρ is water density (kg/m^3), g is gravitational acceleration (~ 9.8 m/s^2), and H_s is significant wave height.

5.5.4. Calibration of optical backscatter sensors

Optical backscatter sensors transmit an optical signal into the water column of which the wave length is near to infrared light (wave length 880 nm) (Seapoint Sensors Inc., 2000). The intensity of the backscattered light, in this case technically expressed as a change in output voltage, can be understood as the amount of the suspended matter concentration (SPMC) in the water. However, the sensor's response not only depends on the number of scatters but also on the composition and size of the suspended particles. That means that for precise turbidity measurements an "on site calibration" is needed, that takes account of the specific suspended matter composition. The aim of such a calibration is to mathematically formulate a close relationship between the sensor's mV responses to actual concentrations of a site specific particle composition, measured on discrete samples in mg/l. For this purpose, one day prior to a measurement campaign, all available sensors are installed very close to each other at a location (Figure 5.11), for which it is assumed that the characteristics are very much comparable to those of the actual sites. Calibration samples are taken every 30 minutes (60 minutes around the slack water phases) over one full diurnal tidal cycle. To separate solids from water the suspension samples are filtered using 0.63 µm filters. The solids are dried and the total dry mass of suspended matter per volume unit of sea water is calculated. In our case the relationship between the real world concentrations and the sensor's signal strength mostly results in a straight line linear best fit (Figure 5.11). The describing equations later allow converting all indirect measurement results into real concentration values.

Besides the calibration of each sensor, the labor intensive field calibration procedure is used to inter-calibrate all sensors and to detect shortcomings of single sensors.

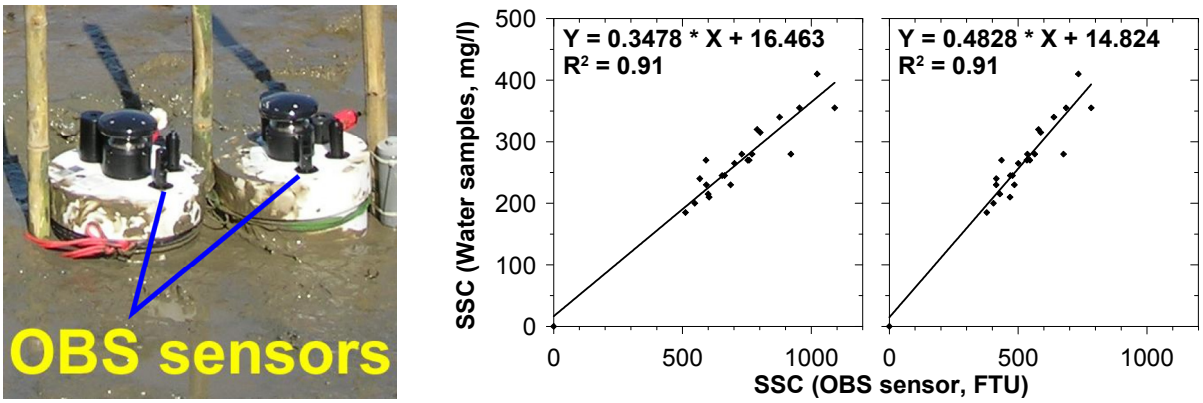

Figure 5.11. Deployment of two directional wave and current recorder devices, which also integrate optical backscatter sensors (OBS) for in-situ (inter-)calibration (left fig.); 'best fit curves' for two OBS sensors (right fig.).

5.5.5. Interpretation grain size distribution

Normally, the mangrove cliff soil is mainly characterized by bimodal grain size distributions with one mode in the range of fine silt or medium silt (4 - 16 μm) and the other mode representing very fine sand or fine sand (63-250 μm) (Figure 5.12a). However, some sediment samples have three dominant modes where the grain sizes of the third mode represent medium sand to very coarse sand. In fact, this mode dose not represent lithogenic parts of the mangrove cliff soil but represent organic materials of mangrove root fragments.

In some samples, the root fragments could not be removed completely, although the sediment samples were treated to dissolve all organic matter before carrying-out the grain size analysis (see Chapter 5.2.2). Those samples, where a lot of root fragment appear, derive mostly from the top parts of the cliff. Here the root systems of mangrove trees are dense. At the lower parts of the cliff, these third modes are not present. The grain size of the cliff soil does not inherit medium to coarse sand. Therefore, it was necessary to remove these soil components manually. After this procedure, the grain size distributions were recalculated. (see Figure 5.12b).

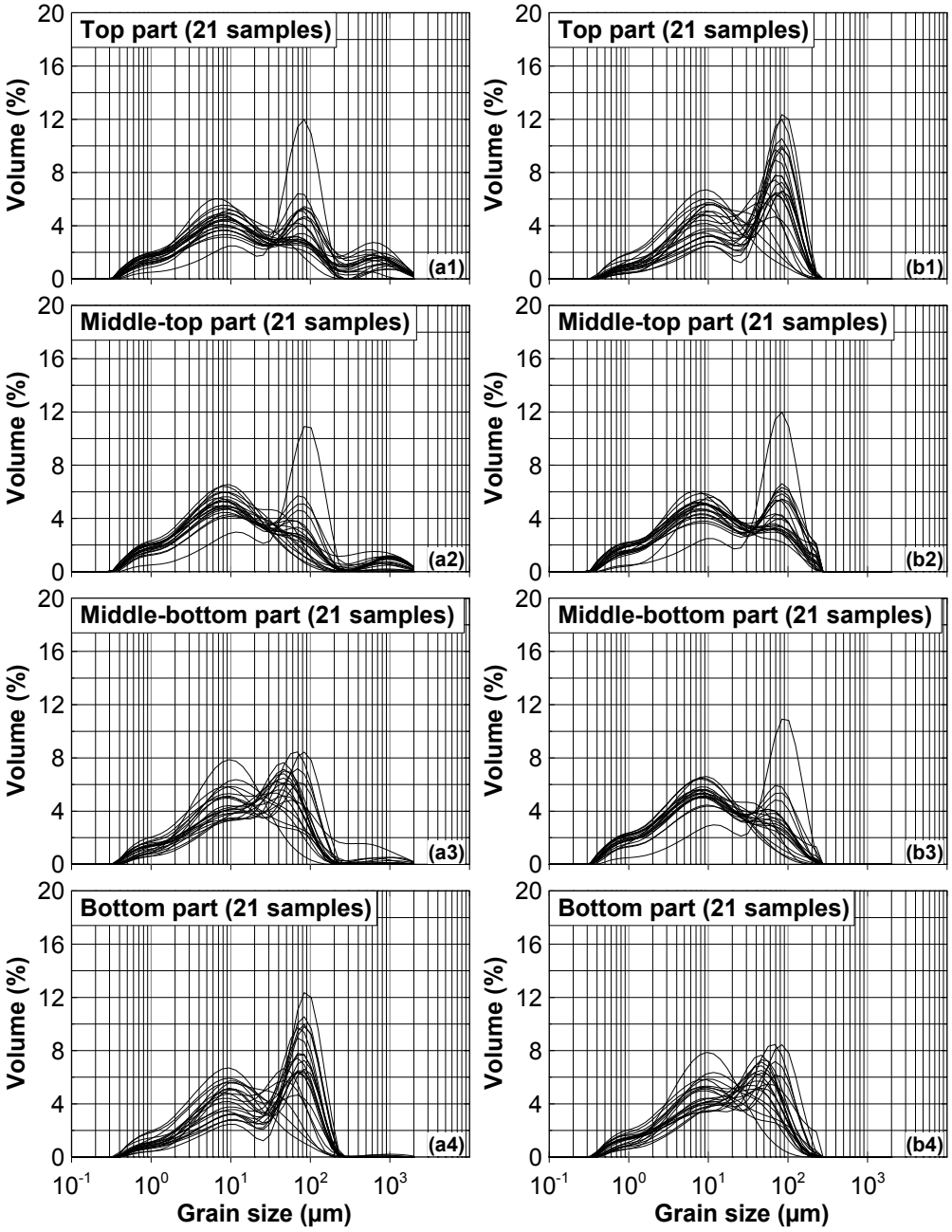

Figure 5.12. Grain size distributions of the soil of the mangrove cliff in Can Gio. Figures a1-4 (left column) show results of the original grain size analysis, which hold the third mode in the ranges from medium sand to very coarse sand. This third mode, in fact, belongs to mangrove root fragments, and therefore has been removed. Figures b1-4 show the grain size distributions after removing those parts, which are created due to the abundance of organic particle.

6. RESULTS

6.1. Tidal characteristics along the coast of the study area

6.1.1. Analysis of tides along the coast from Vung Tau to Ganh Hao

6.1.1.1. Tidal regime at seven coastal stations in Southern Vietnam

In general, the water level fluctuations along the coast from Vung Tau to Ganh Hao are similar (Figure 6.1). The results of the harmonic analysis (Table 6.1) from datasets of hourly water level from the year 2008 show that the tidal regimes at these locations are the same along this coast.

The F numbers (or tidal form numbers) along this coast range from 0.81 to 0.97 showing that the tide is mixed, mainly semi-diurnal according to the tidal classification by Courtier (1938) in (Defant, 1960, p.306-307). The amplitude of M_2 contributes dominantly to the tidal amplitude. The tidal phases (Greenwich lag phases) are mostly increasing from Vung Tau to Ganh Hao indicating that the tidal wave propagates southward (Table 6.1).

For a 19 years period, each station has 508 of 'single' high-low waters (turning points). On average, there are 26.74 turning points per year, which means that every 13.66 days such a point occurs with a standard deviation of app. 1 day.

The highest tidal range at spring tide usually occurs about 1-3 days after full moon or new moon. The lowest tidal range during neap tide occurs about 1-2 days after the first quarter or the last quarter. The tidal ranges of two consecutive spring tides from new moon to full moon or vice versa are usually unequal (Figure 6.1).

The diurnal inequalities of high water (DHQ) values vary from 9.3 cm at VT-TG station to 14.3 cm at GH-TG station. The mean DHQ for all seven stations (Table 6.2) along the Mekong Delta is 10.7 cm. The diurnal inequality of low water (DLQ) values are lowest (62 cm) at MT-TG station, highest (71.7 cm) at VT-TG station with a mean of 65.6 cm (see Table 6.2 for values of all 7 stations). On average, the DHQ is about 55 cm higher than DLQ.

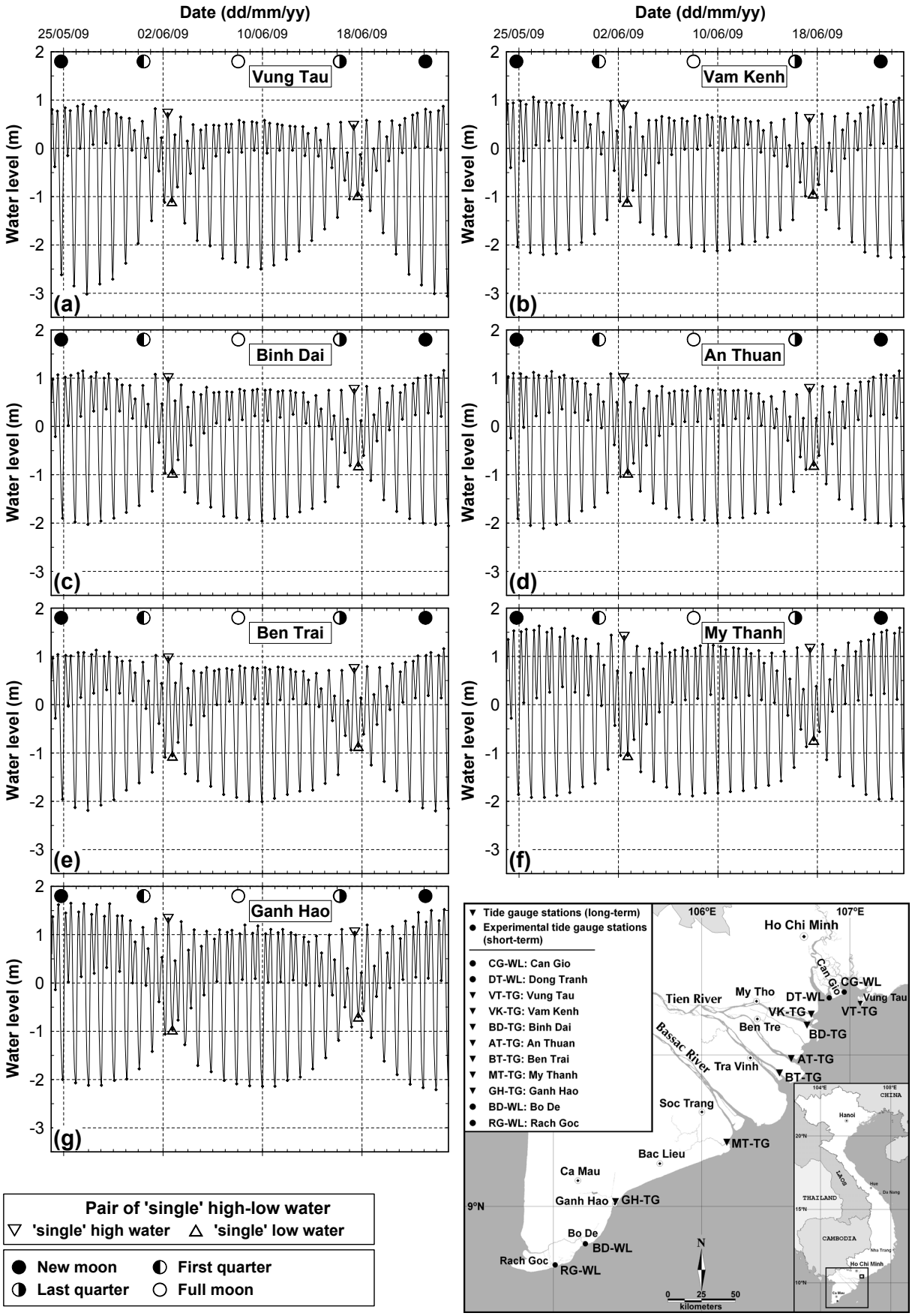

Figure 6.1. Time series plots of typical water level variations of mixed tide, mainly semi-diurnal at seven stations along the coast from Vung Tau to Ganh Hao for the spring and neap tidal cycles (a-g) and the locations of these stations. The zero levels are referenced to the Hon Dau datum.

Table 6.1. Tidal amplitudes and tidal phases of ten major tidal constituents at seven coastal stations.

	Station	Vung Tau	Vam Kenh	Binh Dai	An Thuan	Ben Trai	My Thanh	Ganh Hao
		Tidal phase (degree) or Greenwich lag phase						
Tidal constituents	M2	35.89	54.79	58.02	58.66	65.15	79.03	76.15
	K1	312.69	322.42	324.47	324.76	328.41	337.83	339.25
	O1	263.06	271.52	273.64	274.04	277.53	287.16	289.96
	S2	78.49	99.56	101.87	102.78	109.51	125.30	123.93
	SA	354.08	354.07	354.74	4.39	349.57	346.59	353.39
	P1	307.23	316.98	318.95	320.71	323.18	331.76	336.45
	N2	11.17	31.39	33.92	34.62	40.01	51.26	49.29
	Q1	241.03	250.46	253.00	253.90	256.70	266.73	271.05
	K2	89.80	102.54	104.59	105.21	113.61	124.86	124.96
	SSA	109.85	119.91	107.10	114.32	109.87	102.41	131.11
		Amplitude (m)						
Tidal constituents	M2	0.7636	0.7604	0.7340	0.7635	0.7887	0.8860	0.9153
	K1	0.5871	0.5542	0.5451	0.5649	0.5661	0.5788	0.6350
	O1	0.4456	0.4042	0.3965	0.4117	0.4108	0.4010	0.4297
	S2	0.3022	0.2935	0.2769	0.2857	0.2941	0.3280	0.3590
	SA	0.2227	0.2455	0.2499	0.2775	0.2592	0.2316	0.2505
	P1	0.1821	0.1664	0.1571	0.1648	0.1615	0.1634	0.1885
	N2	0.1554	0.1505	0.1439	0.1491	0.1565	0.1646	0.1715
	Q1	0.0925	0.0778	0.0767	0.0790	0.0782	0.0732	0.0833
	K2	0.0908	0.1032	0.0991	0.1054	0.1060	0.1233	0.1204
	SSA	0.0541	0.0507	0.0525	0.0500	0.0528	0.0616	0.0391
		Form number, F = Tidal amplitude (K_1+O_1) / (M_2+S_2)						
		0.97	0.91	0.93	0.93	0.90	0.81	0.84

Table 6.2. Tidal datums at seven coastal locations. These values were derived from the 19-year (1991-2009) hourly water level datasets. The zero level is referenced to the Hon Dau datum.

	Tidal datums (cm)							
Stations	**MHHW**	**MHW**	**MSL**	**MLW**	**MLLW**	**DHQ**	**DLQ**	**DLQ - DHQ**
Vung Tau	76.3	67.0	-22.1	-107.3	-179.0	9.3	71.7	62.4
Vam Kenh	91.7	81.8	-6.9	-93.3	-157.6	9.9	64.3	54.4
Binh Dai	97.3	87.9	2.0	-81.3	-145.0	9.4	63.7	54.3
An Thuan	101.2	91.5	2.6	-82.6	-146.9	9.7	64.3	54.6
Ben Trai	104.8	94.9	2.5	-86.9	-153	9.9	66.1	56.2
My Thanh	117.1	105.0	-0.8	-97.9	-159.9	12.1	62.0	49.9
Ganh Hao	124.9	110.6	5.5	-94.1	-161.4	14.3	67.3	53.0
					Mean	**10.7**	**65.6**	**55.0**

MHHW: mean higher high water; MLLW: mean lower low water; MHW: mean high water; MLW: mean low water; MSL: mean sea level; DHQ, DLQ: Diurnal inequality of HW, LW.

6.1.1.2. Tidal range variations

The distributions of the tidal ranges at these stations for the 19 years period mostly follow the Gaussian distribution (Figure 6.2a-g). The tidal ranges at all stations are distributed uniformly to both sides of the mean tidal ranges. The differences between the mean tidal ranges and median tidal ranges are almost the same with only 1 cm different.

The mean tidal ranges are decreasing from Vung Tau (VT-TG) to Binh Dai (BD-TG) and increasing from Binh Dai to Ganh Hao (GH-TG). The highest and lowest mean tidal ranges are 2.826 m at Ganh Hao and 2.393 m at Binh Dai. The average of the mean tidal range for the whole area from seven stations is 2.563m (Figure 6.2h, Table 6.3). The mean tidal range for only the area along the mouths of the Mekong Rivers (five stations from Vam Kenh to My Thanh) is 2.520 m. The mean tidal ranges during neap tide and spring tide (mean neap tide and mean spring tide) are also lowest at Binh Dai (2.064 m for mean neap tide and 2.771 m for mean spring tide) and highest at Ganh Hao (2.369 m and 3.260 m) (Table 6.3). The difference between mean neap tide and mean spring tide varies of about 0.651 m at Binh Dai and 0.929 m at Vung Tau. On average of these seven stations, the values of the mean neap tide and mean spring tide are 2.177 m and 2.934 m, respectively.

Similar to the variation trends of mean tidal range, the maximum tidal ranges are also decreasing from Vung Tau to Binh Dai and increasing from Binh Dai to Ganh Hao (Figure 6.2i, Table 6.3). The maximum values of tidal range from highest to lowest values are 4.08 m (at Vung Tau), 4.02 m (Ganh Hao), 3.87 (My Thanh), 3.77 m (Ben Trai), 3.65 m (Vam Kenh), 3.59 m (An Thuan), and 3.46 m (Binh Dai). The average values of the yearly maximum tidal range also show the same pattern but with the exception that at Ganh Hao with a value of 3.893 m the tidal range is higher than at Vung Tau with 3.857 m. On average at seven stations, the mean yearly maximum tidal range is about 3.585 m. When taking into account only the five stations at the mouths of the Mekong River branches (excluding the Vung Tau in the north and Ganh Hao in the south), the average of mean yearly maximum tidal range is 3.469 m.

The minimum tidal ranges vary between 1.07 m (at Vung Tau) and 1.28 m (My Thanh). The mean values of yearly minimum tidal range also show the same trend with the minimum tidal range (Figure 6.2j, Table 6.3) smallest at Vung Tau (1.234 m) and highest at My Thanh (1.483 m). On average at 5 stations at the mouths of the Mekong River branches (excluding Vung Tau and Ganh Hao), the mean yearly minimum tidal range is about 1.356 m. This value is not significantly different compared to the mean of all these seven stations (1.348 m).

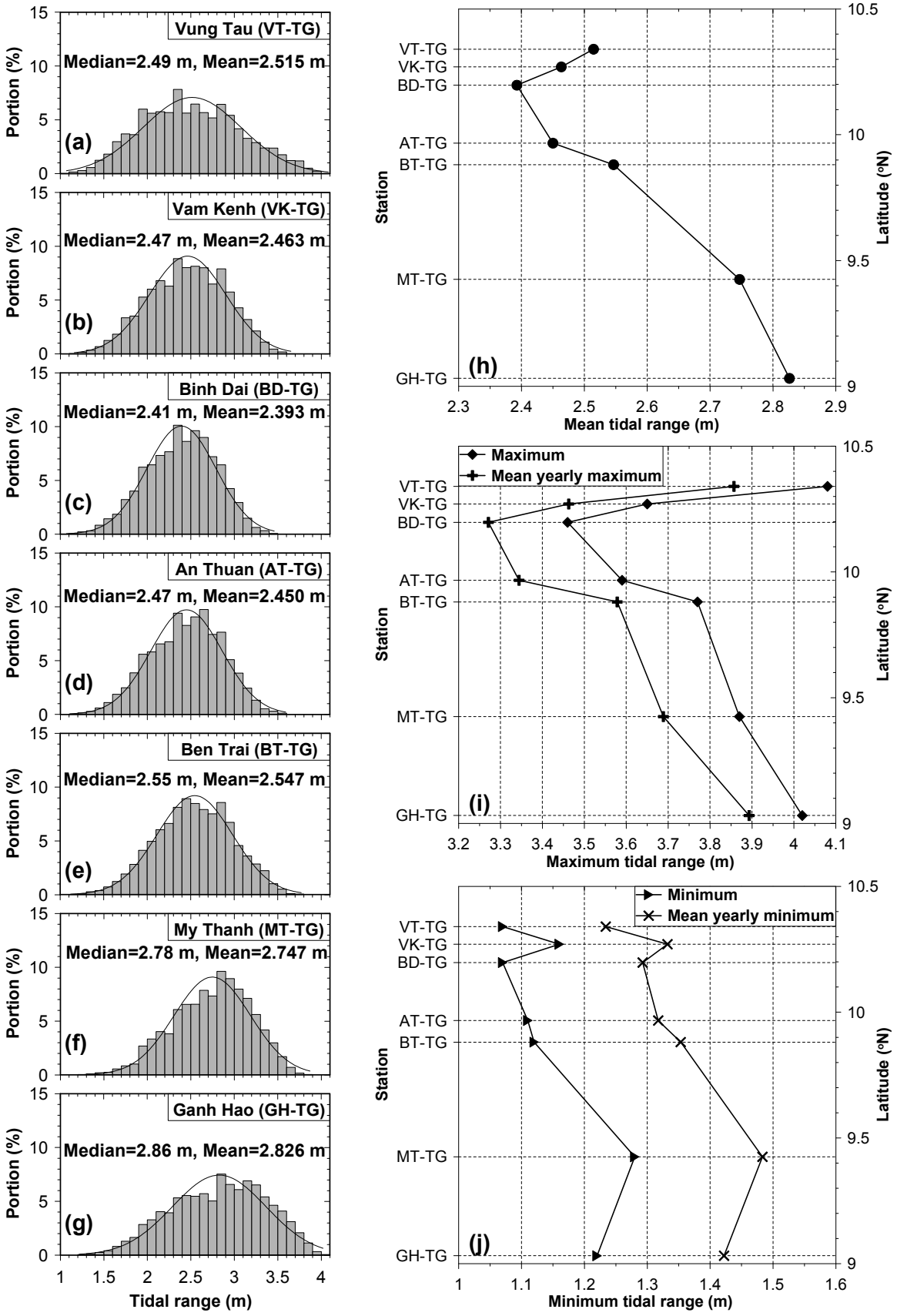

Figure 6.2. Tidal range variations along the coast from Vung Tau to Ganh Hao for the period 1991-2009. Distribution of tidal ranges with Gaussian fits (a-g). The mean (h), maxima (i), and minima tidal ranges (j). The maximum and minimum values are the absolutely highest and lowest tidal ranges during the 19-year period.

Table 6.3. The statistical values of tidal range (in meter) along the coast from Vung Tau to Ganh Hao. These values were derived from hourly water levels for the period 1991-2009.

Station	Min	Median	Max	Mean	SD
Vung Tau	1.070	2.490	4.080	2.515	0.564
Vam Kenh	1.160	2.470	3.650	2.463	0.440
Binh Dai	1.070	2.410	3.460	2.393	0.398
An Thuan	1.110	2.470	3.590	2.450	0.411
Ben Trai	1.120	2.550	3.770	2.547	0.434
My Thanh	1.280	2.780	3.870	2.747	0.439
Ganh Hao	1.220	2.860	4.020	2.826	0.537
Mean all stations	1.147	2.576	3.777	2.563	0.460
Station	**MY Min**	**MY Max**	**Mean neap**	**Mean spring**	**Difference**
Vung Tau	1.234	3.857	2.064	2.993	0.929
Vam Kenh	1.332	3.463	2.096	2.820	0.723
Binh Dai	1.293	3.271	2.060	2.711	0.651
An Thuan	1.317	3.344	2.094	2.769	0.675
Ben Trai	1.353	3.578	2.190	2.897	0.707
My Thanh	1.483	3.688	2.365	3.085	0.720
Ganh Hao	1.422	3.893	2.369	3.260	0.892
Mean all stations	1.348	3.585	2.177	2.934	0.757

Min: minimum (Min); Max: maximum; SD: standard deviation; MY Min: mean yearly minimum, MY Max: mean yearly maximum; Mean neap and Mean spring: the mean tidal ranges of neap and spring periods.

The number of tidal ranges used for all calculation is n = 6957.

MY Min and MY Max values are the arithmetic means of yearly lowest and highest value of tidal ranges during the 19-year period.

Mean neap and Mean spring are the arithmetic means of the tidal ranges, which are lower and higher than the mean tidal range.

6.1.1.3. Seasonal water level fluctuations

The monthly values of mean higher high water (MHHW), mean high water (MHW), mean sea level (MSL), mean low water (MLW), mean lower low water (MLLW), and mean tidal range (MTR) from hourly water levels at seven stations for the period 1991-2009 show the strongly annual variations of the water levels (Figure 6.3, Table 6.4). The water levels during the wet season (in summer) are lower than during dry season (in winter). The MHHW, MHW, MSL, MLLW are lowest in June/July whereas they are highest only in November. In contrast to the water levels, the mean tidal ranges usually reach the highest values during the wet season (or SW monsoon) and lowest values during the dry season (NE monsoon).

On average of seven stations, the differences between highest and lowest of MHHW and MLLW are about 45 cm and 53 cm, respectively. The semi-annual values of MHHW at the

stations in the Mekong river mouths (at Vam Kenh, Binh Dai, An Thuan, My Thanh) are higher than at the two stations (Vung Tau and Ganh Hao). The semi-annual variations of MHHW are highest at Ben Trai (51 cm) and lowest at Vung Tau (38 cm).These differences of MLLW at Vung Tau and Ganh Hao are mostly higher compared to those at the other stations excluded at Ben Trai.

Although the mean tidal range variations show variability during the year, the differences between highest and lowest mean tidal ranges are not significantly higher compared to those of MHHW or MLLW. The arithmetic average of the differences between highest and lowest tidal ranges for all stations is about 0.23 m.

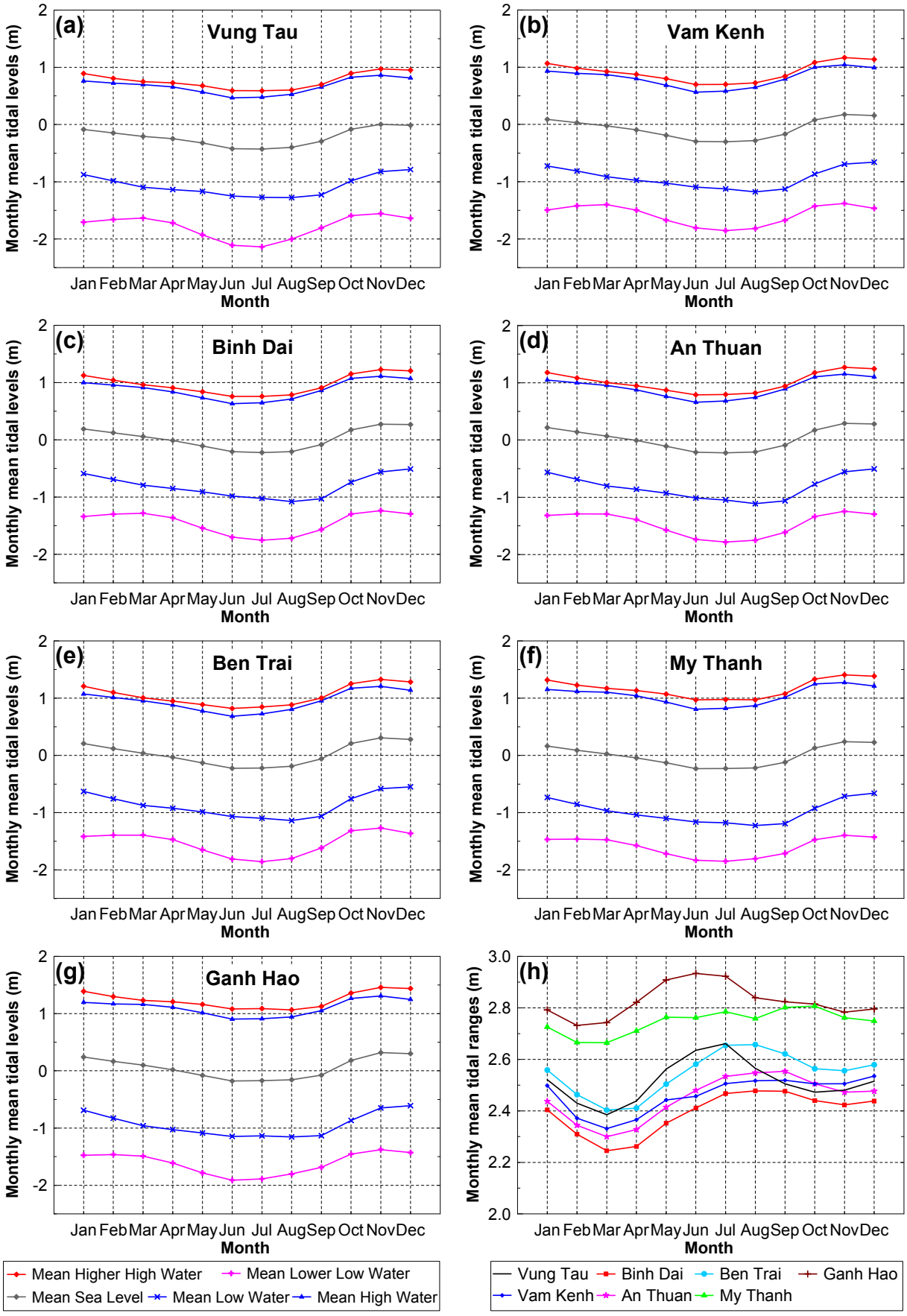

Figure 6.3. Semi-annual variations of the tidal levels (a-g) and the tidal ranges (h) along the coast from Vung Tau to Ganh Hao for the period 1991-2009. The zero levels (excepted for the tidal range) are referenced to the Hon Dau datum.

Table 6.4. Monthly mean values (in meter) of the tidal levels and tidal ranges along the coast from Vung Tau to Ganh Hao for the period 1991-2009.

Station	Vung Tau						Vam Kenh					
Month	**MHHW**	**MHW**	**MSL**	**MLW**	**MLLW**	**MTR**	**MHHW**	**MHW**	**MSL**	**MLW**	**MLLW**	**MTR**
Jan	0.891	0.761	-0.086	-0.874	-1.705	2.521	1.068	0.933	0.089	-0.726	-1.495	2.498
Feb	0.808	0.724	-0.148	-0.984	-1.661	2.430	0.982	0.894	0.030	-0.813	-1.421	2.372
Mar	0.749	0.697	-0.207	-1.095	-1.635	2.385	0.925	0.872	-0.025	-0.914	-1.402	2.331
Apr	0.728	0.657	-0.248	-1.136	-1.719	2.438	0.875	0.801	-0.094	-0.974	-1.497	2.366
May	0.678	0.568	-0.321	-1.170	-1.928	2.562	0.801	0.686	-0.189	-1.024	-1.672	2.442
Jun	0.593	0.467	-0.423	-1.250	-2.109	2.635	0.698	0.566	-0.297	-1.094	-1.807	2.457
Jul	0.590	0.478	-0.428	-1.271	-2.137	2.661	0.700	0.583	-0.302	-1.125	-1.854	2.506
Aug	0.603	0.528	-0.399	-1.276	-2.001	2.565	0.727	0.648	-0.281	-1.177	-1.818	2.517
Sep	0.699	0.655	-0.294	-1.228	-1.805	2.505	0.843	0.792	-0.168	-1.127	-1.675	2.519
Oct	0.896	0.826	-0.082	-0.985	-1.591	2.473	1.084	1.000	0.078	-0.865	-1.427	2.505
Nov	0.972	0.861	0.003	-0.822	-1.556	2.481	1.169	1.043	0.175	-0.693	-1.381	2.505
Dec	0.952	0.814	-0.013	-0.787	-1.637	2.515	1.137	0.992	0.157	-0.658	-1.464	2.535
Max – Min	0.382	0.394	0.431	0.489	0.581	0.276	0.471	0.477	0.477	0.519	0.473	0.204
Month			**Binh Dai**						**An Thuan**			
Jan	1.124	0.999	0.190	-0.588	-1.340	2.404	1.179	1.048	0.218	-0.564	-1.316	2.435
Feb	1.041	0.958	0.124	-0.691	-1.299	2.310	1.084	1.000	0.140	-0.687	-1.291	2.344
Mar	0.963	0.913	0.057	-0.793	-1.283	2.245	1.010	0.954	0.068	-0.803	-1.293	2.302
Apr	0.909	0.838	-0.012	-0.849	-1.363	2.262	0.948	0.876	-0.007	-0.860	-1.389	2.329
May	0.840	0.733	-0.107	-0.909	-1.543	2.352	0.872	0.761	-0.109	-0.928	-1.576	2.415
Jun	0.758	0.632	-0.207	-0.983	-1.701	2.411	0.790	0.661	-0.215	-1.014	-1.738	2.479
Jul	0.758	0.648	-0.223	-1.023	-1.755	2.467	0.796	0.682	-0.224	-1.049	-1.784	2.536
Aug	0.786	0.712	-0.207	-1.080	-1.720	2.478	0.825	0.745	-0.210	-1.113	-1.751	2.549
Sep	0.909	0.864	-0.083	-1.030	-1.569	2.476	0.947	0.892	-0.092	-1.063	-1.612	2.560
Oct	1.151	1.074	0.174	-0.741	-1.298	2.440	1.179	1.103	0.174	-0.771	-1.338	2.510
Nov	1.227	1.111	0.272	-0.560	-1.237	2.423	1.269	1.152	0.291	-0.556	-1.247	2.474
Dec	1.206	1.070	0.266	-0.509	-1.295	2.438	1.244	1.103	0.280	-0.504	-1.298	2.476
Max – Min	0.469	0.479	0.495	0.571	0.518	0.233	0.479	0.491	0.515	0.609	0.537	0.258
Month			**Ben Trai**						**My Thanh**			
Jan	1.209	1.073	0.207	-0.630	-1.415	2.559	1.318	1.153	0.163	-0.734	-1.468	2.726
Feb	1.101	1.013	0.119	-0.757	-1.394	2.463	1.228	1.116	0.089	-0.853	-1.462	2.666
Mar	1.005	0.955	0.037	-0.874	-1.393	2.403	1.172	1.104	0.026	-0.966	-1.474	2.665
Apr	0.950	0.880	-0.034	-0.922	-1.470	2.411	1.134	1.042	-0.042	-1.040	-1.575	2.711
May	0.888	0.776	-0.130	-0.987	-1.649	2.504	1.072	0.932	-0.130	-1.100	-1.719	2.764
Jun	0.820	0.684	-0.225	-1.068	-1.811	2.581	0.971	0.808	-0.230	-1.164	-1.832	2.762
Jul	0.847	0.726	-0.221	-1.097	-1.856	2.654	0.977	0.822	-0.228	-1.177	-1.850	2.785
Aug	0.885	0.804	-0.189	-1.138	-1.801	2.657	0.971	0.868	-0.220	-1.225	-1.805	2.758
Sep	1.004	0.955	-0.059	-1.065	-1.618	2.621	1.078	1.016	-0.120	-1.191	-1.712	2.802
Oct	1.254	1.174	0.208	-0.757	-1.316	2.564	1.334	1.249	0.129	-0.923	-1.473	2.807
Nov	1.328	1.208	0.307	-0.581	-1.269	2.556	1.408	1.274	0.239	-0.713	-1.396	2.762
Dec	1.284	1.138	0.281	-0.549	-1.363	2.579	1.385	1.213	0.228	-0.661	-1.426	2.749
Max – Min	0.508	0.524	0.532	0.589	0.587	0.254	0.437	0.466	0.469	0.564	0.454	0.142
Month			**Ganh Hao**									
Jan	1.39	1.197	0.241	-0.689	-1.471	2.789						
Feb	1.30	1.169	0.166	-0.828	-1.457	2.723						
Mar	1.25	1.161	0.099	-0.960	-1.487	2.753						
Apr	1.22	1.110	0.019	-1.028	-1.611	2.837						
May	1.17	1.013	-0.079	-1.088	-1.787	2.918						
Jun	1.08	0.904	-0.179	-1.147	-1.916	2.939						
Jul	1.09	0.909	-0.172	-1.135	-1.888	2.922						
Aug	1.07	0.942	-0.157	-1.156	-1.797	2.837						
Sep	1.15	1.051	-0.076	-1.133	-1.684	2.843						
Oct	1.38	1.265	0.182	-0.866	-1.459	2.835						
Nov	1.46	1.309	0.317	-0.649	-1.384	2.795						
Dec	1.44	1.246	0.300	-0.610	-1.431	2.799						
Max – Min	0.393	0.405	0.496	0.546	0.532	0.216						

MHHW: mean higher high water; MLLW: mean lower low water;

MHW: mean high water;

MLW: mean low water;

MSL: mean sea level;

MTR: mean tidal range.

6.1.1.4. Annual sea level variations

Yearly mean sea level (MSL) variations at seven coastal stations from Vung Tau to Ganh Hao for the period 1991-2009 are shown in Figure 6.4.

The yearly MSL fluctuations at Vung Tau show the falling and rising phases, which last for about 3-4 years. Peaks of highest or lowest MSL cycle are repeated after about 7-8 years. The rhythms of yearly MSL variations at the other stations are looking similar to each other but are different compared to Vung Tau. They are showing a high-low yearly MSL cycle of about 2-4 years. At Vung Tau, the range between high and low yearly MSL is about 11-13 cm. However, at the other stations such ranges are not clearly estimated due to the rising trends of MSL.

The changing tendency of mean sea level at Vung Tau is not significant (Figure 6.4a). Whereas at the six stations along east coast of the Mekong Delta, the mean sea levels tend to rise, especially at My Thanh (Figure 6.4b-f1). The rates of relative mean sea level rises are from about 6.0 mm/year (at Ben Trai) up to 19.7 mm/year (My Thanh). However, at My Thanh, there are two annual mean sea levels in 2008 and 2009, which look like suddenly jump (Figure 6.4f1). The reason for this jump might be a wrong correction in the adjustment the datum. Excluding the data of these two years, the rate of relative sea level rise at My Thanh is 13.1 mm/year (Figure 6.4f2). On average of six coastal stations along the Mekong Delta, the mean sea level rise is bout 9.6 mm/year.

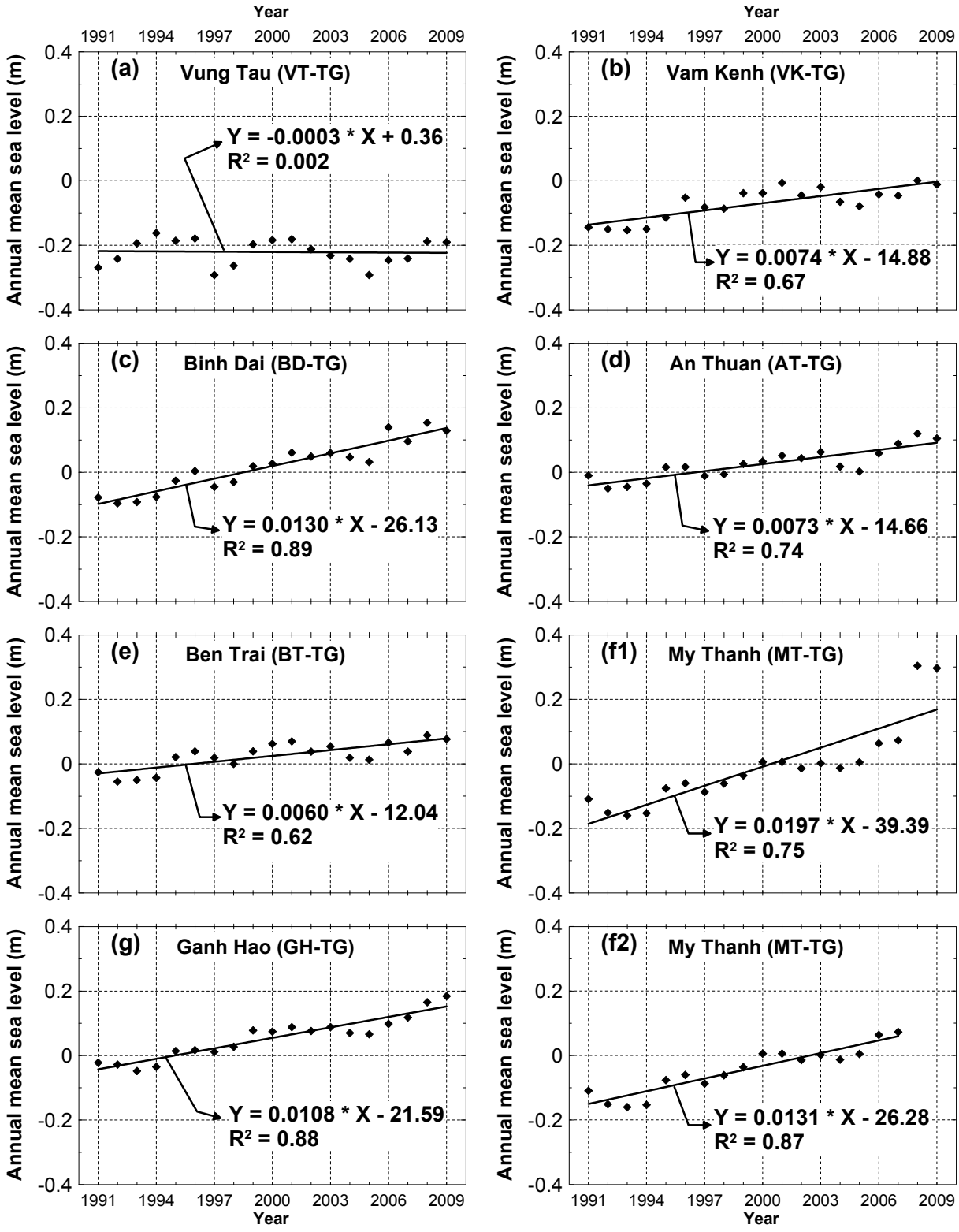

Figure 6.4. Annual mean sea level variations and trends of relative sea level rise along the coast from Vung Tau to Ganh Hao for the period 1991-2009.

6.1.2. Comparison of water levels at the study sites with Vung Tau

In this section, the correlation of the tide at the referenced station in Vung Tau with the other locations at the river mouths in Can Gio (Can Gio (CG-WL) and Dong Tranh (DT-WL)

stations), one in Bo De (BD-WL), and one more station in Rach Goc (RG-WL) (Figure 5.4, Table 5.1, see also Chapter 5 Methods) is shown. Together with the previous section, the tide is studied along the coast Vung Tau toward to the Ca Mau tip.

6.1.2.1. Dong Tranh (DT-WL) vs. Vung Tau (VT-TG)

The tide at the Dong Tranh river mouth (DT-WL, in Can Gio) is almost the same that at Vung Tau (Figure 6.5a, Table 6.5 - the Dataset 3). The mean ebb duration at the Dong Tranh river mouth (DT-WL) is about 13 minutes longer than at Vung Tau (VT-TG) while the mean flood duration at DT-WL is about 13 minutes shorter than at VT-TG. The tidal ranges at DT-WL are higher than at VT-TG. The mean tidal range at DT-WL is about 16 cm higher than at VT-TG. There is no difference in the ranges of tide at both stations. On average, the tidal range of the ebb phase is the same as the tidal range of flood phases. At the Dong Tranh river mouth the flood duration is 41 minutes shorter than the ebb duration.

6.1.2.2. Can Gio (CG-WL) vs. Vung Tau (VT-TG)

In general, the tides at Vung Tau and Can Gio (the Nga Bay river mouth) are similar (Figure 6.5b, Table 6.5 - Dataset 2). The tidal days and periods at both sites are almost the same. On average, the durations of ebb and flood at CG-WL are shorter than at VT-TG. The mean tidal range at Can Gio (CG-WL) is about 23 cm higher than at Vung Tau (VT-TG). The tidal ranges of ebb and flood at CG-TG are also higher than at VT-TG. At both sites, the mean tidal range of ebb is higher than the mean tidal range the flood.

6.1.2.3. Bo De (BD-WL) vs. Vung Tau (VT-TG)

The water level fluctuations at Bo De and Vung Tau are mostly the same (Figure 6.5c, Table 6.5 - Dataset 1). On average, the tidal period and tidal day at Bo De (BD-WL) are not significantly different from those values at Vung Tau (VT-TG). The mean duration of ebb phase at BD-WL is 10 minutes longer than at VT-TG, whereas the mean flood duration is about 10 minutes shorter. Although the mean tidal ranges of ebb and flood phases at BD-WL are higher than at VT-TG, the maximum tidal range of the flood phase at BD-WL is about 16 cm smaller than at VT-TG. The maximum tidal range at BD-WL is about 5 cm less than at VT-TG. At both site, flood duration is shorter than ebb duration, especially at BD-WL.

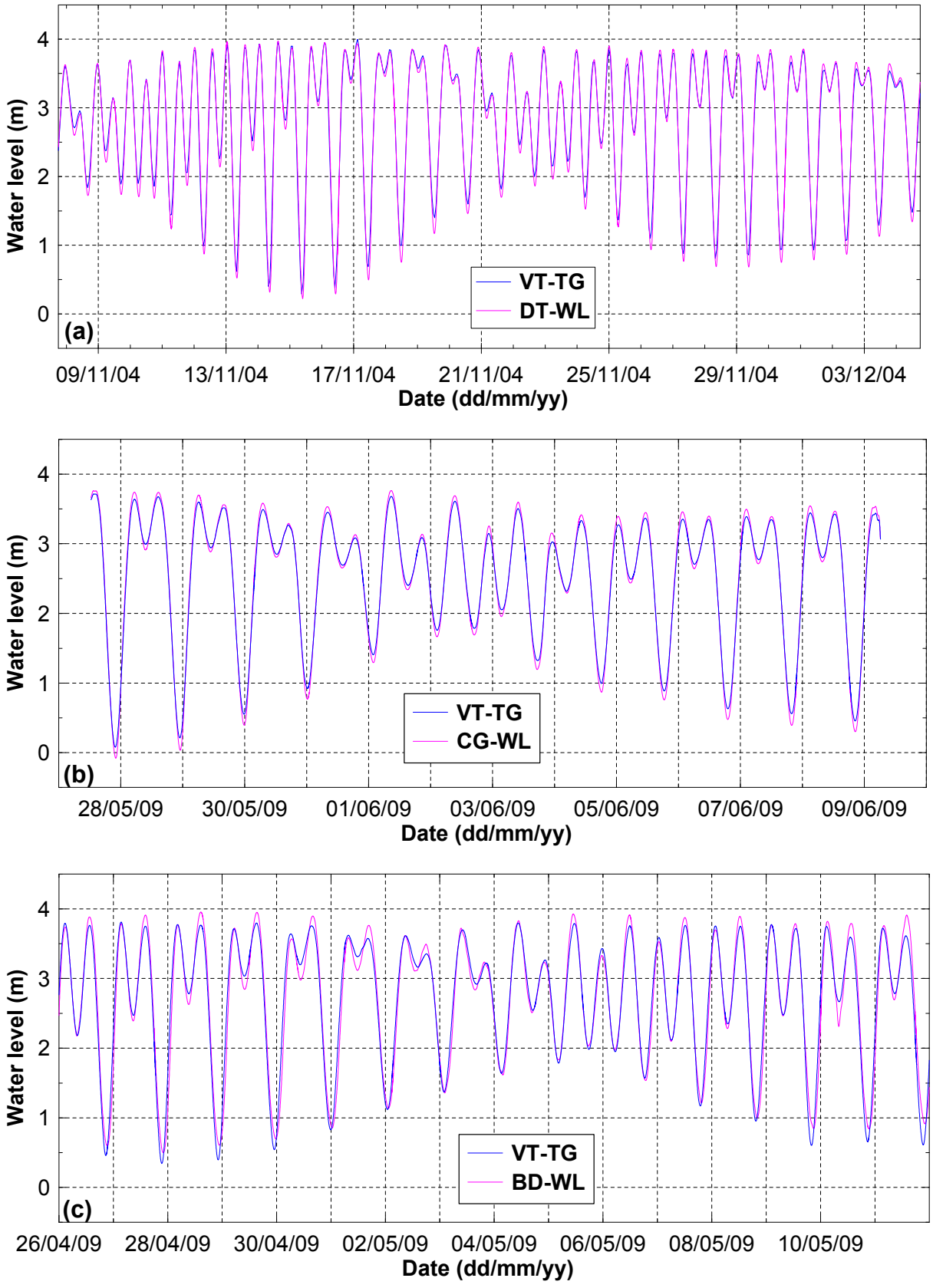

Figure 6.5. Time series plots of water level at Vung Tau (VT-TG) and at the study sites in the Can Gio area (Dong Tranh (DT-WL), Can Gio (CG-WL) stations), and Bo De (BD-WL). For comparison, the times of water levels at the study site stations were shifted backward 19, 3, and 86 min, respectively (Table 6.6). The zero levels at the studying stations are referenced to the zero level at VT-TG.

Table 6.5. Comparisons of tidal characteristics between Vung Tau, Bo De and Can Gio tide gauge stations (VT-TG, DT-WL, CG-WL, BD-WL).

Dataset		1		2		3	
Dataset period	from	25/04 /2009		27/05/2009		07/11/2004	
	to	12/05/2009		09/06/2009		04/12/2004	
Parameter	Statistics	Station		Station		Station	
		VT-TG	BD-WL	VT-TG	CG-WL	VT-TG	DT-WL
Tidal period (hour)	Max	16.62	16.05	15.68	15.58	17.25	16.70
	Min	8.63	9.02	9.17	9.30	7.50	8.17
	Mean	12.37	12.37	12.33	12.33	12.24	12.26
Tidal day (hour)	Max	25.40	25.35	25.55	25.68	25.75	25.40
	Min	24.30	24.65	24.60	24.33	24.25	23.90
	Mean	24.90	24.95	24.89	24.87	24.83	24.83
Duration of ebb phase (hour)	Max	8.62	8.67	8.38	8.43	9.00	8.90
	Min	4.00	3.88	4.37	4.32	3.75	4.40
	Mean	6.31	6.44	6.36	6.30	6.29	6.51
Duration of flood phase (hour)	Max	8.17	7.38	7.82	7.75	9.00	8.20
	Min	3.78	4.13	4.42	4.73	3.00	3.00
	Mean	6.10	5.98	6.03	6.11	6.04	5.82
Tidal range of ebb phase (m)	Max	3.408	3.414	3.463	3.703	3.63	3.66
	Min	0.308	0.467	0.619	0.776	0.25	0.33
	Mean	1.864	1.925	1.678	1.857	1.71	1.83
Tidal range of flood phase (m)	Max	3.431	3.276	3.387	3.664	3.62	3.67
	Min	0.192	0.384	0.392	0.479	0.11	0.11
	Mean	1.820	1.895	1.563	1.739	1.71	1.82
Tidal range (m)	Max	3.467	3.414	3.463	3.705	3.69	3.75
	Min	1.807	1.896	1.826	2.001	1.72	1.91
	Mean	2.747	2.755	2.535	2.762	2.64	2.80

[1] Souce datasets at Vung Tau (VT-TG): 'Intergovernmental Oceanographic Commission, IOC' webpage: http://www.ioc-sealevelmonitoring.org/station.php?code=vung

6.1.2.4. Comparison of water level fluctuations at Bo De and Rach Goc

Although, at Rach Goc, the lower low waters during spring tide were not measured because the instrument was installed at a height higher above those levels, the tidal range at Bo De is higher than that at Rach Goc (Figure 6.6). From 28 full ranges of tide (in both ebb and flood phases) the tidal range, on average, at Bo De is about 38 cm higher than that at Rach Goc. The differences in range of tide between the two stations are usually higher at the times of lower low water. The maximum and minimum of these differences are about +65 cm and +6 cm, respectively. The mean time lag of high water from Bo De to Rach Goc is about +14 min (standard deviation of 14).

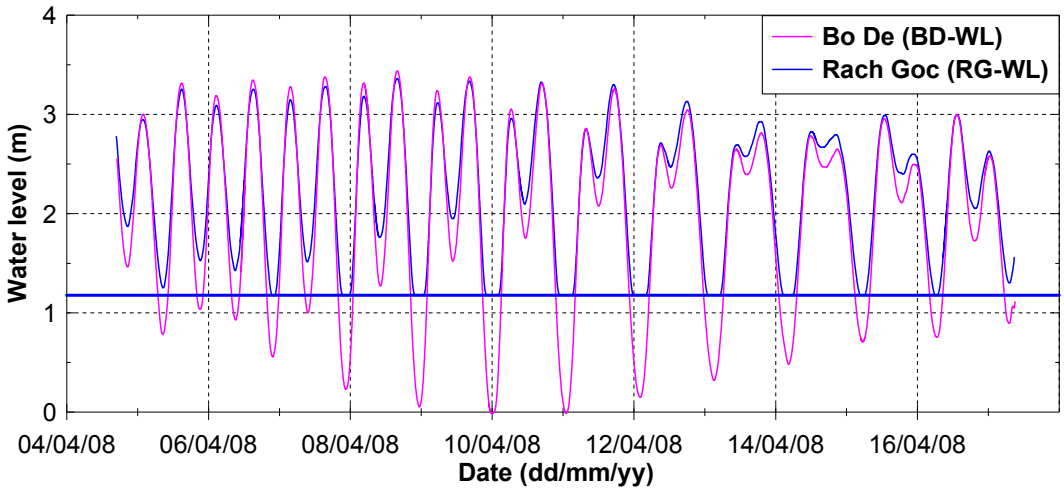

Figure 6.6. Time series plot of water levels at Bo De (BD-WL) and Rach Goc (RG-WL) for about 13 days in April 2008. For comparison, the dataset at Rach Goc, the times of water levels were shifted backward 14 min and the water levels were moved-up 1.18 m (the level of these bold blue line indicates the water level fall below the height of the instrument).

In summary, the type of tidal regimes along the coast from Vung Tau Cape Ca Mau is a mixed tide, dominantly semi-diurnal (Figure 6.5, Figure 6.6). An asymmetry in the duration between ebb and flood phases was found at all stations in Can Gio, Vung Tau, Bo De, and Rach Goc. The duration of the ebb is always shorter than the duration of flood (Table 6.5). From Vung Tau, the tidal wave propagates to upstream of the two rivers in Can Gio and to southerly toward to the tip of Ca Mau.

Table 6.6. Comparison of the time lag of high water (HW) between Vung Tau (VT-TG) and the study sites in Can Gio (DT-WL, and CG-WL), Bo De (BD-WL), and Rach Goc (RG-TG)..

Station	DT-WL	CG-WL	BD-WL	RG-WL*
Number of HW	46	25	33	24
Mean time lag (min)	+19	+3	+86	+100
Standard deviation, SD	12	6	19	NA

* This is the result of the comparison between the stations RG-WL and BD-WL and the comparison between the stations BD-WL and VT-TG.

6.1.3. Latitudinal changes of the tidal ranges along the studied coast

It's difficult to estimate the long-term maximum tidal ranges at the study sites in Can Gio, Bo De, and Rach Goc because the experimental water level datasets were short and carried-out in summer during low inundation periods. The estimation of mean tidal ranges for long-term, however, were done by the comparison of water level datasets at the study sites with the reference site at Vung Tau as mentioned in Chapter 6.1.2. Then these results are combined with the mean tidal range variations of the seven long-term stations (see Section 6.11.4, Figure 6.2h, Table 6.4) to show trend of variation of the tidal ranges along coast from Vung Tau to Rach Goc.

Along the coast from Vung Tau to Rach Goc including (included two sites: the Dong Tranh and Can Gio), the mean tidal range variations also tend to follow latitudinal changes. From Binh Dai (BD-TG), the tidal ranges are increasing in both directions: to the north until Can Gio (CG-WL) and to the south until Ganh Hao (GH-TG). From Ganh Hao to Rach Goc (RG-WL), the tidal ranges tend to decrease (Figure 6.7).

From the northern sites down to Binh Dai and from Ganh Hao down to the south of Binh Dai locations, the tidal ranges decrease following latitudinal decrease with almost the same rate. The gradient of the decrease is almost the same. The gradient of the linear trends of these decrements are about 0.59 (Figure 6.7). By contrast, from Binh Dai to Ganh Hao, the tidal ranges increase from north to south. The rate of increasing tidal ranges is smaller than the decreasing rate of north of Binh Dai and south of Ganh Hao (Figure 6.7). This increment of increasing the tidal range is about four times smaller than the decrement.

Along this coast, the greatest mean tidal range is at Ganh Hao. In the north of Ganh Hao, the lowest mean tidal range is at Binh Dai. Although in the south of Ganh Hao the mean tidal range might be lowest at location further to the south of Rach Goc river mouth, as far as these datasets show that the tidal range at Rach Goc is lowest on entire the studied coast.

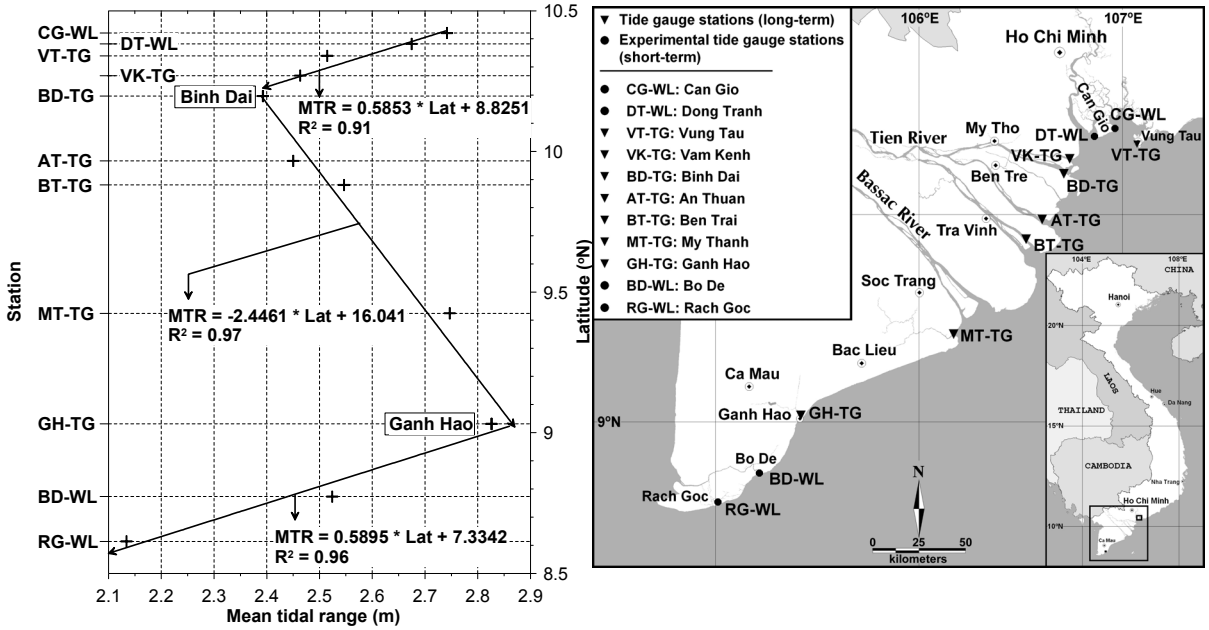

Figure 6.7. Temporal variations of mean tidal range (MTR) along the studied coastal areas (left fig.). The stations are ordered from north to south. The mean tidal ranges in the left figure is the combination of the mean tidal ranges at seven long-term stations for the 19-year period (Figure 6.3h) and the mean tidal ranges at the "experimental" stations in Can Gio (CG-WL, DT-WL), Bo De (BD-WL), and Rach Goc (RG-WL). The MTR at Rach Goc was referenced to Bo De and all other stations were referenced to Vung Tau. The left figure shows the MTR variation trend following the latitudinal changes.

6.2. Driving factors of mangrove cliff retreat in Can Gio

6.2.1. General introduction

To give an overview of the whole river system including the western side of Can Gio (the Dong Tranh river mouth) the main driving forces, e.g. the tide and flow regime as well as the morphology in Can Gio are presented (Figure 4.1b). The bathymetry map for Can Gio was combined from two datasets, the first one taken in 2004 and the second taken in 2009. West of Can Gio, the bathymetric data were collected during several surveys in 2004 in the Dong Tranh River from the river mouth to the upstream of the Mui Nai River. East of Can Gio the bathymetric data were collected in 2009. Water depth fluctuations due to the tide were corrected by CTD data, which were taken close to the study area. The zero level for the bathymetry map was referenced to the zero level at Vung Tau tide gauge station.

At the Nga Bay river mouth the water levels were measured at the tidal river (CG-WL, Figure 4.1b, Figure 5.4) close to the main site for studying the mangrove cliff retreat. At the main channel of the Nga Bay river mouth the current velocities were measured at the mooring station (MS1-CG, Figure 3.1b) using an ADCP (WHSW600, RD Instruments). The current velocities at MS1-CG were collected two times during spring and neap tide stages in May 2008 with a measuring period of 2 days for each stage. During this period, the current velocities were also collected at two stations on the tidal flat (ST1-CG and ST2-CG, Figure 4.1, Figure 5.1a1, a2), west of the mooring station. At the tidal flat stations, currents were measured using the directional wave and current recorders (DWR, Valeport, Co., LTD). Waves were only collected in front of the mangrove cliff at the tidal flat stations (ST1-CG and ST2-CG), where data of suspended sediment concentration, water temperature, and salinity were also collected as well.

6.2.2. Bathymetry around Can Gio

Can Gio area is bordered by the Dong Tranh River in the western part and the Nga Bay River in the eastern part; both discharging into the open sea. The bathymetry of the area indicates that the main channel of the Dong Tranh River is narrower and shallower than the main channel of the Nga Bay River. Moreover, the mouth of the Dong Tranh estuary is also is also smaller compared to the mouth of the Nga Bay (Figure 6.8).

West of Can Gio, in the Dong Tranh River from the river mouth towards upstream, the main channel becomes narrower and more shallow. The slopes on the east side of the channel are steeper compared to those on the western side (Figure 6.8a, b1-4).

East of Can Gio, a cross-section from the tidal flat via the main channel of the Nga Bay River shows that the channel width is about 500 m with a water depth of about 11 m above the zero level, which is referred to Vung Tau tide gauge station (Figure 6.8c3). From this transect downstream the main channel becomes wider and shallower (Figure 6.8c1, c2). By contrast, towards upstream, the main channel is narrower and deeper (Figure 6.8c4).

In the inner estuary along the western part of the Nga Bay River the tidal flat is characterized by gentle slopes. As spring tide low water, this tidal flat extends more than 500 m from the rim of the mangrove forest. In front of the cliff shoreline, the tidal flat slope is about 0.4% (Figure 6.8c5).

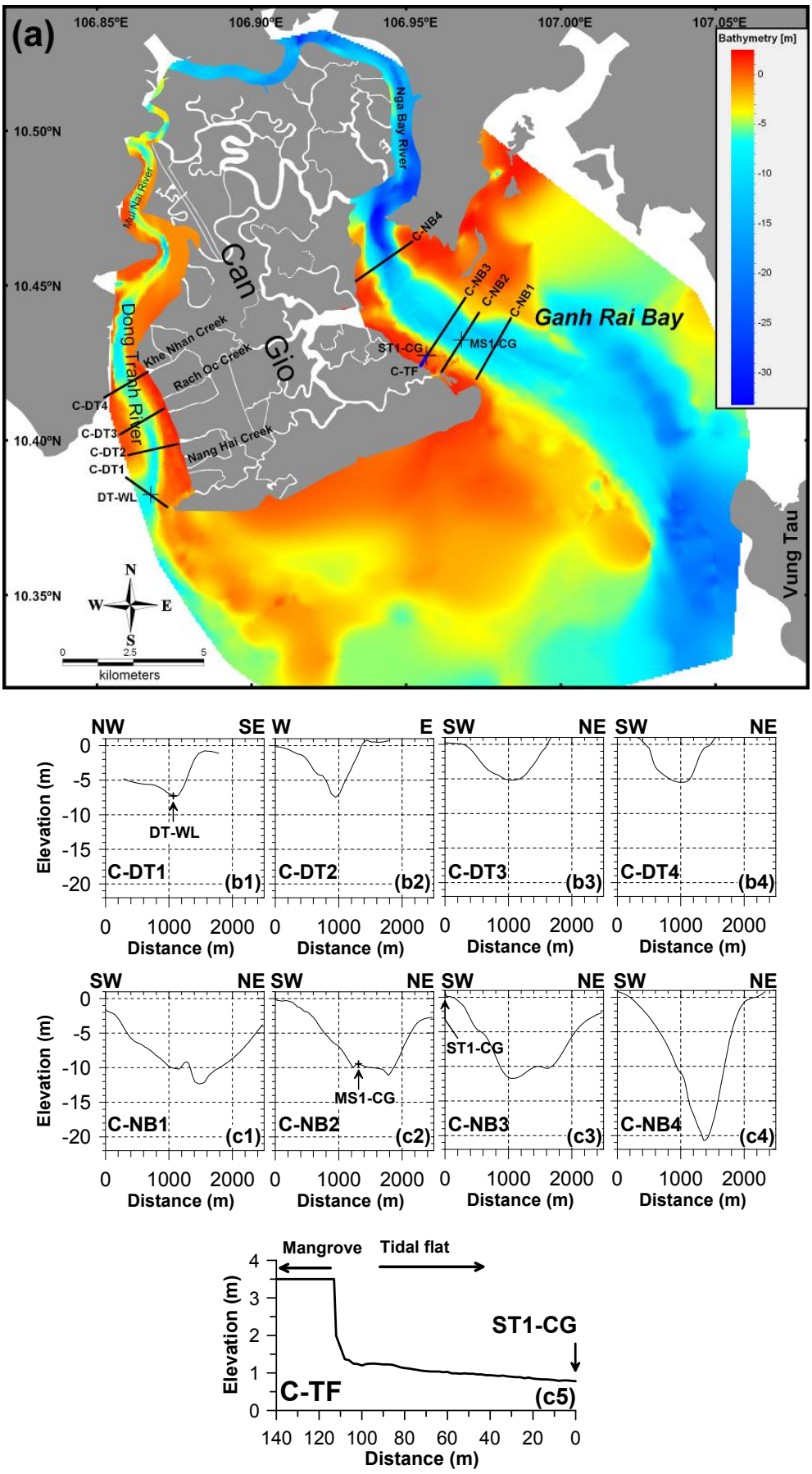

Figure 6.8. (a) Bathymetry around Can Gio. Bathymetrical profiles along the Dong Tranh River (b1-4) and the Nga Bay River (c1-4) and a topographical profile on the tidal flat in front of the mangrove cliff (c5). The zero elevation is referenced to the zero level at Vung Tau.

6.2.3. Tidal asymmetries around the river mouths at Can Gio

6.2.3.1. Tidal characteristics

Although the tidal ranges at the two river mouths (the Dong Tranh and Nga Bay river mouths) in Can Gio are higher than the tidal range at Vung Tau, the tidal regimes (mixed tide, mainly semi-diurnal) are basically similar to the tide at Vung Tau. Therefore, the data from Vung Tau are used for the long-term statistical estimation of tides.

At the Dong Tranh river mouth the tide is characterized by an about 35 min shorter flood duration compared to ebb tide. At the Nga Bay river mouth, the average flood duration is about 11 min shorter than the ebb duration. The tidal range at the Dong Tranh river mouth is less than that at the Nga Bay river mouth (see also Chapter 6.1.2, Table 6.5).

6.2.3.2. Tidal current at the Dong Tranh river mouth

The dataset of current velocities measured close to the bottom and the water level variations at the Dong Tranh river mouth station (DT-WL) during 22 days in November 2004 show a flood dominant tidal flow regime (Figure 6.9). The directions of the ebb and flood currents are inversely, mainly in south and north directions, respectively (Figure 6.9c, d).

Current velocities of the flood are usually stronger, especially during spring tide. Highest current speeds during flood and ebb tide are about 1.48 m/s and 1.28 m/s, respectively (Figure 6.9a, b).

During higher spring tide, the maximum flood currents are usually higher than the maximum ebb currents; while the differences between maximum flood and ebb currents are not significant during lower spring tide or neap tide (Figure 6.9e). The flood durations are mainly shorter than ebb durations, but the tidal ranges of these flood phase are almost the same than tidal ranges of ebb phase (see definitions in Table 5. 2, Figure 6.9f, g). Therefore, the dominated flood current is strongly related to the asymmetry of tidal durations between the ebb and flood phases.

For the period, which was recorded 22 days, the average of maximum flood speeds (0.70 m/s) is about 7.5% higher than the average of maximum ebb speeds (0.65 m/s). The mean flood duration is about 35 min (or ~ 9%) shorter than the mean ebb duration. The mean tidal range of flood is about 4 cm higher than the mean of ebb.

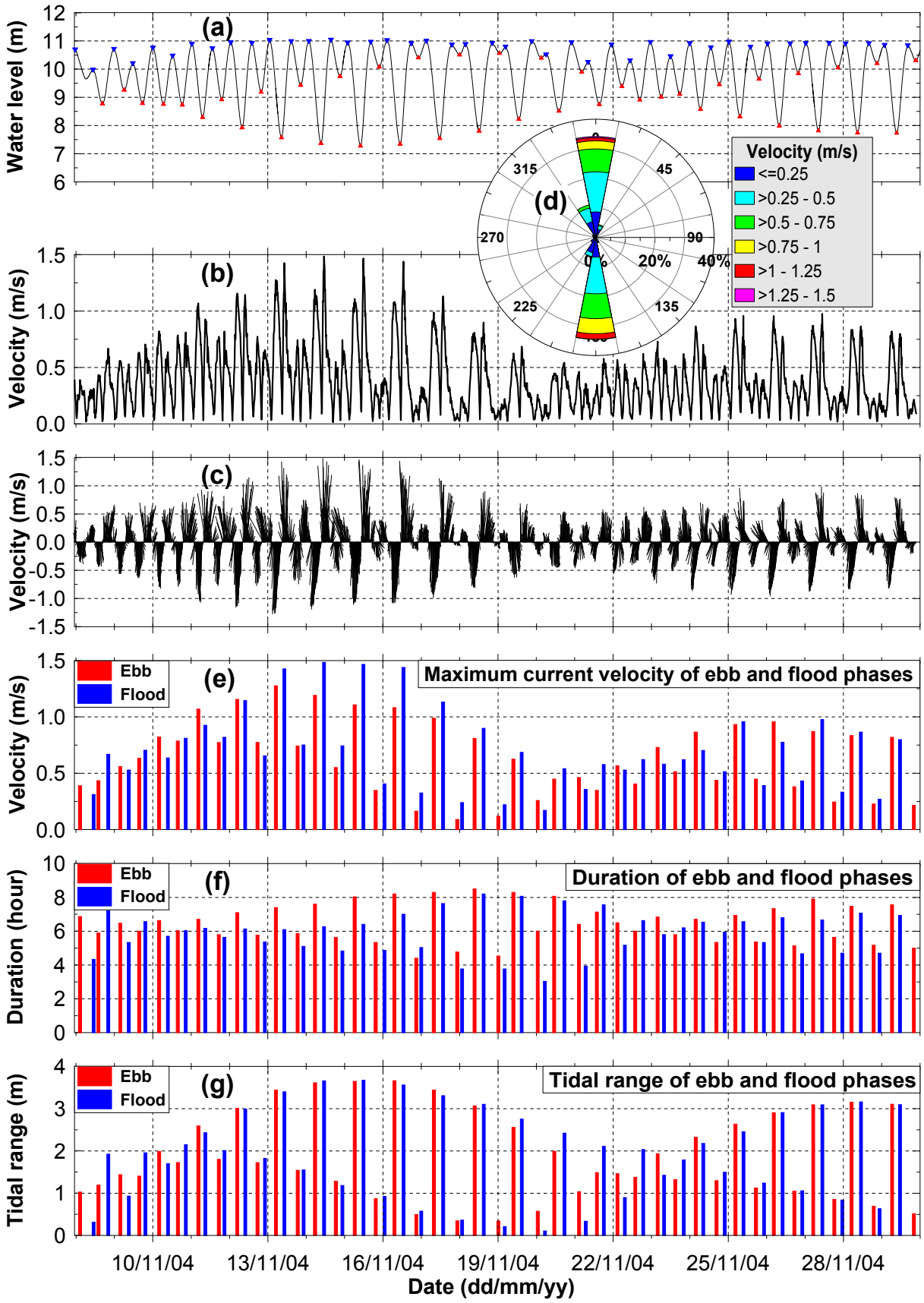

Figure 6.9. (a) Time series plots of water level, (b) current velocity, (c) current vector, (d) directional distribution of current velocity, maximum current speed, duration of ebb and flood phases (f) and tidal range (g), at the Dong Tranh river mouth, Can Gio (DT-WL station). During spring tide, the flood current is stronger than during the ebb current.

6.2.3.3. Tidal current at the Nga Bay river mouth

At the main channel of the Nga Bay river mouth, the currents were measured at the mooring station (MS1-CG, Figure 4.1b) during spring tide for a period of 49 hours (from 06 May 2008 at 08:00) and during neap tide for a period of 46 hours (from 14 May 2008 at 19:00). For these periods, current data were also collected at two stations on the tidal flat in front of the mangrove cliff (ST1-CG and ST2-CG, Figure 4.1b). The datasets of currents from these locations show that in front of the cliff as well as in the main channel the ebb current speed is faster than the flood current speed especially during spring tide. This indicates ebb dominance.

In the channel of the Nga Bay river mouth the directions of ebb and flood currents are almost reverse. The dominant ebb and flood directions are ESE and WNW during spring tide as well as during neap tide (Figure 6.10a8-10; b8-10).

During spring tide, a vertical current profile in the river mouth shows that the current velocities decrease significantly from the surface to the bottom (Figure 6.10a1-7). The maximum ebb and flood current speeds were about 1.64 m/s and 1.04 m/s at the surface, and 1.22 m/s and 0.82 m/s near the bottom. The maximum of the depth averaged velocities of all ebb and flood measurements were about 1.42 m/s and 0.89 m/s, respectively. In comparison between the maxima of ebb and flood currents, the surface and near bottom velocities of the ebb phase are about 33% and 37% higher than during the flood phase.

During the neap tide stage, the current velocities also decrease from the surface to the bottom. However, only at the surface the maximum ebb current (1.03 m/s) is faster than the maximum flood current (0.8 m/s) (Figure 6.10b1-7). In contrast, near the bottom these values amount to 0.49 m/s and 0.55 m/s for the ebb and flood phase, respectively. The maximum depth averaged ebb and flood speed were about 0.66 and 0.61 m/s, respectively.

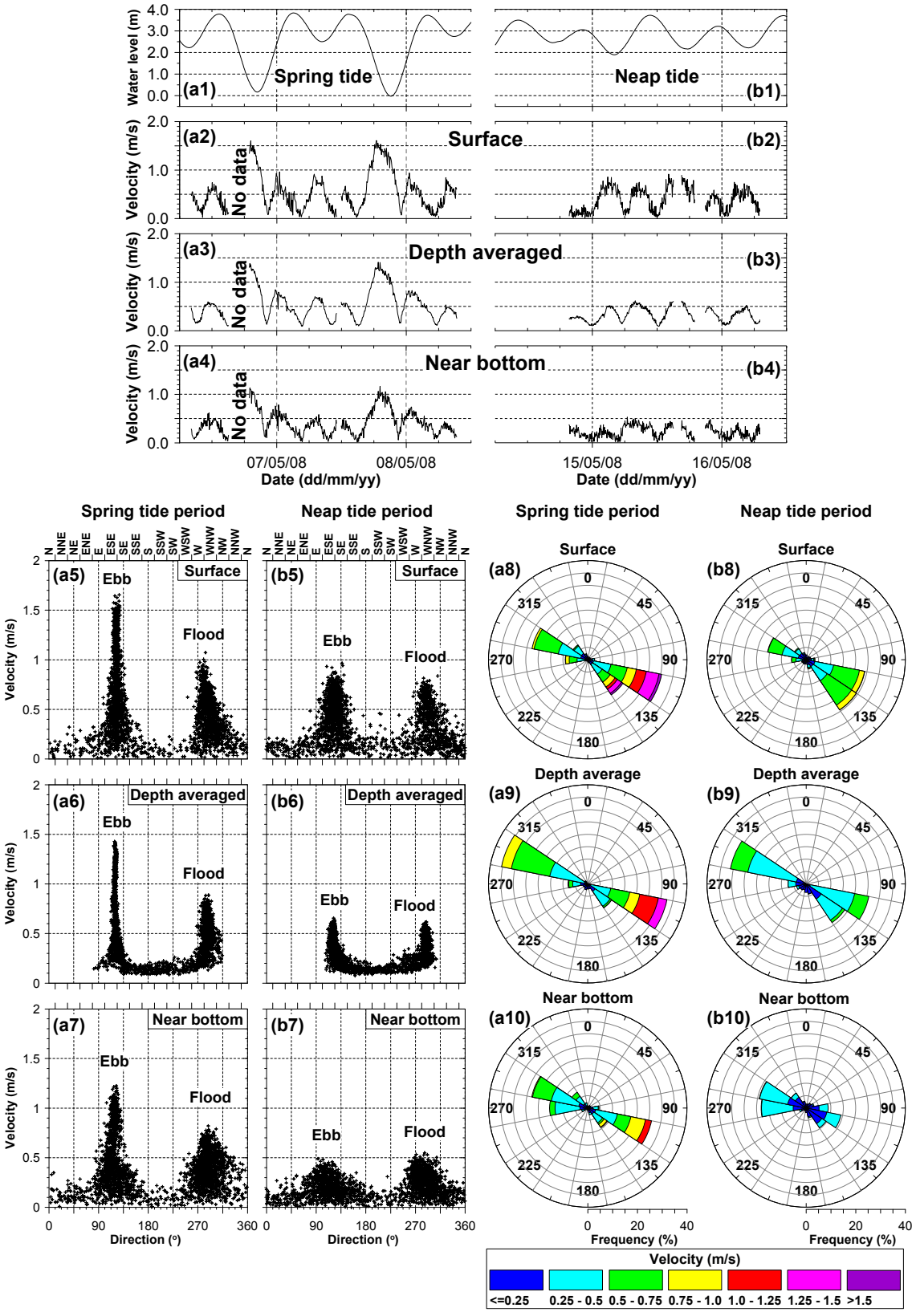

Figure 6.10. Water level at Vung Tau (VT-TG) and current velocities at the Nga Bay river mouth station (MS1-CG) during spring and neap tides (for locations of these stations see Figure 4.1b). Diagrams indicated by "a" show the situations for spring tide, "b" for neap tide. Figures a, b (1-4) are time series plots of water level, current velocities: at the surface, the depth averaged, and at near the bottom. The Figures a, b (5-7) are the diagrams of current speeds versus directions at the surface, the depth averaged, and at near the bottom. The Figures a, b (8-10) are directional distribution, of current velocity at the surface, the depth averaged, and near the bottom.

6.2.3.4. Currents on the tidal flat

This section is based on a 14-days period dataset that was collected from 6-20 May 2008 at two stations on the tidal flat (ST1-CG, ST2-CG; Figure 5.1). During this measuring period the tidal flat (from ST1-CG to the cliff) was exposed for about 50 hrs (or ~ 8% of the measuring time) at eight lower low waters of the spring tides.

At ST1-CG the currents on the tidal flat are ebb dominant (Figure 6.11). The ebb current direction was mainly SW, while the flood current direction was in the range between NNE to NE (Figure 6.11b, c). On average for the whole dataset, the mean ebb and flood current speeds were about 0.09 m/s and 0.05 m/s, respectively. The peaks of ebb current are higher than those of the flood current, especially during spring tide (Figure 6.11a, b). The maximum speeds of ebb and flood were 0.24 m/s and 0.13 m/s (at two ebb tides on 7-8 May 2008 during spring tide). Beside these maximum speeds, the current speeds seldom exceed 0.2 m/s for the ebb phase, and 0.1 m/s for the flood phase. During 14 days, about 80% of the current velocities were less than 0.1 m/s, 19% in between 0.1-0.2 m/s, and 1% exceeds 0.2 m/s but the currents were never stronger than 0.25 m/s (Figure 6.11d).

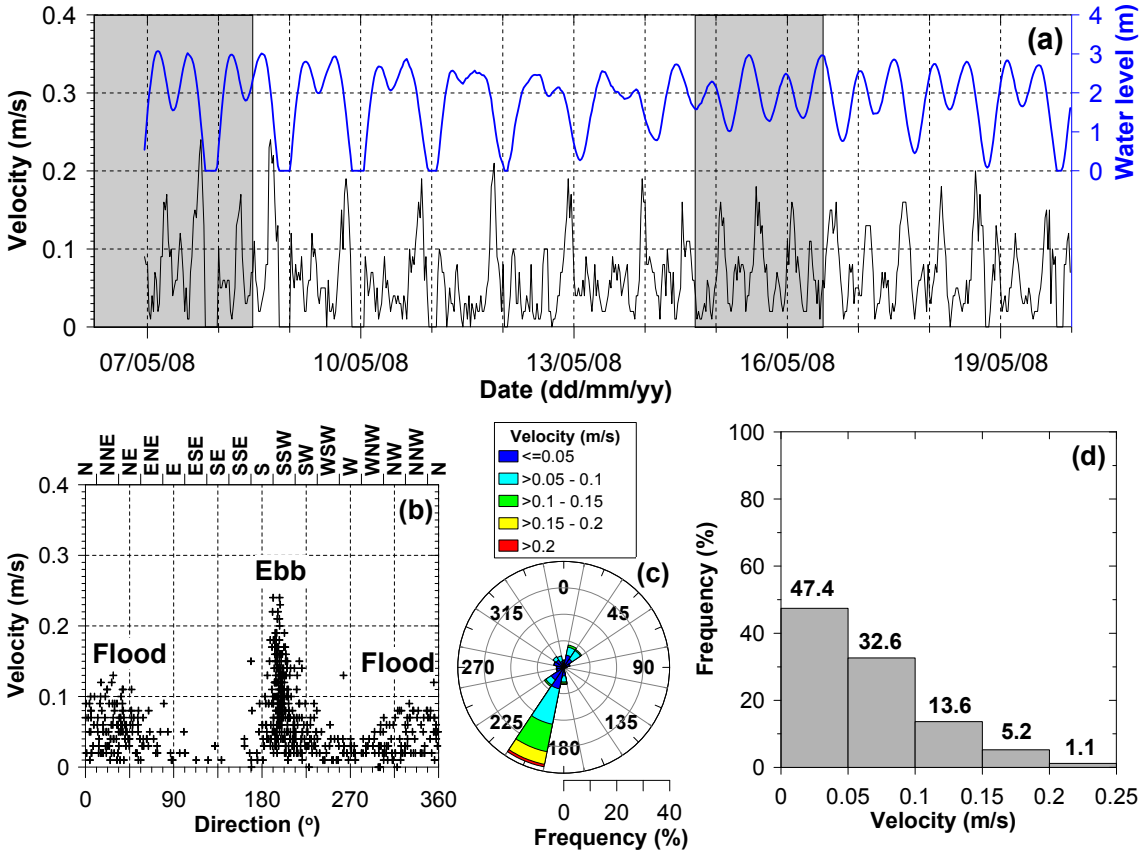

Figure 6.11. (a) Time series plots of current velocity and water level at tidal flat station (ST1-CG). (b) Diagram of current velocity versus direction. (c) Directional distribution of current velocity. (d) Frequency distribution of current velocity. The grey rectangles are marked for the periods when the current velocities were measured at the main channel of the Nga Bay River (MS1-CG).

At ST2-CG, close to the mangrove cliff, the current velocities are very slow. The flood and ebb directions are the same as those at ST1-CG. The peaks of the speeds are neither significant dominant in ebb nor flood current directions. These peaks are even not different between neap and spring tide (Figure 6.12a, b, c). During the 14 days period, there are only 2.1% current speeds in the range 0.1-0.15 m/s, 16.7% from 0.05-0.1 m/s, and 81.2% below 0.05 m/s (Figure 6.12d).

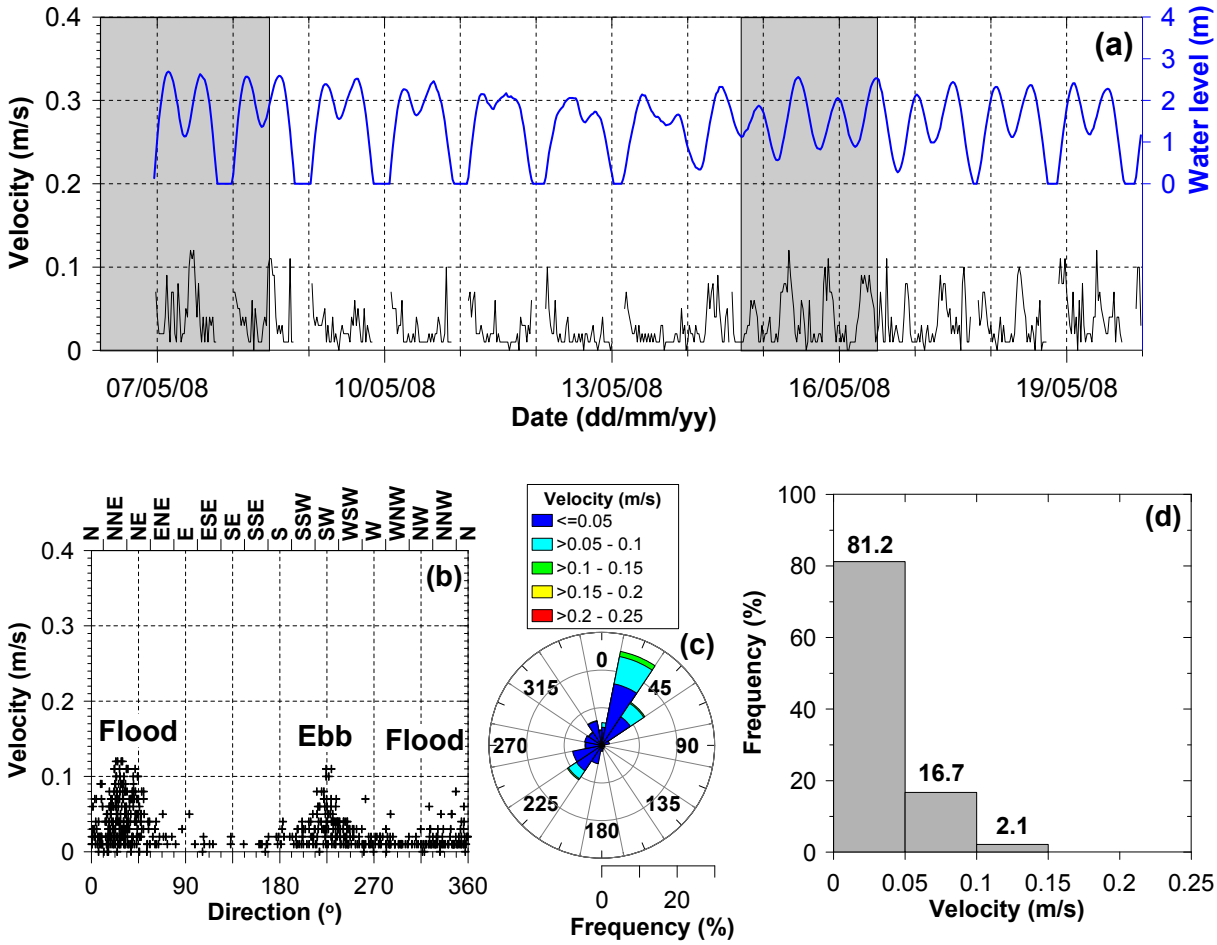

Figure 6.12. (a) Time series plots of current velocity and water level at tidal flat station (ST2-CG). (b) Diagram of current velocity versus direction. (c) Directional distribution of current velocity. (d) Frequency distribution of current velocity. The grey rectangles are marked for the periods when the current velocities were measured at the main channel of the Nga Bay River (MS1-CG).

6.2.4. Soil properties of the mangrove cliff and tidal flat

6.2.4.1. Shear strength of the mangrove cliff soil

The strength of the soils building up the mangrove-cliff in Can Gio was measured with a 'pocket van tester' at the cliff retreat stations at the beginning of the field campaign (See 5.2.2). In total 84 values of the shear strengths were collected along the whole 125 meters long the profile.

The shear strength of the mangrove cliff soil is not uniform (Figure 6.13, Table 6.7). The values are scattered ranging from 0.0547 to 0.2461 kg/cm^2, with 0.1273 kg/cm^2 as average value (SD (standard deviation) = 0.0421). However, the averaged shear strengths at the four different positions of each of the vertical profiles show that the shear strength values from the top positions are higher than the values of the other positions. These values also indicate that the part from the middle to the bottom show the lowest shear strength (Figure 6.13a1-a4). Moreover, the shear strength is dominated by certain values: 0.08-0.09 (count number n = 9), 0.10-0.11 (n=30), 0.12-0.13 (n=11), and 0.14-0.15 (n=19). These ranges account for about 82% of the total 84 measured values (Figure 6.13b).

Table 6.7. Shear strengths of the cliff soil at the site in Can Gio. The measurements were carried-out totally at 84 stations on 21 profiles (4 positions at each profile from the top to bottom of the cliff).

Shear strength (kg/cm^2)					
Profile name	**Position 1 (top)**	**Position 2 (middle-top)**	**Position 3 (Middle-bottom)**	**Position 4 (bottom)**	**Mean**
1	0.1914	0.1914	0.1367	0.1094	0.1572
2	0.0547	0.1094	0.1094	0.1094	0.0957
3	0.1094	0.1094	0.1367	0.1640	0.1299
4	0.1640	0.1094	0.1094	0.1094	0.1230
5	0.1367	0.1094	0.0820	0.1367	0.1162
6	0.0820	0.0547	0.0547	0.1094	0.0752
7	0.1094	0.0547	0.1367	0.1094	0.1025
8	0.1094	0.1094	0.0820	0.1094	0.1025
9	0.1094	0.0820	0.1640	0.1640	0.1299
10	0.1640	0.1094	0.0547	0.0820	0.1025
11	0.1640	0.1640	0.0820	0.1914	0.1504
12	0.1367	0.1640	0.1640	0.0547	0.1299
13	0.2461	0.2187	0.1640	0.1367	0.1914
14	0.1640	0.1094	0.1094	0.1640	0.1367
15	0.1640	0.0547	0.1094	0.1094	0.1094
16	0.1367	0.1640	0.0820	0.1094	0.1230
17	0.1914	0.1094	0.1640	0.0820	0.1367
18	0.2187	0.1640	0.1094	0.1094	0.1504
19	0.1640	0.1640	0.1094	0.1094	0.1367
20	0.1094	0.1094	0.0820	0.1367	0.1094
21	0.1640	0.1367	0.1367	0.2187	0.1640
Mean	0.1471	0.1237	0.1133	0.1250	
Max					0.2461
Min					0.0547
Mean					0.1273
Standard deviation, SD					0.0421

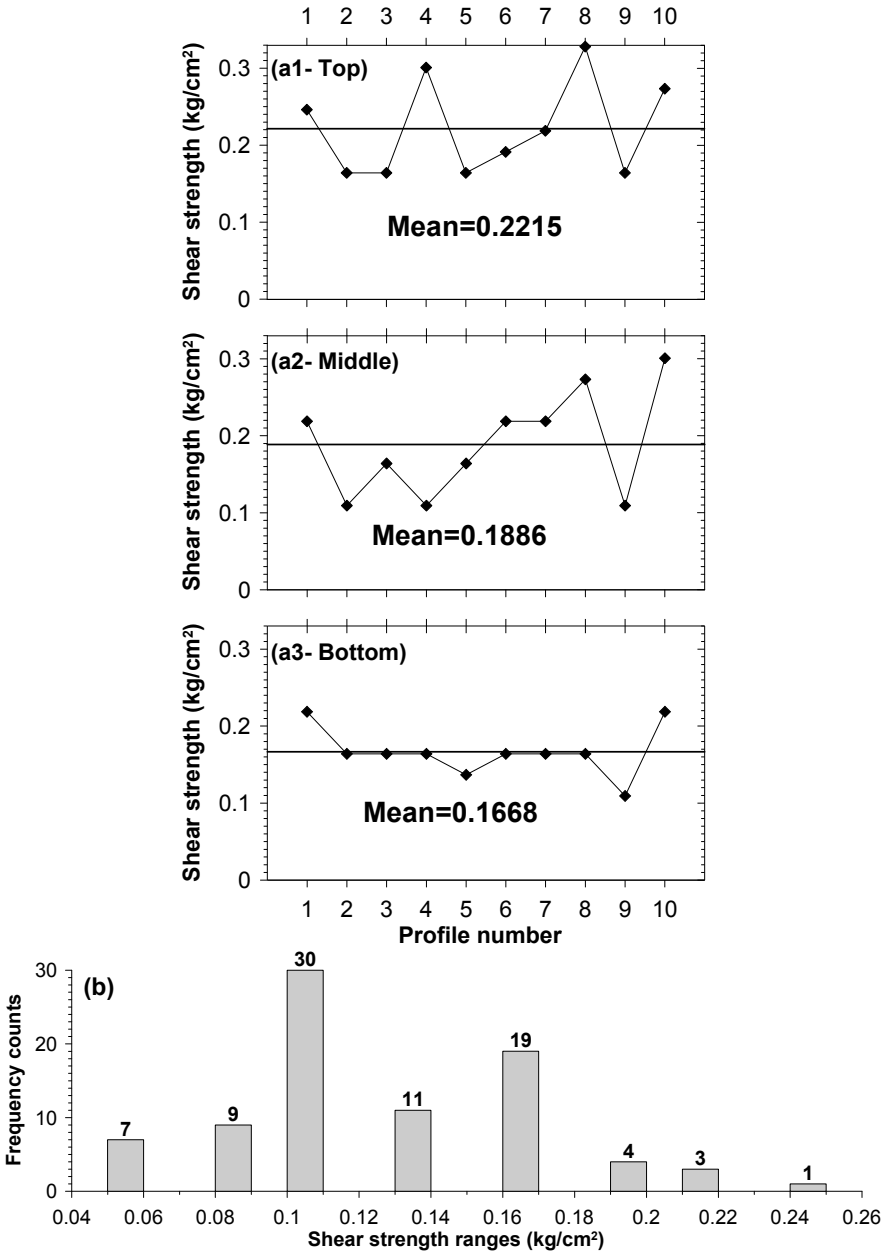

Figure 6.13. Shear strengths of the mangrove cliff soil in Can Gio. Figures a1-a4 show the shear strength variations at four vertical positions at 21 locations (profiles). The mean shear strength values at each horizontal profile are marked by the bold horizontal lines; Figure b shows the distribution of all shear strengths values due to their occurring frequencies.

6.2.4.2. Grain size distributions of the mangrove cliff and tidal flat soils

The mangrove cliff soil in Can Gio is mainly characterized as bimodal type of grain size distribution. One mode represents medium silt and the other mode represents very fine sand (Figure 6.14). About one third samples (30 samples) show unimodal grain size distribution, which are mainly in the range from medium silt to coarse silt. The rest sediment samples (54 samples) are characterized as bimodal type. The first mode is mainly in the range of medium silt and the second mode in the range from very fine sand to fine sand. On average of 84 sediment samples, mud content is 78% and sand content is 22%.

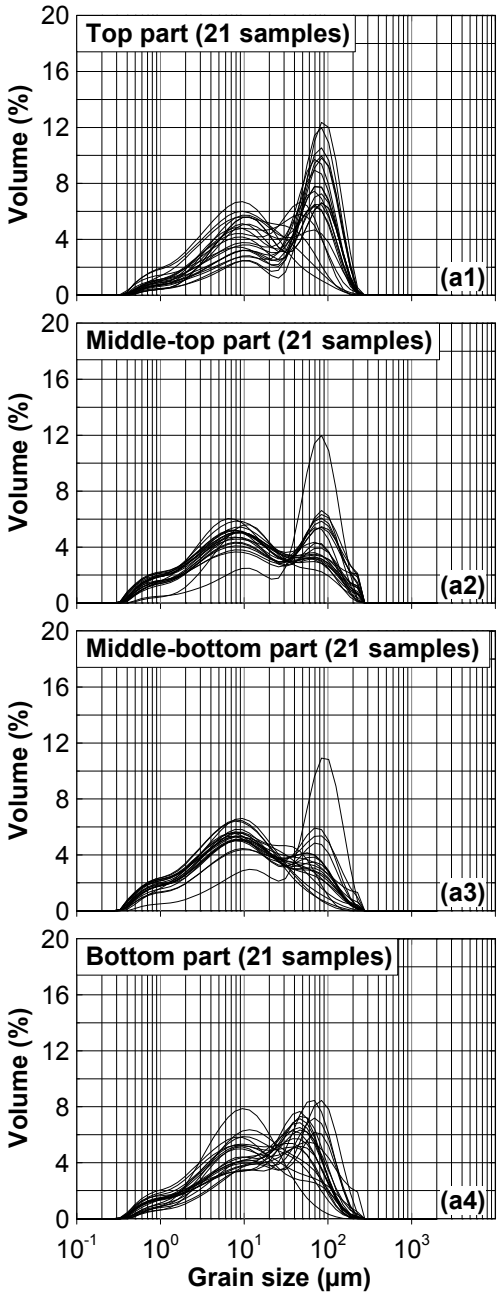

Figure 6.14. Grain size distributions of the soil of the mangrove cliff.

Nine sediment samples from the tidal flat were taken in front of the mangrove cliff on three transects, each 100 m long. The sampling stations were close to cliff foot, the middle of the transet, and 100 m offshore. Among these nine samples, there are three samples, which are composed mainly of fine sand showing unimodal grain size distributions. All other samples show bimodal grain size distributions with the first dominant mode in the range of fine sand and the second mode is in the range of fine and medium silt (Figure 6.15). The sediment on the tidal flat is represented by sand. On average of nine samples, the sand content is 54.7% and mud content amounts to 45.3%.

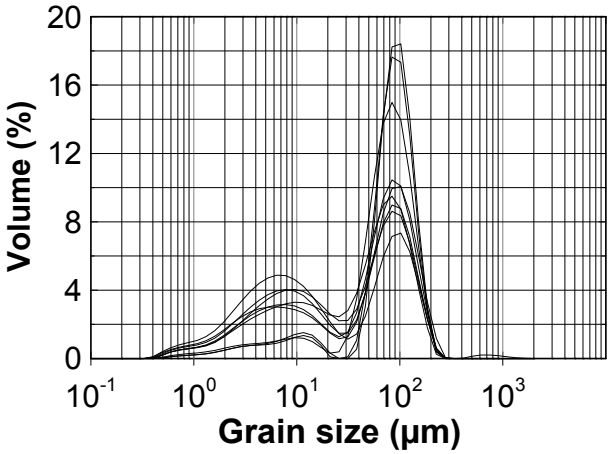

Figure 6.15. Grain size distributions of the soil on the tidal flat in Can Gio.

6.2.5. Short-term mangrove cliff retreat in Can Gio and influencing parameters

To ascertain the main hydrological parameters influencing mangrove cliff retreat in Can Gio, a field survey was designed to measure daily the cliff retreat and the hydrodynamic inputs by e.g. waves, currents, and tides from 26 May to 8 June 2009. At two stations on the tidal flat (ST1-CG and ST2-CG) offshore the mangrove cliff wave-recorder, current meter, CTDs and OBS-sensors were installed to measure continuously hydrodynamic parameters and the concentration of suspended load. The distances from the mangrove cliff to ST2-CG and ST1-CG are about 12 m and 110 m (Figure 5.1a1, a2). Compare to Vung Tau tide gauge station, the elevation of ST1-CG is +80 cm, of ST2-CG +130 cm, and for the cliff base, it is +170 cm.

6.2.5.1. Meteorological oceanographic conditions

Water level variations and inundation

The water level fluctuations during the 13-day period are shown in Figure 6.16. The beginning and the end of the field survey are dominated by spring tides while in between neap tide happens. During this short term measuring campaign, the tidal flat, considered from the mangrove cliff to ST1-CG, was exposed totally for about 20 hours at five lower low waters. The mangrove cliff was exposed completely for about 59 hours accounting for about 19% of the survey period.

There were 12 coupled pairs of high-low waters (two high waters and two low waters) and one single pair of high-low water (called the turning point) (Figure 6.16a). The higher high waters of the first spring tide are higher than those of the second spring tide. The higher high waters during neap tide are also as high as those of the first spring tide. The levels of lower low waters are increasing from the beginning of the measuring period until reaching

the highest level at the turning point in neap tide on 2 June. Then the lower waters are decreasing until the end of the measuring campaign. The high waters occurred during the day and the lower low waters mostly appeared during the night.

The tidal periods (see Table 5. 2) are decreasing from the beginning of the measurement during spring tide until meeting the turning point at neap tide and were then increasing until the end of the measurement at the second spring tide (Figure 6.16b).

The water level changes during spring tide are faster than during the neap tide. The tidal periods during spring tide are longer than during neap tide. Moreover, the lower low water levels during neap tide are higher than during spring tide. The time of inundation of the cliff increases from the first spring tide to the turning point and reach their highest value during neap tide and then decrease again towards the second spring tide (Figure 6.16a).

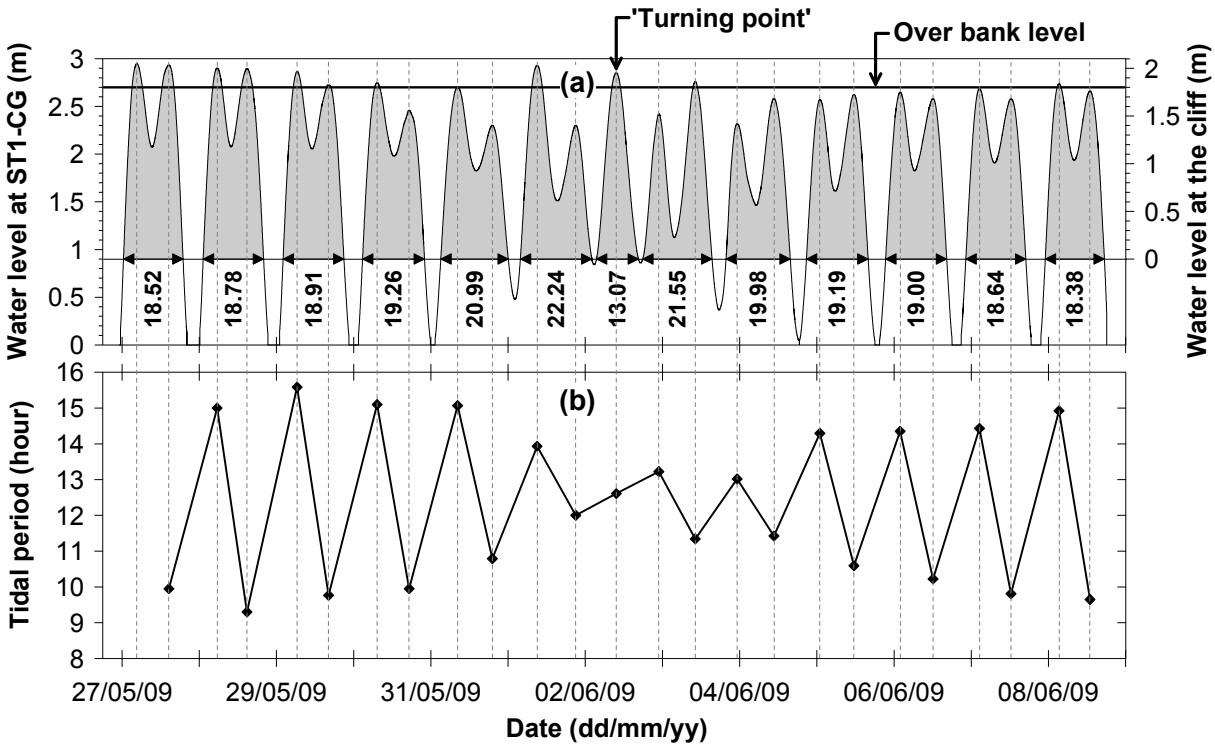

Figure 6.16. Time series plots of water level (a) and tidal period (b) at the tidal flat station (ST1-CG). In Fig. a, the grey part above 0.9 m level is marked as the inundation level at the foot of the mangrove cliff. The bold line at 2.7 m (left axis) is marked for the over bank level (cliff fully inundated). The arrows with the numbers below indicate the duration of inundation (in hours) of the cliff. The zero level on the left axis of Fig. a indicates the water level of the height from station ST1-CG. The tidal periods in Fig. b provide the duration between two consecutive high waters.

Salinity and water temperature

The changes of salinity of the water body on the tidal flat follow the tide (Figure 6.17a, b). During spring tide, the salinity fluctuations are lower than during neap tide. The salinity

maxima and minima occur around slack high water and slack low water. The highest and lowest values of salinity were about 28.5 ppt (part per thousand) and 25.5 ppt (25.8 on average).

Changes in water temperature are small (Figure 6.17a, c). The water temperatures range between 28.1 °C and 31.0°C with a mean of 29.7 °C. In comparison to the air temperature, which reaches from 25.4 °C in the evening to 34.3 °C in the after noon, the water temperature fluctuations are small. Especially in the afternoon, the air temperatures were higher than the water temperatures. These differences between water temperature and air temperature occurred strongly during spring tide periods.

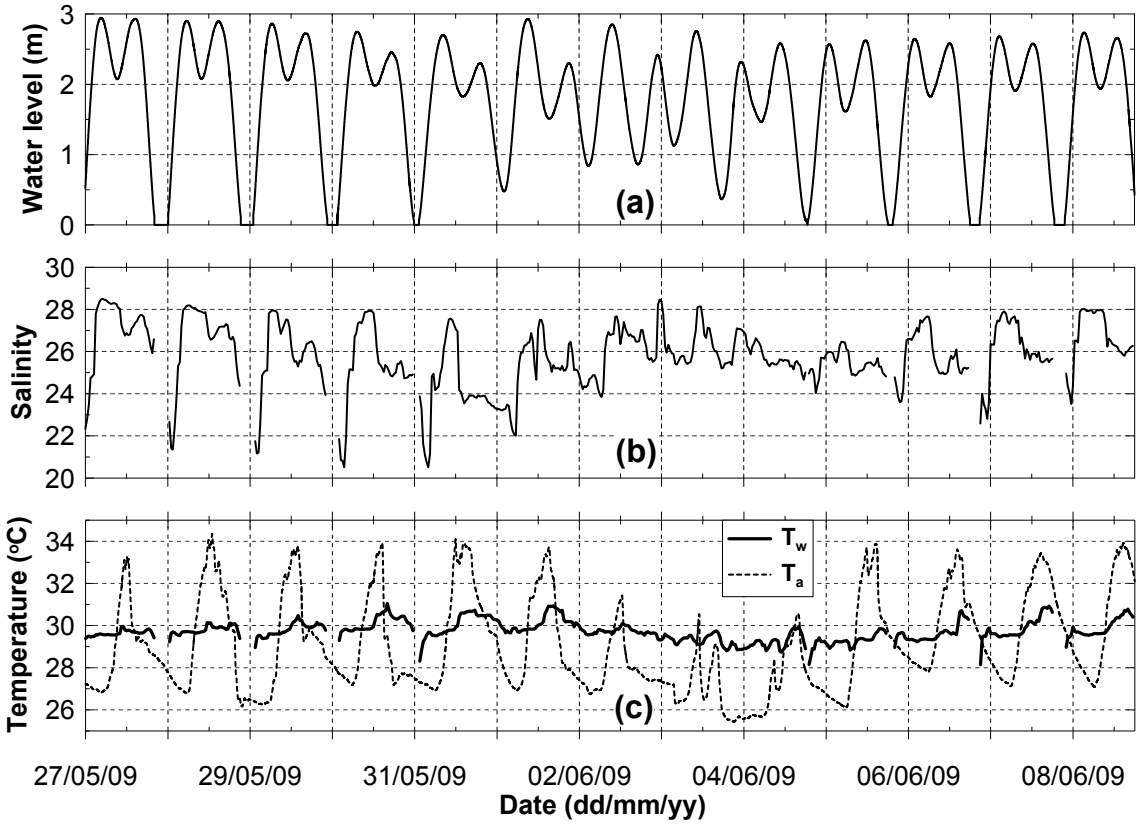

Figure 6.17. Time series plots of water level, salinity, water- and air temperatures (T_w and T_a), at the ST1-CG station.

Wind and waves

Even if wind velocities were not measured, the study site in Can Gio can be regarded as calm. Wind of the southwest monsoon was not observed. The only winds mainly started to blow in the afternoon as breezes (below 1m/s, own measurement) that were formed due to the difference in temperatures between air and sea (Figure 6.17c).

During the measuring campaign, the sea state was very calm except for the days from 5-6 June 2009. The incident waves mostly attack perpendicular to the mangrove cliff. The peaks of wave heights usually occurred at high tides during the day (Figure 6.18).

At ST1-CG most of the waves approached from NE to E directions. The energy of these waves accounts for about 96.1% of the total wave energy, which was transferred to the coast; most of the energy (80.3%) is transferred from the very small sector ENE (Figure 6.18c1, c2, Figure 6.19a). The wave periods (about 90%) are from 3-6 seconds, with a dominance of 5 seconds (Figure 6.19b). The H_s values were mainly in the range between 0.05 m to 0.15 m and do not exceed 0.3 m (accounting for 66%, Figure 6.18a, c1, c3). The highest and the mean value of H_s were about 0.29 m and 0.10 m.

Close to the cliff, at ST2-CG, the wave directions are scattered and mainly in the range between NE and ESE, where ESE is the most dominant direction (Figure 6.18d1, d2). The significant wave heights do not exceed 0.4 m. They were dominant and distributed (about 60%) in the range from 0.05 to 0.15 m (Figure 6.18b, d3). The highest and mean values of H_s are about 0.38 m and 0.12 m.

The wave heights at ST2-CG are relatively higher than at ST1-CG because of wave reflection. The ST2-CG station is located about 12 m in front of the active cliff as well as near to blocks of eroded mangrove cliff. Therefore, the incident waves are reflected and hence enhanced the wave heights at ST2-CG. On average, for only those times when the mangrove cliff was inundated, the mean significant wave height at ST2-CG is about 0.02m higher than that at ST1-CG.

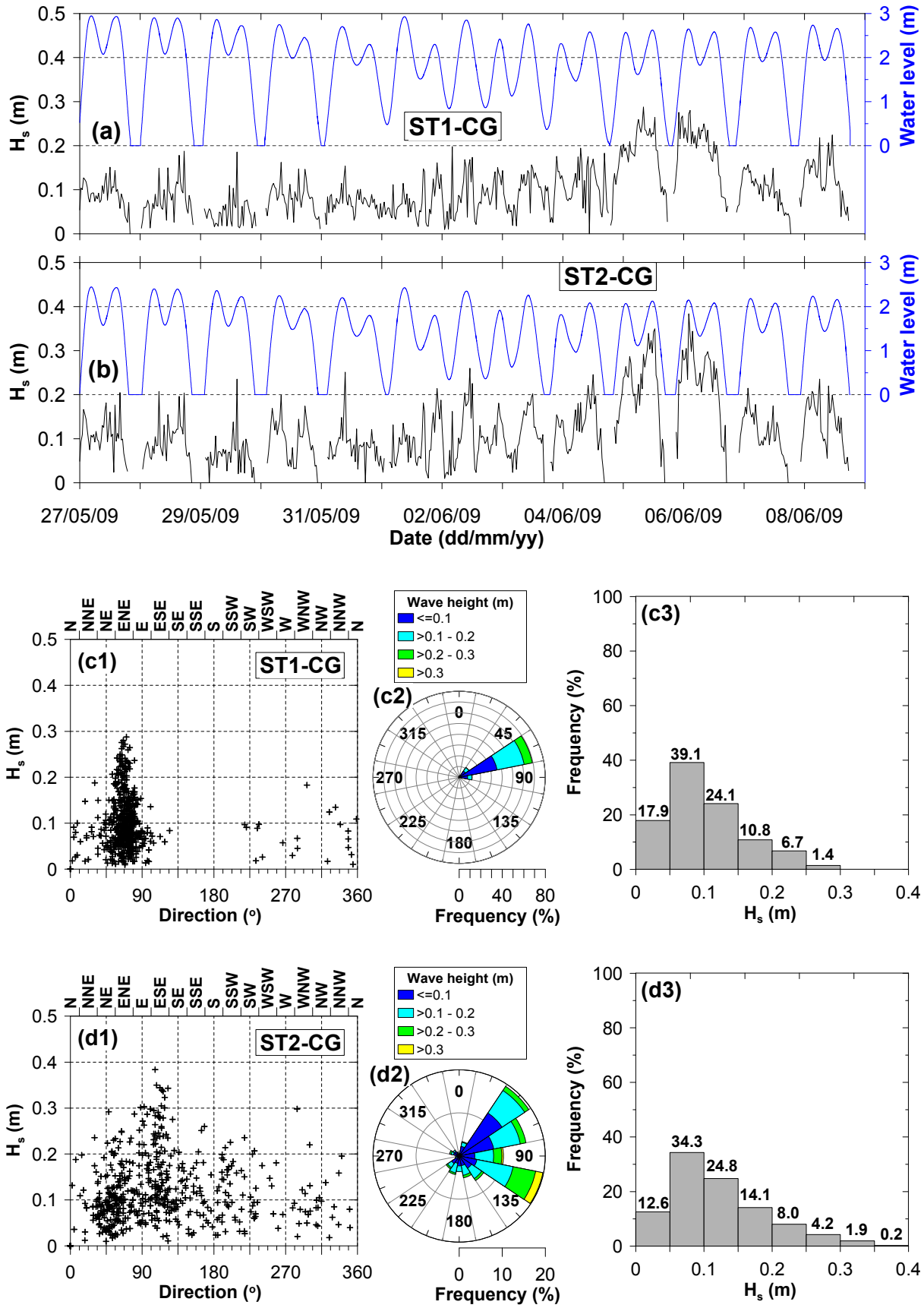

Figure 6.18. Time series plots of water level and significant wave height (H_s) at ST1-CG (a) and ST2-CG (b). The figures (c1, d1) show diagrams of H_s versus wave direction, c2, d2 show rose plots of directional distribution of Hs, and c3, d3 show frequency distribution of H_s.

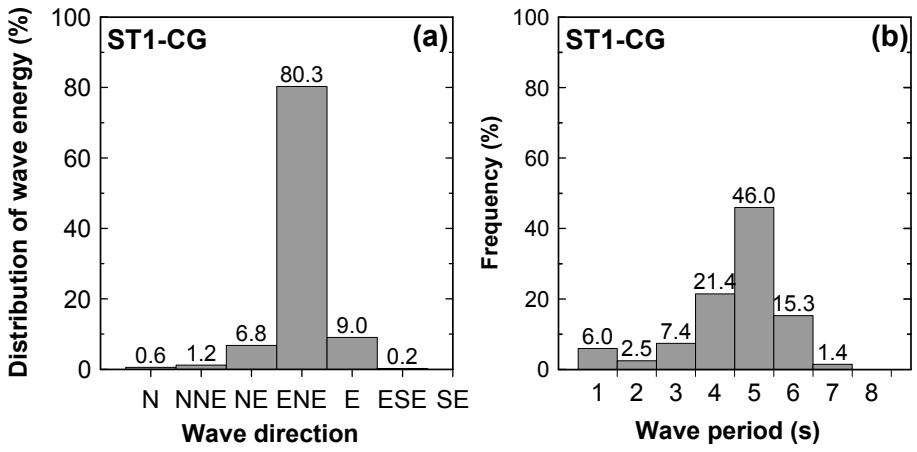

Figure 6.19. Directional distribution of wave energy (a) and frequency distribution of the wave period (b) at ST1-CG for the same dataset showing in Figure 6.18.

Current

The currents at about 110 m offshore the mangrove cliff (ST1-CG) are slow and ebb dominant. The flood and ebb current directions are dominant towards NNE and SSW. The ebb current is usually stronger than the flood current. The maximum ebb and flood current speed are 0.23 m/s and 0.18 m/s. The mean ebb current speed (0.08 m/s) is also higher than the mean flood current speed (0.06 m/s). During most of the current speed was less than 0.2 m/s (Figure 6.20a, b, c). About 95.2% of the current speeds are less than 0.15 m/s and only 4.6% are in the range between 0.15-0.2 m/s (Figure 6.20d).

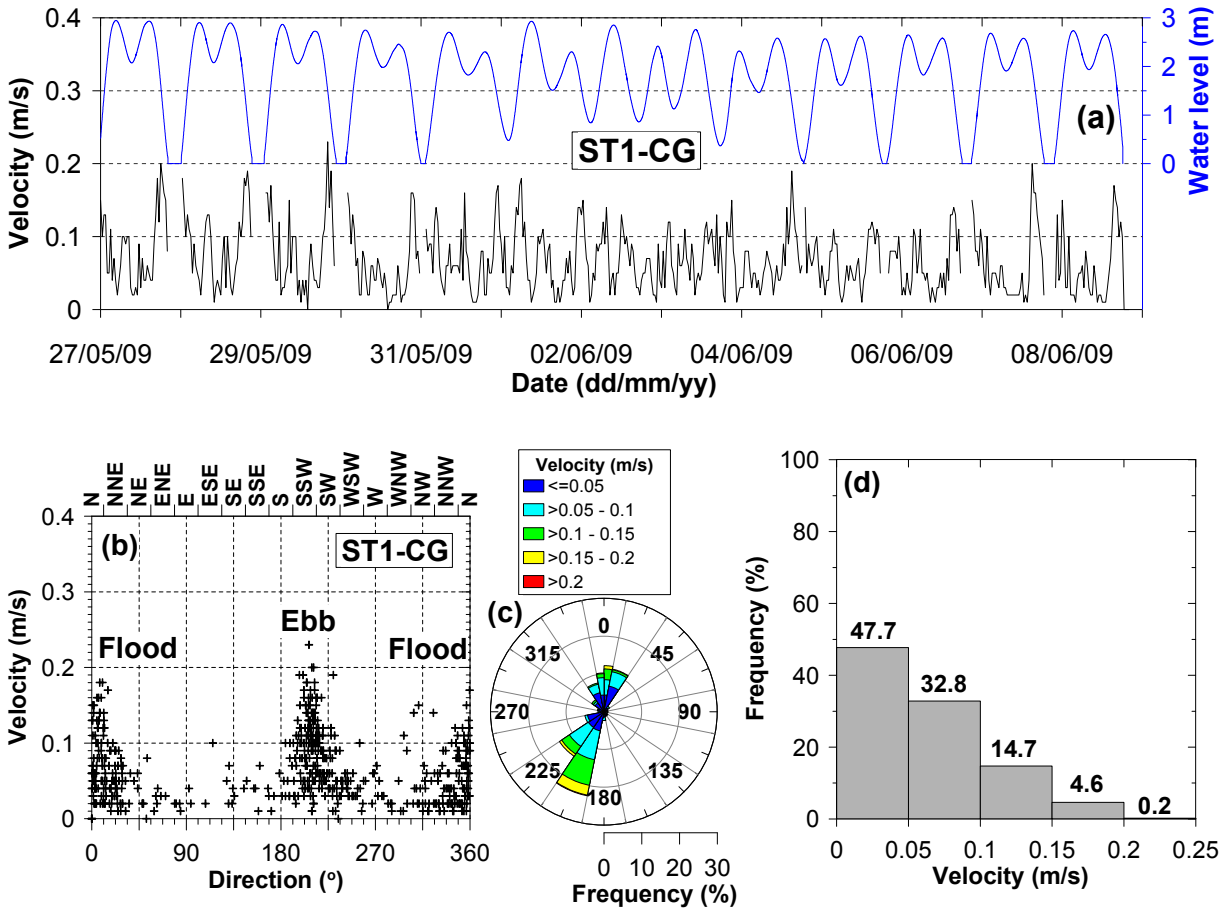

Figure 6.20. Graphs of water level and current velocity at the tidal flat station (ST1-CG). Time series plot of water level and current velocity (a). Diagrams of current velocity versus direction (b), directional distribution of current velocity (c), and frequency distribution of current velocity (d).

Close to the mangrove cliff (ST2-CG station), the current flow is very slow. The current directions of flood and ebb are dominant towards NE and SW. The ebb current speed is not significantly different from the flood current speed (Figure 6.21a, b, c). About 98.8% of measured current speeds are less 0.1 m/s, where about 88.8% is below 0.05 m/s (Figure 6.21d). The maximum ebb and flood currents are about 0.16 and 0.11 m/s. The mean speeds of ebb and flood current are the same (0.03 m/s).

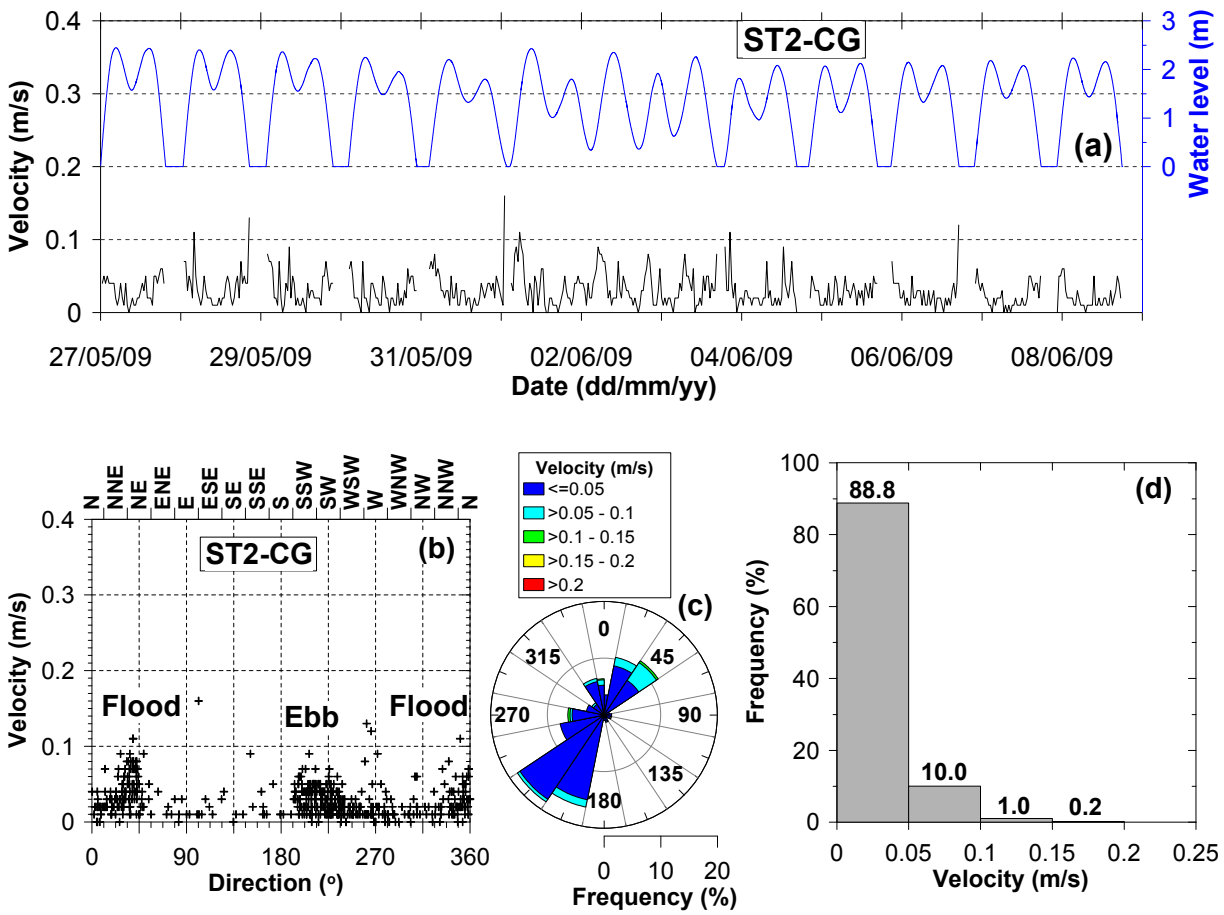

Figure 6.21. Graphs of water level and current velocity at the tidal flat station (ST2-CG). Time series plot of water level and current velocity (a). Diagrams of current velocity versus direction (b), directional distribution of current velocity (c), and frequency distribution of current velocity (d).

Suspended matter

The suspended sediment concentration (SSC) on the tidal flat in front of the mangrove cliff (ST1-CG) almost follows the tide and wave conditions (Figure 6.22). The peaks of SSC usually occurred at the beginning of the rising phase and at the end of falling phase, when the water levels were low and the current speeds reach maximum values (Figure 6.22b, c). High SSC values also occurred under conditions of relatively high waves even at high tides (Figure 6.22a, c). During neap tide, the water turbidities are small compared to those during spring tides. The maximum SSC was about 0.851 g/l (at near slack low water on 0/06/2009 18:00). During the 13 days field campaign the mean SSC was about 0.176 g/l. There is no clear difference in SSC between ebb tide and flood tide.

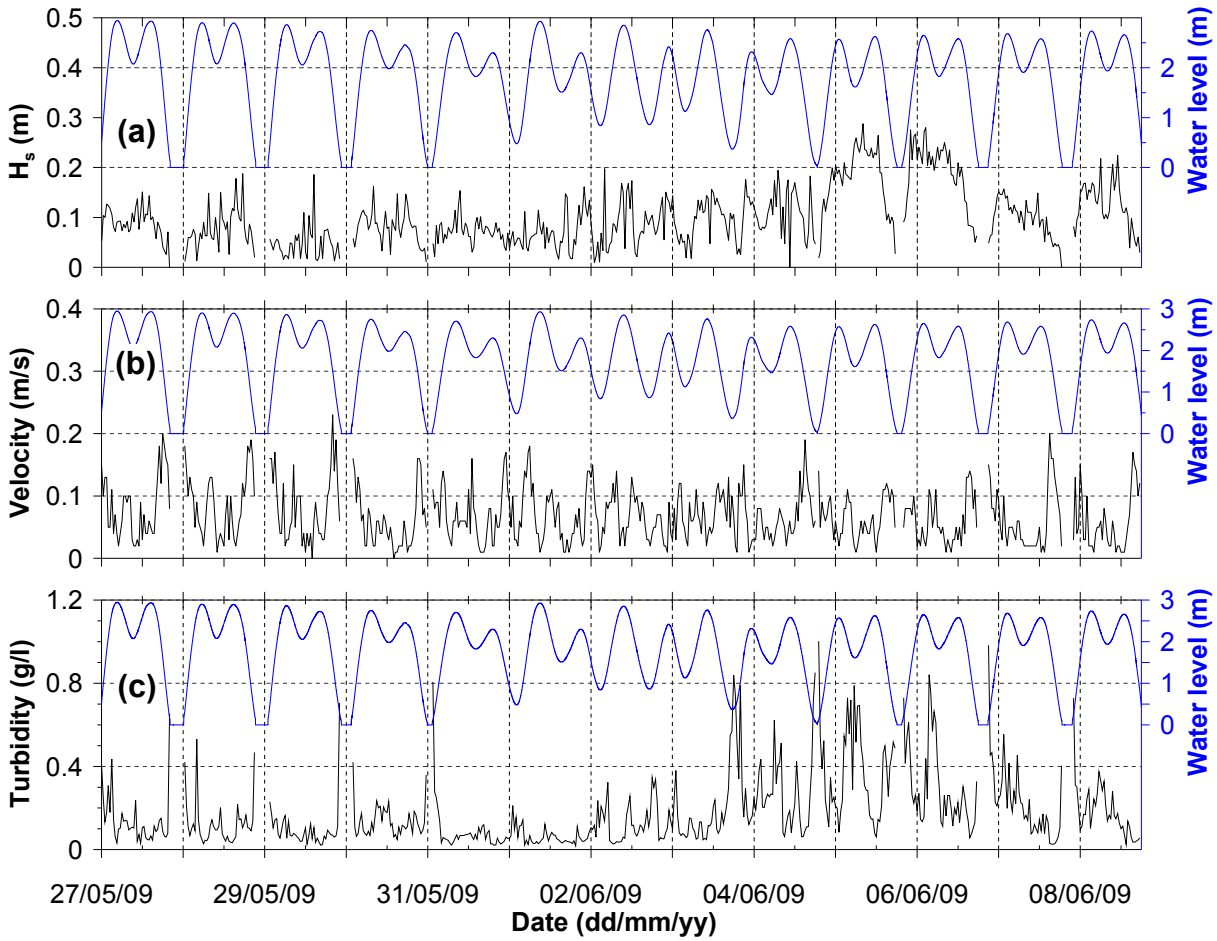

Figure 6.22. Time series plots of (a) significant wave height, (b) current velocity, and (c) suspended sediment concentration. Water level is included in all figures.

6.2.5.2. Short-term mangrove cliff retreat and affecting factors

The measurement strategy for collecting cliff retreat data was described in Chapter 5.2.1. Thirteen repeated measurements on 21 profiles, with four measurement stations at each vertical profile from bottom to top of the cliff resulted in 1092 values of which 881 values (accounting for 80.7%) show no retreat. The maximum retreat value was 32.0 cm; the mean retreat value was about 0.37 cm with a standard deviation of about 1.93. This shows that the data are not uniform in time and space. Table 6.8 lists thirteen retreat measurements on 21 profiles, where the retreat data obtained from the four measuring points in each of the vertical profile are averaged. Therefore, the 1092 retreat values were reduced to 263 values.

Inundation due to tides and total wave energy input to the cliff are considered as the hydrological driving forces for cliff retreat. The total wave energy input was calculated as a sum of wave energies, which are collected only during those times when the cliff was inundated (see Chapter 5). To correlate cliff retreat data with wave energy input and duration of inundation, all retreat values from one measuring period have been reduced to one representative value. A measuring period is defined as the time from one inundation of

the cliff base to the next inundation. The mean retreat is the arithmetic mean of all cliff retreat values at 84 stations (21 profiles, four stations each).

During this measuring campaign, the cliff foot has been inundated for about 307 hours. For the whole measuring campaign, thirteen mean cliff retreat values could be calculated (see MR in Table 6.8).

The mean cliff retreat (MR in Table 6.8) varies from 0 cm (at the thirteenth value, see Table 6.8 period 13) to 0.91 cm (period 7) with an average of 0.37 cm for the whole campaign. The rate of mean retreat (RMR in Table 6.8) varies from 0.0 cm/day to 1.56 cm/day with an average of 0.42 cm/day (Table 6.8). Although the mean retreat shows non-uniformity in time, the linear retreat trend from the mean retreat values shows that the retreat rate amounts to 0.36 cm/day, which is almost the same as the mean retreat (0.37 cm) (Figure 6.23).

Table 6.8. Data of short-term mangrove cliff retreat in Can Gio. Thirteen repeated measurements from 26 May 2009 at 23:00 to 08 June 2009 at 17:00 are shown.

	Periods of dataset												
Period name	**1**	**2**	**3**	**4**	**5**	**6**	**7**	**8**	**9**	**10**	**11**	**12**	**13**
From: dd/mm	26/05	27/05	28/05	29/05	30/05	01/06	02/06	02/06	03/06	04/06	05/06	06/06	07/06
hh	23	23	23	23	23	02	03	17	16	16	17	17	17
To: dd/mm	27/05	28/05	29/05	30/05	01/06	02/06	02/06	03/06	04/06	05/06	06/06	07/06	08/06
hh	23	23	23	23	02	03	17	16	16	17	17	17	18
Period (day)	1.00	1.00	1.00	1.00	1.13	1.04	0.58	0.96	1.00	1.04	1.00	1.00	1.04
Profile name	**Mean cliff retreat from 4 stations at a profile (cm)**												
1	0.00	1.25	0.25	0.00	0.00	1.83	2.38	0.83	0.35	0.00	0.08	0.38	0.00
2	0.00	0.13	0.13	0.00	0.00	0.00	0.00	0.60	0.00	0.00	1.50	0.00	0.00
3	0.13	0.88	0.08	0.00	0.00	1.75	6.08	1.18	5.20	0.13	1.65	0.00	0.00
4	0.00	0.13	0.00	0.15	0.13	0.00	0.75	0.00	0.00	0.00	0.18	0.00	0.00
5	0.00	0.35	0.08	0.00	0.00	0.00	0.50	0.18	1.00	0.33	0.93	0.00	0.00
6	0.00	0.00	0.00	0.15	0.00	0.50	0.25	8.15	0.00	1.00	15.93	0.00	0.00
7	0.10	0.00	0.00	0.23	0.00	0.00	0.00	0.13	0.00	0.00	0.00	0.00	0.00
8	0.13	0.63	0.08	0.00	0.00	0.00	0.00	0.00	0.00	0.00	0.15	0.00	0.00
9	0.13	0.13	0.25	0.28	0.00	0.13	0.15	0.00	0.00	2.25	0.50	0.00	0.00
10	0.13	0.13	0.00	0.00	0.00	5.40	0.00	0.88	0.20	0.00	0.63	0.00	0.00
11	0.10	0.00	0.00	0.08	0.00	0.00	1.88	0.15	0.00	0.50	0.58	0.13	0.00
12	0.00	0.13	0.00	0.25	0.00	0.25	1.13	0.00	0.00	0.00	0.00	0.00	0.00
13	0.13	0.00	0.00	0.11	0.08	0.15	0.00	0.25	0.00	0.00	0.00	0.00	0.00
14	0.88	0.18	0.13	0.13	0.13	0.13	0.38	0.75	0.10	0.08	0.30	0.00	0.00
15	0.13	0.08	0.00	0.13	0.00	0.70	2.25	0.28	0.50	0.00	3.38	0.00	0.00
16	0.00	0.13	0.00	0.00	0.08	0.20	0.38	1.13	0.30	0.00	0.95	0.08	0.00
17	0.00	0.13	0.95	0.20	0.00	0.23	0.00	0.00	0.25	0.33	0.25	0.00	0.00
18	0.00	0.00	0.08	0.15	0.00	0.00	0.60	0.38	0.00	0.00	0.10	0.00	0.00
19	0.00	0.00	0.13	0.08	0.00	0.00	0.15	0.38	0.00	0.20	0.20	0.08	0.00
20	0.00	0.15	0.00	0.00	0.00	1.13	2.18	1.63	0.75	0.18	0.35	0.23	0.00
21	0.25	0.25	0.00	0.00	0.00	0.23	0.00	0.00	0.00	0.00	0.00	0.08	0.00
	Mean cliff retreat (cm) from 21 profiles (84 stations)												
MR	0.10	0.22	0.10	0.09	0.02	0.60	0.91	0.80	0.41	0.24	1.32	0.05	0.00
CMR	0.10	0.32	0.42	0.51	0.53	1.13	2.04	2.84	3.25	3.49	4.80	4.85	4.85
MRR (cm/day)	0.10	0.22	0.10	0.09	0.02	0.58	1.56	0.83	0.41	0.23	1.32	0.05	0.00

MR: Mean Retreat; CMR: cumulative MR; MRR: Mean Retreat Rate.

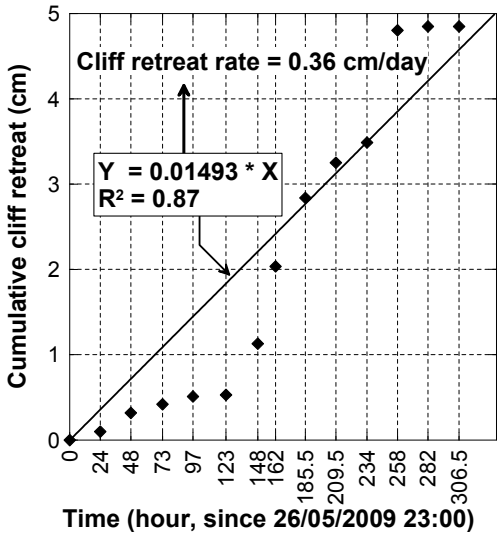

Figure 6.23. Cumulative values of cliff retreat. The linear trend is based on the 13 mean cliff retreat values.

Among the 13 cliff inundation values, the longest duration of inundation (in hour) exists for period six (see Figure 6.24a). From the first period until the seven period, the duration of cliff inundations are increasing. Period seven, which lasts 13.07 hours, represents only one high water; It is the turning point from neap tide to spring tide. From here, the duration of inundation is decreasing toward period thirteen.

During the whole measuring period, the wave directions at ST1-CG are almost perpendicular to the cliff; while close to cliff at station (ST2-CG) the wave directions are scattered. The wave heights close to the cliff (ST2-CG) are higher than the wave heights measured 100 m offshore (ST1-CG) (Figure 6.18). Consequently, the total wave energy at ST2-CG is higher compared to ST1-CG (Figure 6.24b). Normally, when waves propagate from deeper water into shallow water, the wave heights are decreasing. The opposite is observed here due to wave reflection from the cliff.

The cliff retreat together with hydrodynamic input is shown in Figure 6.24. There are two peaks of cliff retreat. The first peak (period seven) occurs during neap tide under low wave energy input, which does not change very much from periods one to seven. The cliff retreat is very small until period five and then suddenly increased during period six and seven During period seven, the time of inundation is highest. The second peak happens at the last stage of the dataset (period eleven) under relatively high wave energy input and shorter time of inundation.

From period seven to ten, the wave energy is increasing, while the retreat is decreasing. The retreat is highest at the eleventh values due to the highest total wave energy input. From periods eleven to thirteen, the retreats are decreasing rapidly. At the last value (period

thirteen), there is no any erosion although the wave energy is higher compared to the wave energy at the twelfth value. These data show that the cliff retreat is not only related to high wave energy input but is also influenced by the duration of tidal inundation.

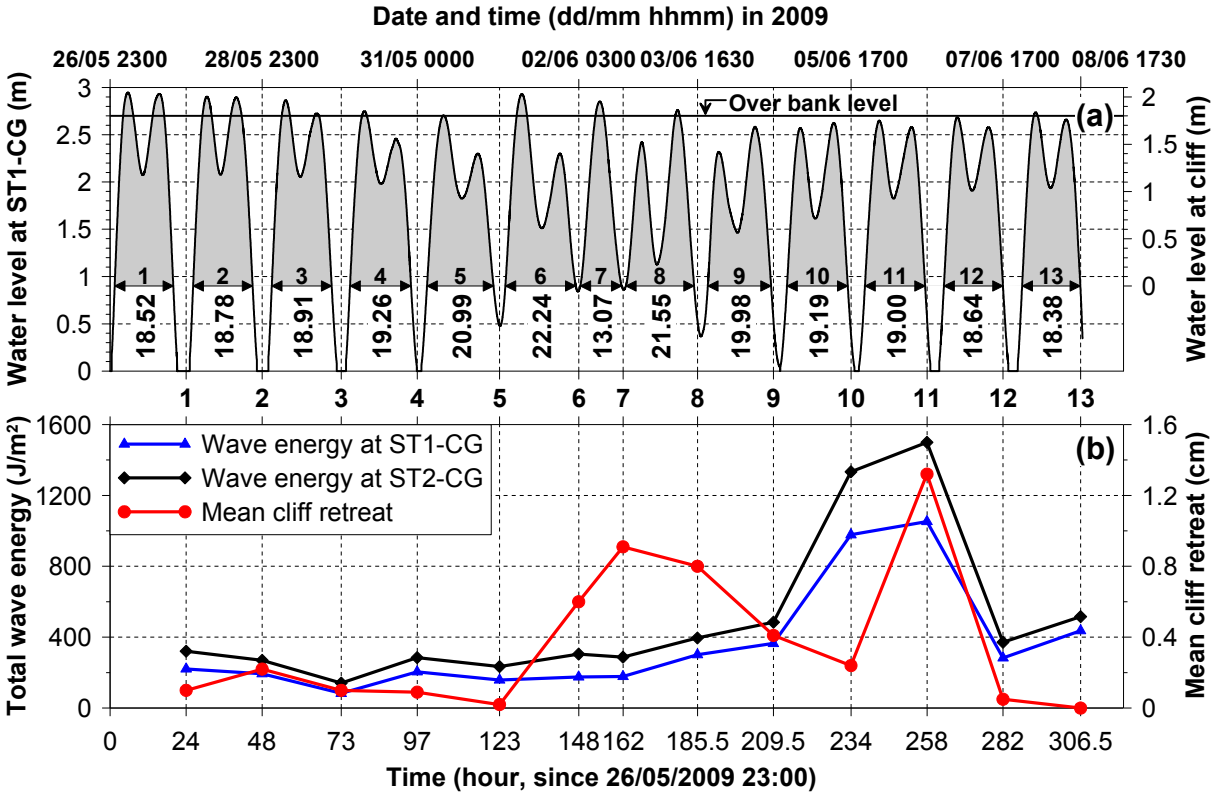

Figure 6.24. (a) Water level at the ST1-CG station and cliff inundation (grey area), numbers below the grey area indicate the durations of inundation (in hours). (b) Mean cliff retreat and wave energy at the ST1-CG and ST2-CG stations. The mean cliff erosion is the arithmetic mean of the cliff retreat at 84 stations.

This dataset shows clearly that the tide (or water level fluctuation) plays a key role in the process of mangrove cliff retreat in Can Gio. The cliff retreats are faster during neap tide than during spring tide. Without tides, waves would not reach the cliff to cause erosion. In addition, if water level changes are fast (during spring tide), or in other words, tidal inundations are short, waves not always cause erosion immediately. Even without wave energy influence, the mangrove cliff can retreat due to inundation.

6.2.6. Annual mangrove cliff retreat in Can Gio

The data regarding the annual mangrove retreat in Can Gio are listed in Table 6.9. This dataset is based-on 14 repeated measurements representing 315 days from 26 December 2007 to 5 November 2008. The time between the measurements lasted from one day up to 93 days. Because the time between to consecutive measurements was long, some erosion pins disappeared (length of erosion pin: 47 cm, erosion must have been ≥ 47 cm). This

happen especially for period three (93 days between two consecutive measurements) and period eight (63 days). Since 20/09/2008 (period ten), at each cliff retreat profile, were marked with benchmarks, which were deployed inside the mangrove forest (see Methods). In those cases when erosion pins on the profile were lost, the distance from the edge of cliff to the benchmark was measured to get the cliff retreat value. However, detail measurement from the vertical cliff profile were missed.

This dataset shows that the mangrove cliff retreats are not uniform in space and time. Therefore, in order to find the trend of the retreat, at each period, the mean retreat (MR) was calculated by averaging the retreats at 84 stations (from 21 profiles, 4 stations at each profile). The cumulative value of mean cliff retreat (CMR) was also calculated. The results are shown in Figure 6.25. Although there are some gaps, the linear trend from these values shows that the rate of cliff retreat is about 0.76 cm/day (or app. 2.76 m/year).

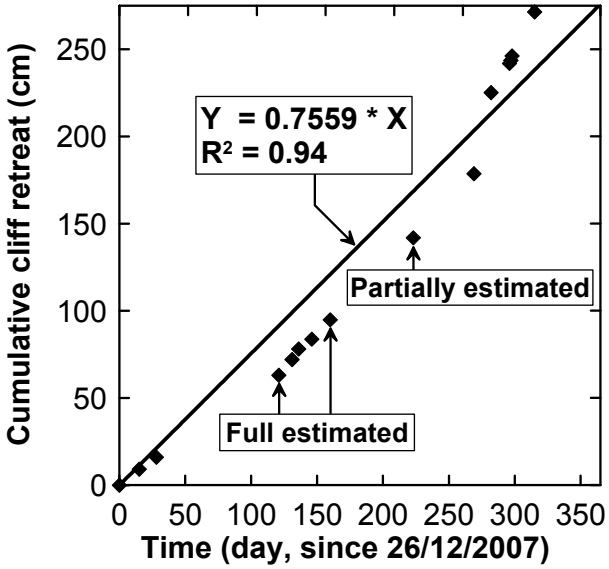

Figure 6.25. Cumulative values of cliff retreat. The linear trend is based on the 14 mean cliff retreat values (see also Table 6.9).

Filling the gaps

At some stations, the erosion pins could not be found, which indicate that the retreat was higher than 47 cm (which represents the length of an erosion pin). In those cases, gaps of data have been filled by data of the retreat trend, which was calculated from reliable values (Figure 6.26). In order to find the trend for filling these gaps, two datasets, (1) from period 4 to 7 and (2) from period 10 to 14, were chosen. Their linear trends show that the rate of cliff retreat varies from 0.839 cm/day (Figure 6.26a) to 2.233 cm/day (Figure 6.26b). These rates are very different from each other. Therefore, the gaps are filled by replacing the values of 47.0 cm at periods 3, 8, 9 using the following three trends:

(1) Lowest retreat: y = 0.839*Nd (trend (1), Figure 6.26a)

(2) Highest retreat: y = 2.233*Nd (trend (2), Figure 6.26b)

(3) Mean retreat: y = 1.536*Nd (the mean of trend (1) and (2))

Nd is number of days between two consecutive measurements. The results of these treatments are also listed in Table 6.9.

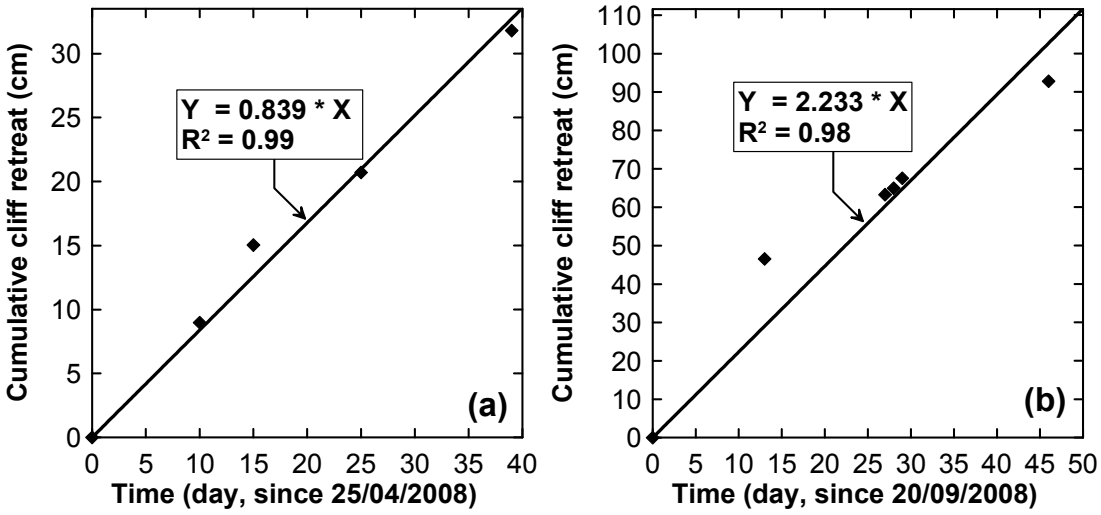

Figure 6.26. Cumulative cliff retreat and the linear trends for the reliable datasets. Fig. a for the dataset periods from 4 to 8 (4 measurements during 39 days). Fig. b for the dataset periods from 10 to 13 (5 measurements during 46 days).

The linear trends of the modified datasets show the rates of cliff retreat of about 0.89, 1.73, and 1.31 cm/day for the gaps. These gaps are filled by the three trends describe above, shown in Figure 6.27. From these trends, the annual rates of cliff retreat in Can Gio are estimated. They range from about 3.25 m/year to 6.32 m/year with a mean of 4.79 m/year (Figure 6.27). The minimum estimated annual rate of cliff retreat of 3.25 m/year, calculated from the modified dataset, is even higher than the original annual rate of retreat (2.76 m/year) where the gaps were filled with data representing 47.0 cm (length of erosion pin). Therefore, the annual mean rate of cliff retreat in Can Gio of about 4.79 m/year should be used.

Table 6.9. Annual mangrove cliff retreat in Can Gio including 14 repeated measurements from 26 December 2007 to 05 November 2008.

	Periods of dataset													
Period name	1	2	3	4	5	6	7	8	9	10	11	12	13	14
From: dd/mm/yy)	26/12/07	10/01/08	23/01/08	25/04/08	05/05/08	10/05/08	20/05/08	03/06/08	05/08/08	20/09/08	03/10/08	17/10/08	18/10/08	19/10/08
To: dd/mm/yy	10/01/08	23/01/08	25/04/08	05/05/08	10/05/08	20/05/08	03/06/08	05/08/08	20/09/08	03/10/08	17/10/08	18/10/08	19/10/08	05/11/08
Nd [1]	15	13	93	10	5	10	14	63	46	13	14	1	1	17
CNd [2]	15	28	121	131	136	146	160	223	269	282	296	297	298	315
Profile name	**Mean cliff retreat (cm) from 4 stations at a profile**													
1	4.7	**47.0**	**47.0**	8.6	20.7	14.3	**47.0**	**47.0**	**47.0**	11.7	5.6	0.6	1.0	25.8
2	1.9	0.9	**47.0**	23.9	15.7	0.2	**47.0**	**47.0**	**47.0**	4.2	24.4	0.8	3.4	42.3
3	4.9	3.1	**47.0**	13.6	1.5	18.8	18.6	**47.0**	35.4	15.5	15.4	18.7	7.0	28.1
4	3.2	0.3	**47.0**	1.8	0.0	1.0	2.8	**47.0**	**47.0**	2.6	0.6	0.2	0.4	2.1
5	5.9	1.0	**47.0**	0.6	0.7	0.3	1.8	**47.0**	**47.0**	1.9	2.3	0.3	0.2	1.9
6	3.5	0.5	**47.0**	1.3	**47.0**	2.6	27.3	**47.0**	29.6	10.7	27.5	0.2	1.9	19.6
7	3.0	0.8	**47.0**	24.2	22.8	4.4	0.4	**47.0**	15.5	6.3	36.4	0.2	2.2	9.1
8	32.5	2.7	**47.0**	8.4	3.0	10.7	6.5	**47.0**	36.5	17.1	135.7	0.0	0.6	1.0
9	2.0	4.9	**47.0**	3.0	0.5	2.8	2.5	**47.0**	25.4	98.0	3.4	0.3	1.6	5.7
10	0.8	12.0	**47.0**	11.0	5.5	8.8	26.1	**47.0**	**47.0**	114.0	2.1	0.5	1.1	88.0
11	6.5	3.8	**47.0**	4.0	0.0	0.5	1.1	**47.0**	36.9	19.7	36.5	6.5	12.9	38.6
12	21.8	10.4	**47.0**	1.6	0.6	0.8	0.8	**47.0**	27.9	114.0	2.6	0.2	0.0	4.1
13	**47.0**	3.8	**47.0**	3.9	0.5	3.8	3.1	**47.0**	32.0	4.9	26.1	0.3	5.6	23.6
14	9.9	7.4	**47.0**	15.0	5.4	28.6	13.9	**47.0**	39.0	107.0	1.3	0.2	6.7	114.0
15	7.3	2.5	**47.0**	5.4	0.1	0.1	0.5	**47.0**	37.5	96.0	2.6	0.1	1.3	1.7
16	16.2	18.8	**47.0**	6.0	0.4	2.3	3.8	**47.0**	**47.0**	152.0	1.7	0.5	0.0	2.2
17	6.5	8.0	**47.0**	2.6	0.8	1.0	3.1	**47.0**	35.8	155.0	0.5	0.2	0.0	32.1
18	3.3	3.7	**47.0**	24.8	0.5	16.6	1.8	**47.0**	**47.0**	18.3	0.3	0.4	1.4	17.0
19	5.0	2.8	**47.0**	6.3	1.0	0.6	3.4	**47.0**	22.9	2.3	1.3	0.2	0.6	**47.0**
20	3.9	6.0	**47.0**	10.3	0.5	0.0	7.0	**47.0**	21.8	17.8	18.6	4.6	3.8	6.8
21	2.9	4.4	**47.0**	12.4	0.2	1.1	14.5	**47.0**	**47.0**	8.5	7.0	0.2	3.2	19.6
	Mean cliff retreat (cm) from 21 profiles (84 stations)													
MR[3]	9.2	6.9	**47.0**	9.0	6.1	5.7	11.1	**47.0**	36.8	46.5	16.7	1.7	2.6	25.2
CMR[4]	9.2	16.1	63.1	72.0	78.1	83.8	94.9	141.9	178.6	225.2	241.9	243.6	246.2	271.4
Modified data: for stations with lost erosion pins, the value of cliff retreat is replace by calculation using the linear trend 'y = 0.839*Nd'														
MR1	9.2	6.9	78.0	9.0	6.1	5.7	11.1	52.9	38.6	46.5	16.7	1.7	2.6	25.2
CMR1	9.2	16.1	94.1	103.1	109.1	114.8	125.9	178.7	217.3	263.9	280.6	282.3	284.9	310.1
Modified data: for stations with lost erosion pins, the value of cliff retreat is replace by calculation using the linear trend 'y = 2.233*Nd'														
MR2	9.2	6.9	207.7	9.0	6.1	5.7	11.1	140.7	102.7	46.5	16.7	1.7	2.6	25.2
CMR2	9.2	16.1	223.7	232.7	238.8	244.4	255.5	396.2	498.9	545.5	562.2	563.9	566.5	591.7
Modified data: for stations with lost erosion pins, the value of cliff retreat is replace by calculation using the linear trend 'y = 1.536*Nd'														
MR3	9.2	6.9	142.8	9.0	6.1	5.7	11.1	96.8	70.7	46.5	16.7	1.7	2.6	25.2
CMR3	9.2	16.1	158.9	167.9	173.9	179.6	190.7	287.5	358.1	404.7	421.4	423.1	425.7	450.9

[1] Nd: number of days of two consecutive measurements; [2] CNd: cumulative number of days since 26/12/07; [3] MR: mean cliff retreat from 21 profiles; [4] CMR: cumulative MR.
Estimated data are in bold.

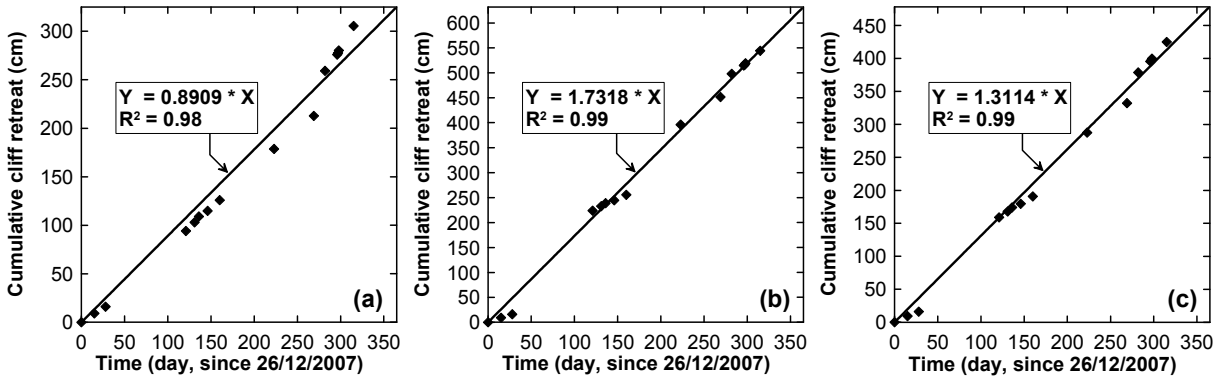

Figure 6.27. Cumulative cliff retreat and linear trends from the modifications of the original data by replacing gaps. For figure a, the trend was calculated using CMR1 (see Table 6.9), for figure b the trend was calculated using CMR2, and for figure c, the trend as derived from CMR3.

6.2.7. Mechanism of mangrove cliff retreat

The mangrove cliff in Can Gio is eroded in various ways. It is either eroded relatively uniform from the top to bottom, named surface erosion, (Figure 6.28a) or notched from the bottom, which means the lower part is eroded faster than the top part, Figure 6.28b, when the notch has reached a certain size, the whole block of cliff collapses due to slope failure (Figure 6.28c). Notched erosion and slope failure were observed more often than surface erosion. The surface erosion was found at locations where the cliff height is less than the mean height (1.8 m) and the mangrove trees are distributed less densely.

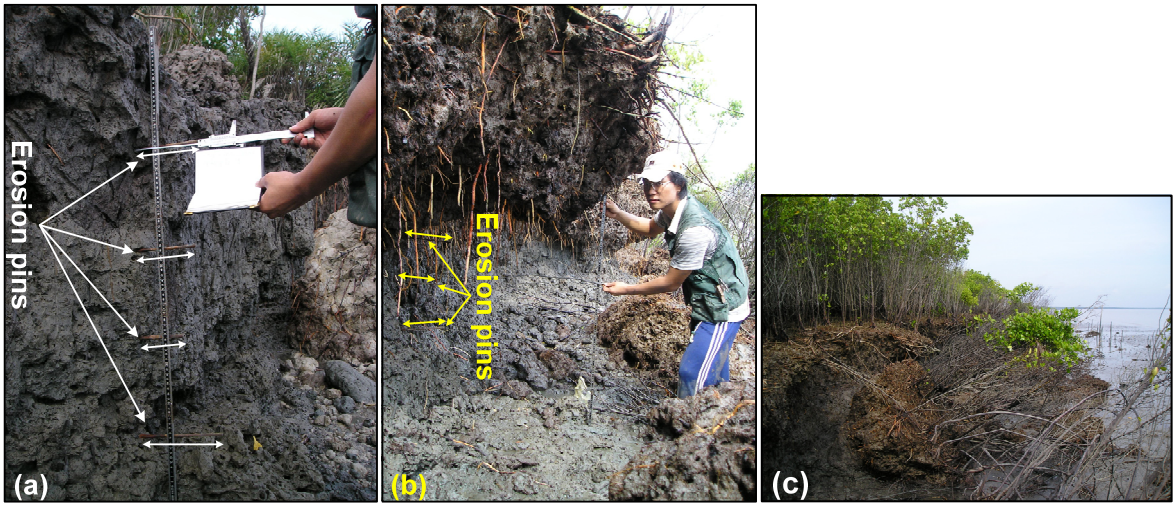

Figure 6.28. Types of mangrove cliff erosion in Can Gio: (a) surface erosion; (b) notch erosion, and (c) slope failure erosion.

6.2.8. Topographical change on the tidal flat

On a transect from the edge of the mangrove cliff to the tidal flat, the topography was measured twice between 17 October 2008 and 26 May 2009 (about seven months). These

topographies show that the cliff has retreated but the topography in front of the cliff almost did not change (Figure 6.29). This demonstrates that the eroded sediment from the cliff is washed out from the area.

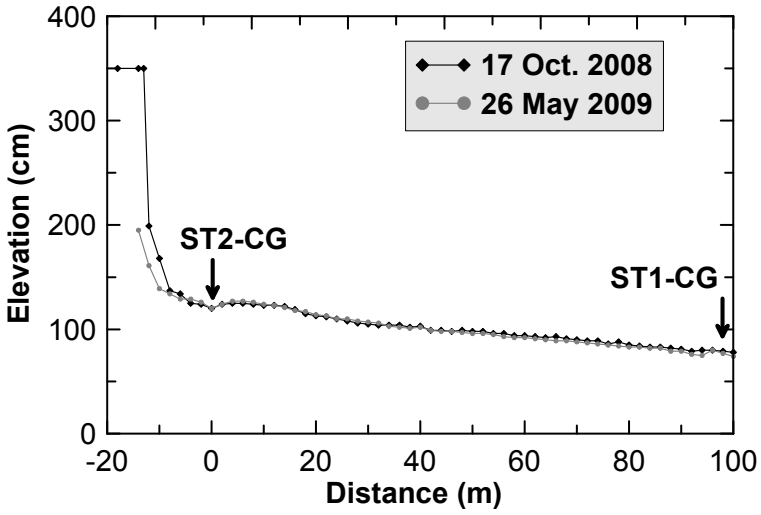

Figure 6.29. Topographical changes on the tidal flat in Can Gio.

6.3. Driving factors of mangrove cliff retreat in Bo De

6.3.1. General introduction

To understand the driving processes on acting on the mangrove cliff causing retreat at Bo De site. The results are mainly based on the measuring campaign, which was carried out from April to May 2009. Besides this measuring campaign, two datasets of current velocity one from inside the river mouth and the second from outside the river mouth, but both close to the study site were collected end of March 2008.

Bathymetry around the river mouth was surveyed on 06 May 2009 (for method see Chapter 54.4). Data of the currents regime around the river mouth are based-on two datasets, which were obtained by using an ADCP at two mooring stations. One at the inner (MS2-BD) mouth, about 3 km inside at the water depth of about 31 m, and the other at outer river mouth (MS1-BD), about 1,5 km out side at the mean water depth of 11 m (Figure 4.1c). The periods covered by these datasets is about 22 hour during spring tide for each position.

Tide data at the study area are based on a 16-day dataset of water levels, which was measured at the tidal creek about 1 km onshore of the study area, at BD-WL station (Figure 4.1, Table 5.1). This water level dataset was analyzed and compared with the water level dataset from Vung Tau tide gauge station to calculate tidal characteristics as well as to estimate the long-term water level fluctuations at this site (see Chapter 6.1.2).

For measuring mangrove cliff retreat and related parameters at the study site in Bo De, a profile long of 110 meters along the shoreline was selected to measure the cliff retreat at 10 profiles, with vertical three positions for each profile (Figure 5.1b1, b3). The height of this cliff varies from 0.4 m to 1.0 m (0.7 m on average). The retreats were measured using erosion pins (see Chapter 5.2.1). There are 13 repeated retreats measured during the period from 27 April to 8 May 2009. The retreats were measured almost every day.

Besides cliff retreat measurement, current and wave data, water level and suspended load data were recorded at two stations located at about 16 m (ST2-BD) and 96 m (ST1-BD) on the tidal flat in front of from the cliff (Figure 4.1a, c, Figure 5.1b1, b2). The period of this survey lasted from 26 April at 23:00 to 11 May 2009 at 19:00. The instruments (Midas DWR devices) were setup to collect the data every 30 min with a 4 Hz sampling rate, and about 17 min burst duration (4096 samples per burst). The CTD recorded the data every 1 min.

The grain size distributions of the sediment of the cliff are based on the samples, which were taken close to cliff retreat stations. Sediment samples from the tidal flat were also taken for grain size analyzes. The shear strength of the cliff soil was measured at positions close to the

cliff retreat stations using the Pocket Vane Tester device. After measuring the shear strength, the sediment samples were taken at those positions.

In addition, air pressure, temperature, and wind velocity were measured at the light house close to the study site at about 5 m above the sea level.

6.3.2. Bathymetry around the study site Bo De

A deep channel and steep slopes characterize the bathymetry around the river mouth. The channel depth reaches more than 30 meters. From the river mouth to the open sea, the main channel becomes narrower and shallower (Figure 6.30a). The channel depth decreases from 18.0 m at the river mouth to 10.4 m at about 1500 m offshore with gradually about 0.5 m every 100 m. From the river mouth to the inner part, the main channel is much deeper and wider compared to the outer part (Figure 6.30a). The width of the channel is about 300 m and the steepness of the channel flank is 16% (Figure 6.30b).

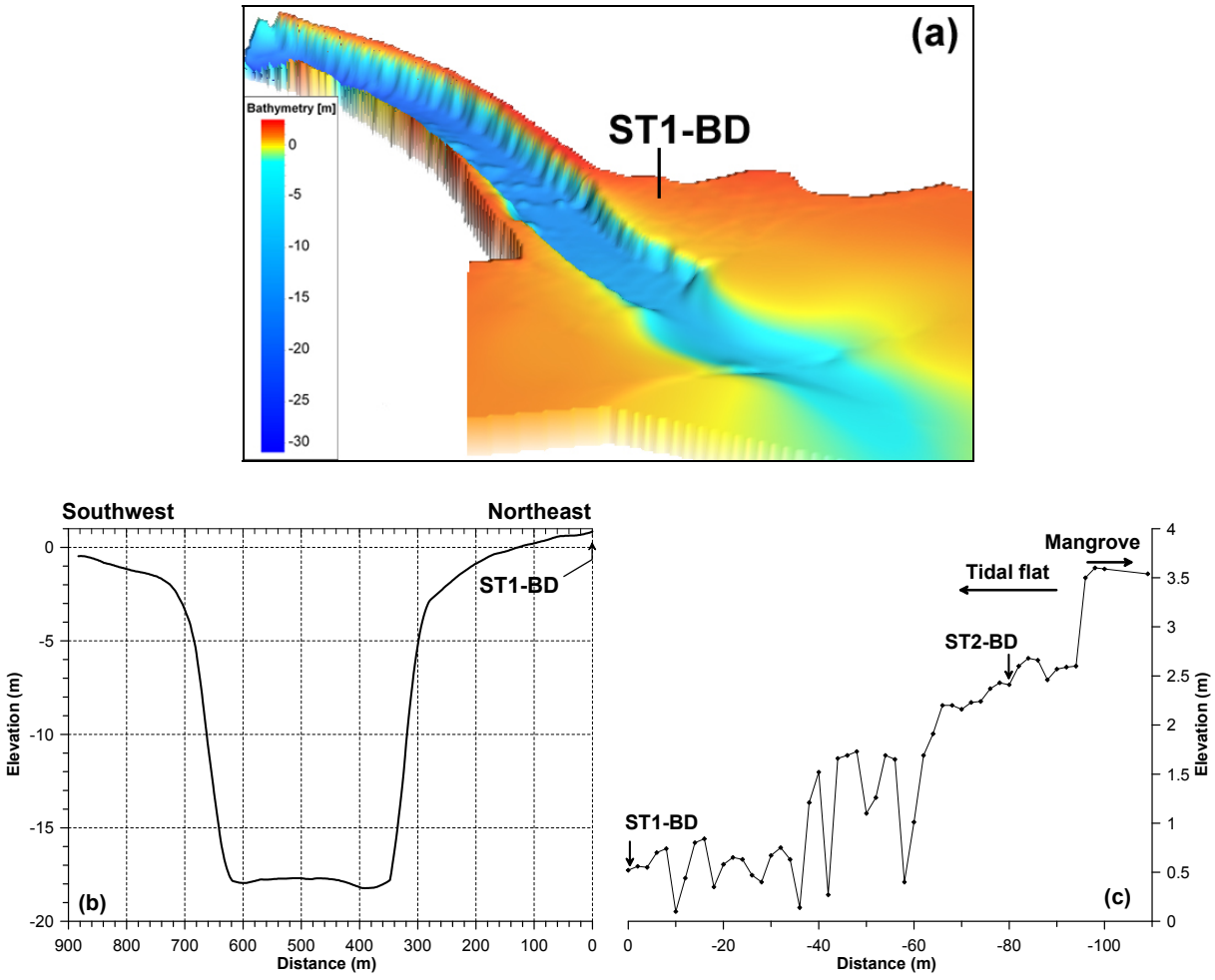

Figure 6.30. (a) 2.5D view of the bathymetry around Bo De tidal channel mouth; (b) southwest-northeast cross-section along the Bo De tidal channel mouth and (c) morphological profile from the tidal flat to the mangrove shoreline crossing the measurement station ST1-BD and ST2-BD. Reference level: Vung Tau tide gauge station.

The tidal flat at the study site in Bo De shows many scour holes. In the past, this area was belonging to the old mangrove belt. Recently, it is exposed as a tidal flat are due to strong erosion processes (Figure 6.30c). The slope gradient along a 100-m transect in the tidal flats amounts about 2.1%, which is very high and not typical for tidal flat.

6.3.3. Asymmetries of tide and tidal current around the Bo De tidal channel

The tide at Bo De tidal channel was measured using a CTD, which was deployed close to the river mouth (station BD-WL, Figure 4.1, Figure 5.4). Water levels were recorded every minute during summer 2009 from 27 May to 10 June 2009, (see Chapter 6.1.2). This dataset was used for calculating the tidal characteristics at this location.

As mentioned in Chapter 6.1, the tide at the Bo De tidal channel is mixed, mainly semi-diurnal. The flood phase is 28 minutes shorter than the ebb phase; the mean tidal range is 2.56 m.

Ebb current speed is faster than the flood current (Figure 6.31, Figure 6.32). At the surface, the maximum ebb speed of 1.15 m/s, which is about 36% higher than the maximum flood speed of 0.74 m/s (Figure 6.31a1-1, b1). Near the bottom, the maximum speeds of the ebb and flood currents are about 0.8 m/s and 0.58 m/s, respectively (Figure 6.31a3). Hence, the maximum ebb current speed is about 27% higher than the flood current. The depth averaged velocities (mean velocities) are also dominated by the faster ebb current, which has a higher mean velocity (0.89 m/s) of 40% compared to the maximum mean flood current (0.53 m/s) (Figure 6.31a2). The highest current speeds from the surface to the near bottom decrease about 30% and 21% for ebb and flood currents, respectively.

Outside Bo De tidal channel (MS1-BD station), the ebb current directions for the whole water column range from ESE-SSE, where SE is the main direction (Figure 6.31b, c), while the flood current directions are scattered around W-NNW. The mean flood current direction is mainly NW but at the surface and near the bottom, they differ by about 45 degrees. The main direction at the surface is WNW while it is NNW near the bottom.

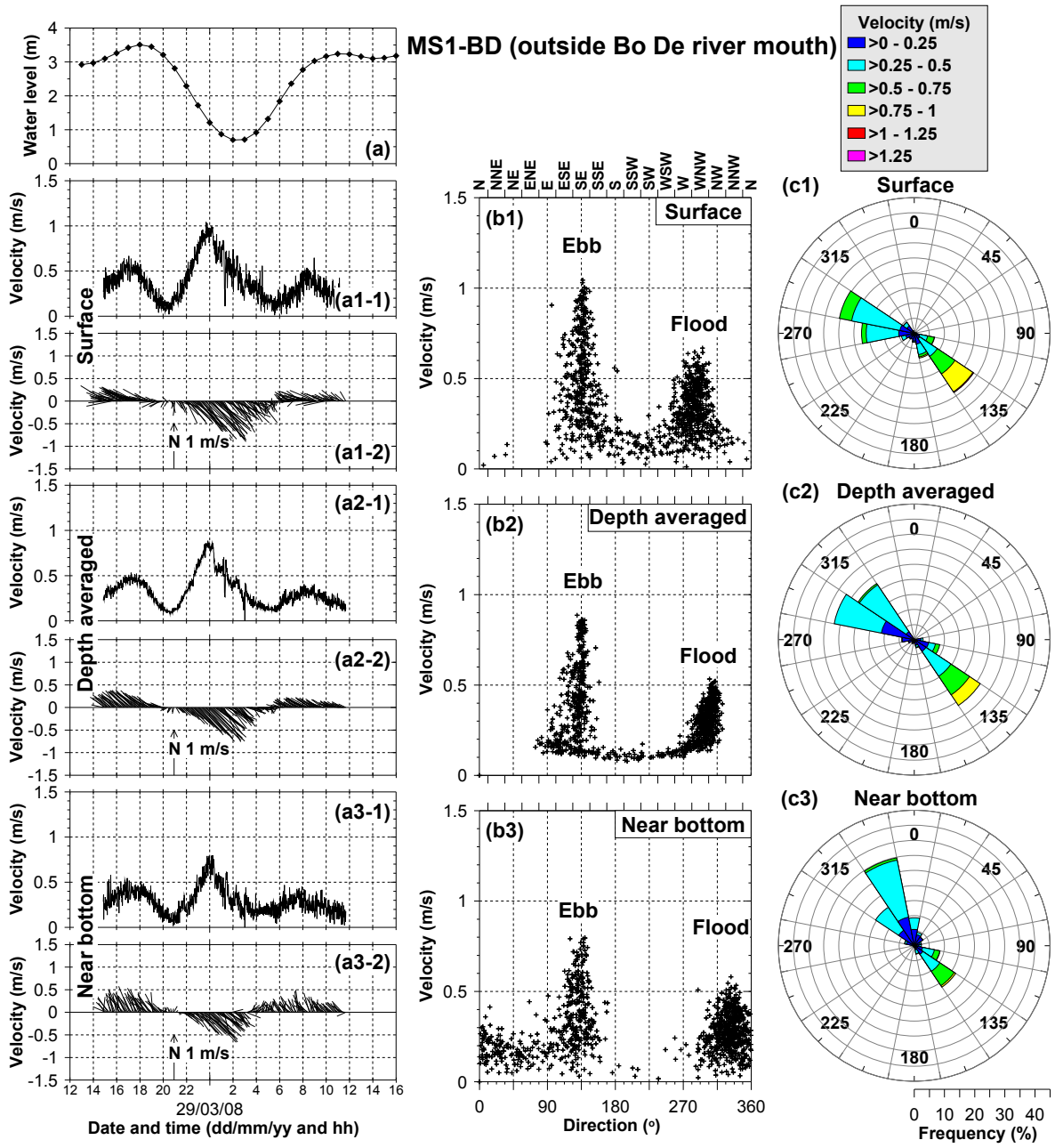

Figure 6.31. Station MS1-BD: Diagrams showing the current velocities outside Bo De tidal channel mouth. (a) Time series plot of predicted water levels at Bo De tidal channel mouth (BD-WL station). (b) Time series graphs of current speed and vector of current velocities at the surface(a1-1, a1-2), the depth averaged (a2-1, a2-2), and near the bottom (a3-1, a3-2). Diagrams of current speeds and directions at the surface (b1), the depth averaged (b2), and near the bottom (b3). Directional distribution of current velocities at the surface (c1), depth averaged (c2), and near bottom (c3).

At the inner Bo De tidal channel mouth station (MS2-BD), the ebb current directions range from ENE-E (Figure 6.32b, c), while the flood current directions range from WSW to W, with the dominant direction being WSW. The speed of the ebb current is almost homogeneous from the surface to the bottom, while the speeds of the flood current decrease from the surface to the bottom. At the surface, maximum ebb and flood current speeds are about 1.1 m/s. However, higher speeds of 1.0 m/s occur more often during flood period compared to ebb period (Figure 6.32a1, b1).

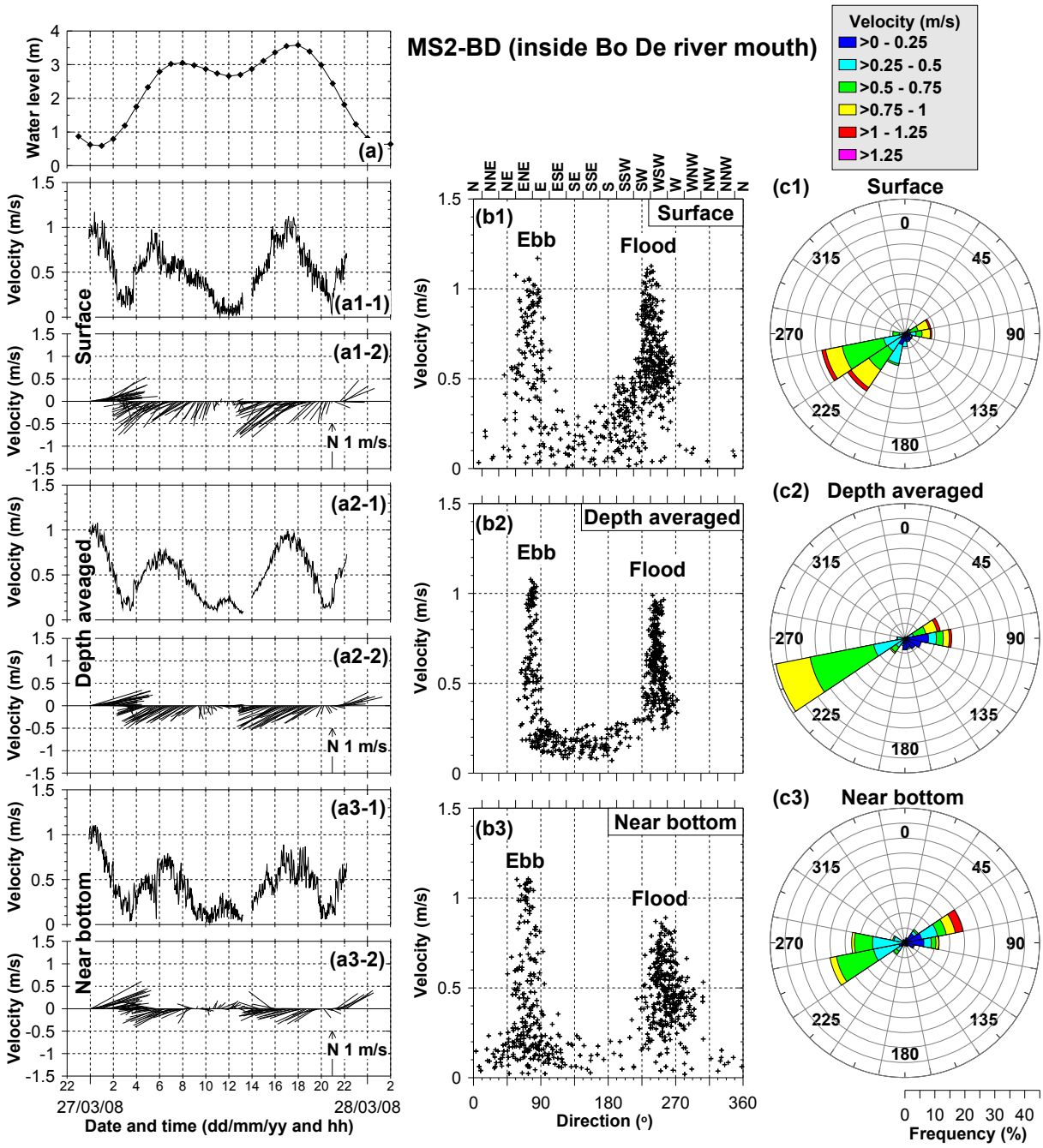

Figure 6.32. Station MS2-BD station: Diagrams showing the current velocities insides Bo De tidal channel mouth. (a) Time series plot of predicted water levels at Bo De tidal channel mouth (BD-WL station). (b) Time series graphs of current speed and vector of current velocities at the surface(a1-1, a1-2), the depth averaged (a2-1, a2-2), and near the bottom (a3-1, a3-2). Diagrams of current speeds and directions at the surface (b1), the depth averaged (b2), and near the bottom (b3). Directional distribution of current velocities at the surface (c1), depth averaged (c2), and near bottom (c3).

Near the bottom, the maximum ebb current speed is 1.1 m/s, which is approximately 18% higher than the maximum flood current (0.9 m/s) (Figure 6.32a3, b3). Regarding the entire water column, the highest depth averaged velocity occurs during the ebb phase. In summary, the maximum speeds of the ebb and flood phase are 1.1 m/s and 1.0 m/s (Figure 6.32a2, b2). The maximum flood speeds mostly decrease from the surface to the bottom. In

contrast, the maximum ebb speeds are almost uniform from the surface to the bottom (Figure 6.32b1-3). In the flood phase, the maximum speed at the bottom is about 18% less than that at the surface.

6.3.4. Soil properties of the mangrove cliff and tidal flat

6.3.4.1. Shear strength of the mangrove cliff soil

The shear strength values of the mangrove cliff in Bo De are distributed inconsistently. Its values vary from 0.1094 to 0.33 kg/cm^2, where shear strengths of 0.16-0.17 kg/cm^2 are the most dominant values (see Figure 6.33). The shear strengths at the top and the middle are quite scattered (0.1094 - 0.3281 kg/cm^2), while those at the bottom are concentrated around the mean value of 0.1668 kg/cm^2. The mean shear strengths decrease from top to bottom (Table 6.10, Figure 6.33). On average of all 30 stations, the mean shear strength is 0.1923 kg/cm^2 (standard deviation of 0.0594).

Table 6.10. Shear strength values of the mangrove cliff soil at all 30 stations of the study site in Bo De.

Shear strength (kg/cm^2)				
Profile name	**Position 1 (Top)**	**Position 2 (Middle)**	**Position 3 (Bottom)**	**Mean**
C1	0.2461	0.2187	0.2187	0.2278
C2	0.1640	0.1094	0.1640	0.1458
C3	0.1640	0.1640	0.1640	0.1640
C4	0.3007	0.1094	0.1640	0.1914
C5	0.1640	0.1640	0.1367	0.1549
C6	0.1914	0.2187	0.1640	0.1914
C7	0.2187	0.2187	0.1640	0.2005
C8	0.3281	0.2734	0.1640	0.2552
C9	0.1640	0.1094	0.1094	0.1276
C10	0.2734	0.3007	0.2187	0.2643
Mean	0.2214	0.1886	0.1668	
Max				0.3281
Min				0.1094
Mean				0.1923
Standard deviation, SD				0.0594

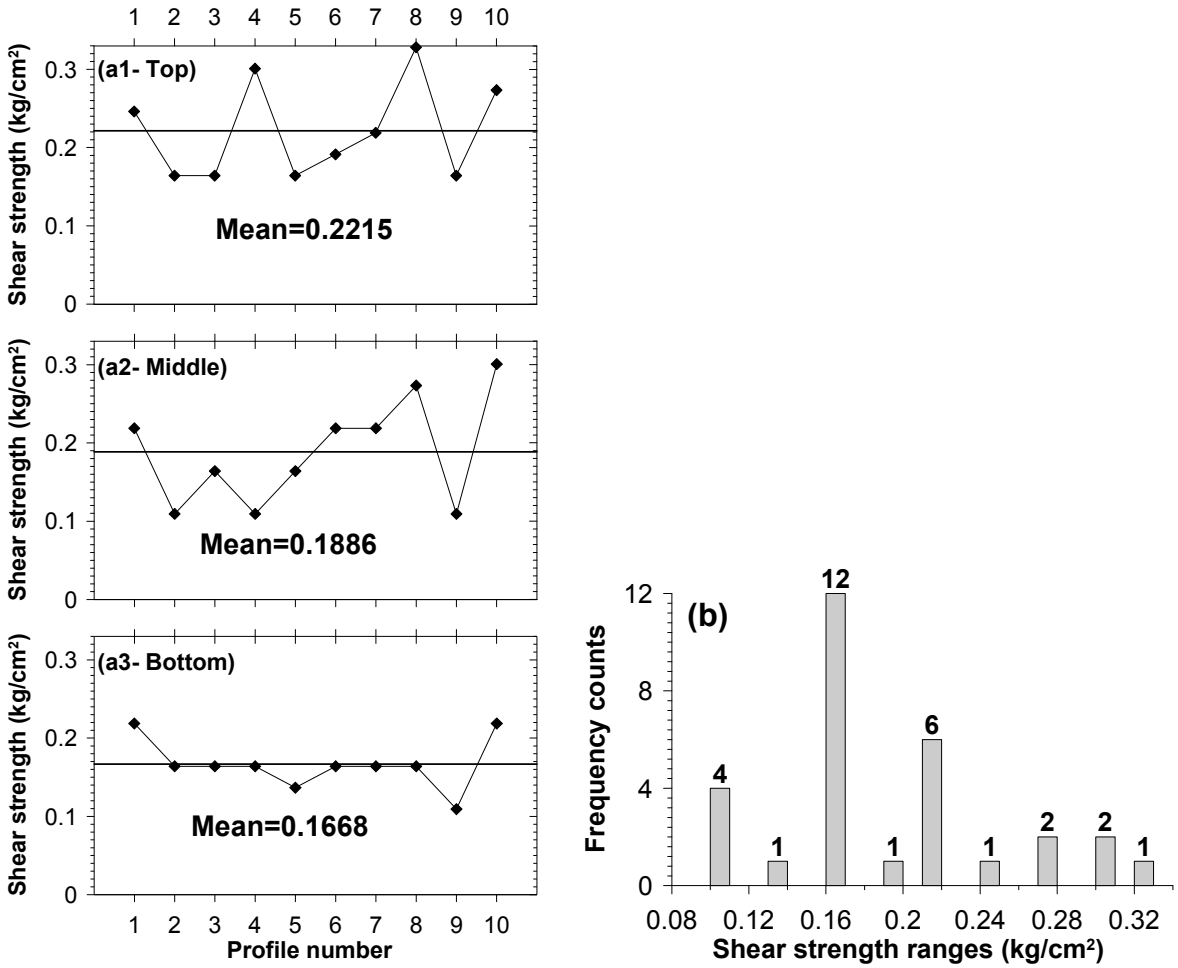

Figure 6.33. Shear strengths of the mangrove cliff in Bo De. Figures (a1-a3) show the shear strength variations at three levels on 10 locations along a profile. Mean shear strength values at each part are marked by bold line; Figure b shows the distribution of all shear strengths values due to their occurring frequencies.

6.3.4.2. Grain size distributions of the mangrove cliff and tidal flat soils

In Bo De, 30 sediment samples were taken along the 10 profiles at three vertical positions of each profile (top, middle, and bottom). Its grain size distributions are shown in Figure 6.34a. Bo De cliff sediment consists of very fine material with the dominant mode ranging from fine to medium silt. Within 30 samples, 22 samples are unimodal and 8 samples show bimodal grain size distribution. The first mode ranges from 5.83 to 10.56 µm (from fine to medium silt). The second mode ranges from 42.24 to 206.03 µm (from very coarse silt to fine sand). On average of 30 samples, the mud content is 93.5% and sand content is 6.5%.

Two samples from the tidal flat (taken at ST1-BD and ST2-BD) were also analyzed to compare the sediment grain size distribution from the tidal flat with those from the mangrove cliff. Their grain size distributions show the dominant mode at 8-10 µm (medium silt). At ST2-BD, the second mode has a grain size of 76 µm (very fine sand, Figure 6.34b). These results imply

that the grain size distribution of the tidal flat sediments correlate with the mangrove cliff sediments. Additionally, it reflects that the tidal flat was the mangrove area in the past.

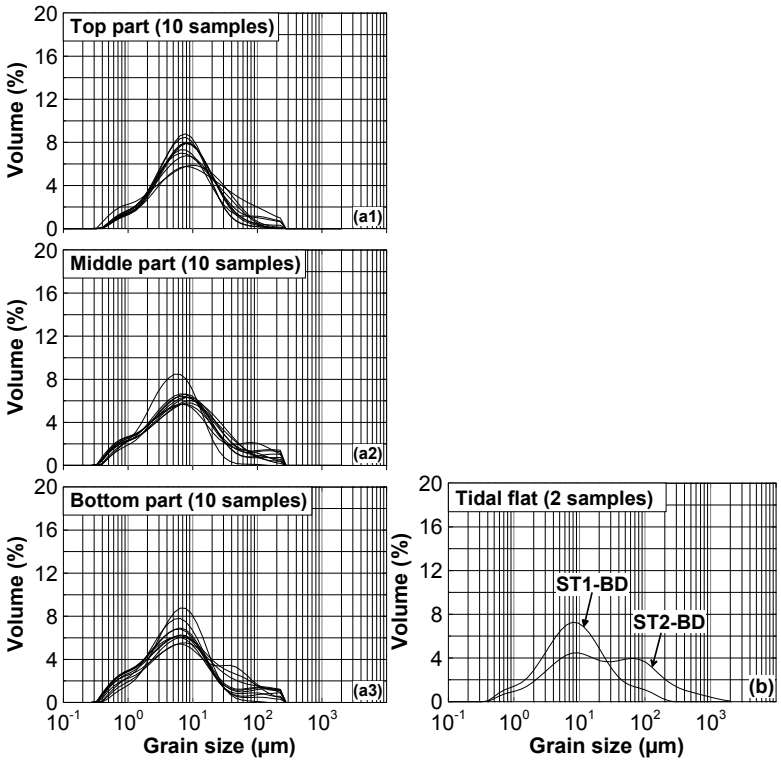

Figure 6.34. Grain size distributions of the soil on the mangrove cliff (a) and tidal flat (b) in Bo De.

6.3.5. Short-term mangrove retreat in Bo De and influencing parameters

6.3.5.1. Meteorological oceanographic conditions

Wind

During the measuring campaign, wind directions from SSW to W prevailed (Figure 6.38). The wind usually blows strongly in the afternoon. Its maximum speed was about 6 m/s. During the measuring period, the area was influenced by a tropical storm that was formed from a tropical depression on 03 May 2009 at 12:00. The low pressure center was about 600 km from the study site in Bo De. On 03 May at 18:00, it was upgraded to tropical storm called the *Chan-hom.* This storm moved northerly in the South China Sea. After 06 May 2009, this storm was no longer any influence on the study area (Figure 6.35).

Although this tropical storm was located far from the coast and did not influence the study site directly, nonetheless some impacts were observed from 02 May 2009. During the tropical storm period it was camp. The sea surface state was very smooth and only swell waves were observed. Light rains occurred with highest rainfall measured about 13 mm.

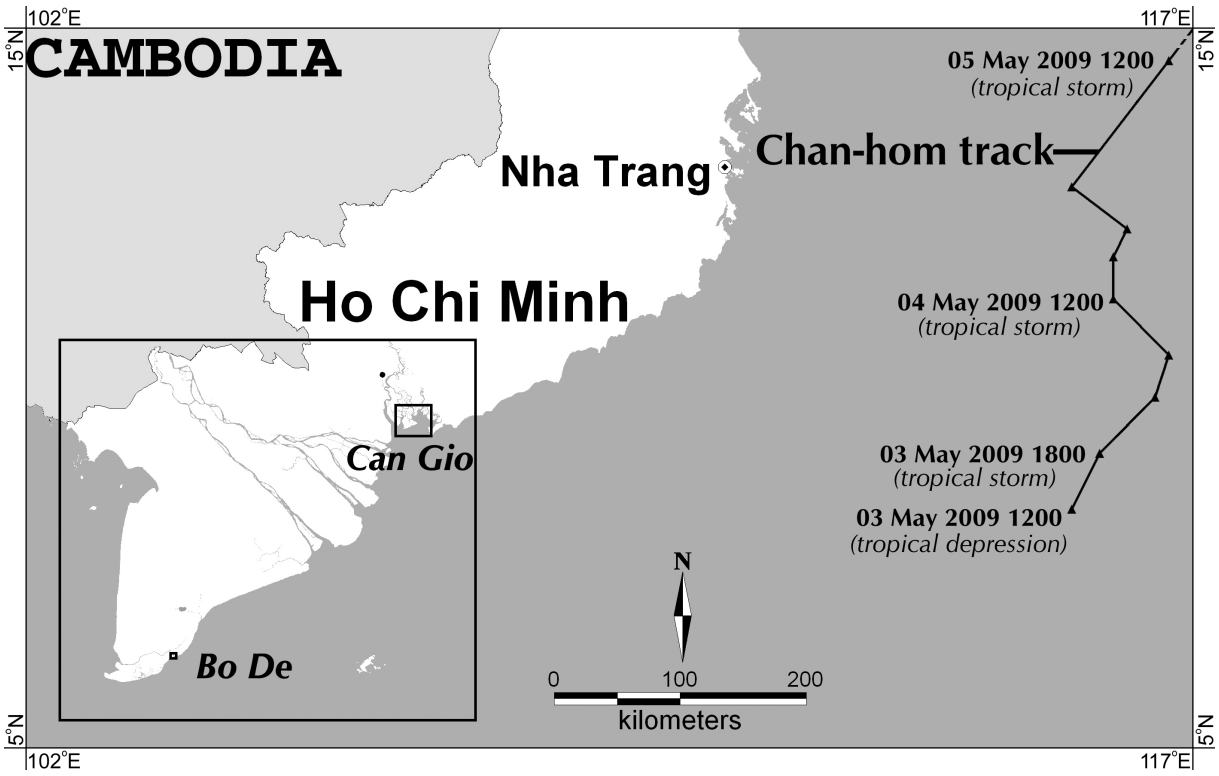

Figure 6.35. The study area showing the first stage of the track of the tropical storm, the Chan-hom 2009.

Water level variations and inundation

For the measuring campaign, the water level variations on the tidal flat are shown in Figure 6.36. This dataset from station ST1-BD (tidal flat) was captured one full neap tide (at middle stage) and two half spring tides (the beginning and end stages). During this period, the tidal flat (considered from ST1-BD station to the cliff) was exposed totally for about 6.6 hours at six lower low waters during spring tide. The cliff was exposed for about 5.68 days, accounting for about 41% of the total time span of the field campaign.

There are 13 coupled two pairs of high-low water and one single pair of high-low water (or the turning point at period eight, Figure 6.36c). In total, there are 27 high waters and 26 low waters (excluding two low waters at the beginning and end of the dataset). The high water of this single pair occurs on 5 May 2009 at noon during neap tide. From the beginning of the dataset until the turning point, there are seven coupled two pairs of high-low water. Six coupled two pairs of high-low water occur after the turning point until the end of the measurements. At each coupled two pairs of high-low water, the high water heights are almost the same during spring tides but differ of about 0.7 m during neap tide. The lower low water (LLW) levels increase from the beginning of the dataset until the turning point of the neap tide. Afterwards, the LLW levels decrease again until the end of the measurements (Figure 6.36a).

At each coupled two pairs of high-low waters, the tidal periods during neap tide are usually longer than those during spring tide (Figure 6.36b). Additionally, the levels of lower low waters are higher during neap tide. Therefore, the water level changes (or range of tide) during neap tide are slower. Hence, the area is inundated longer during neap tide (Figure 6.36c).

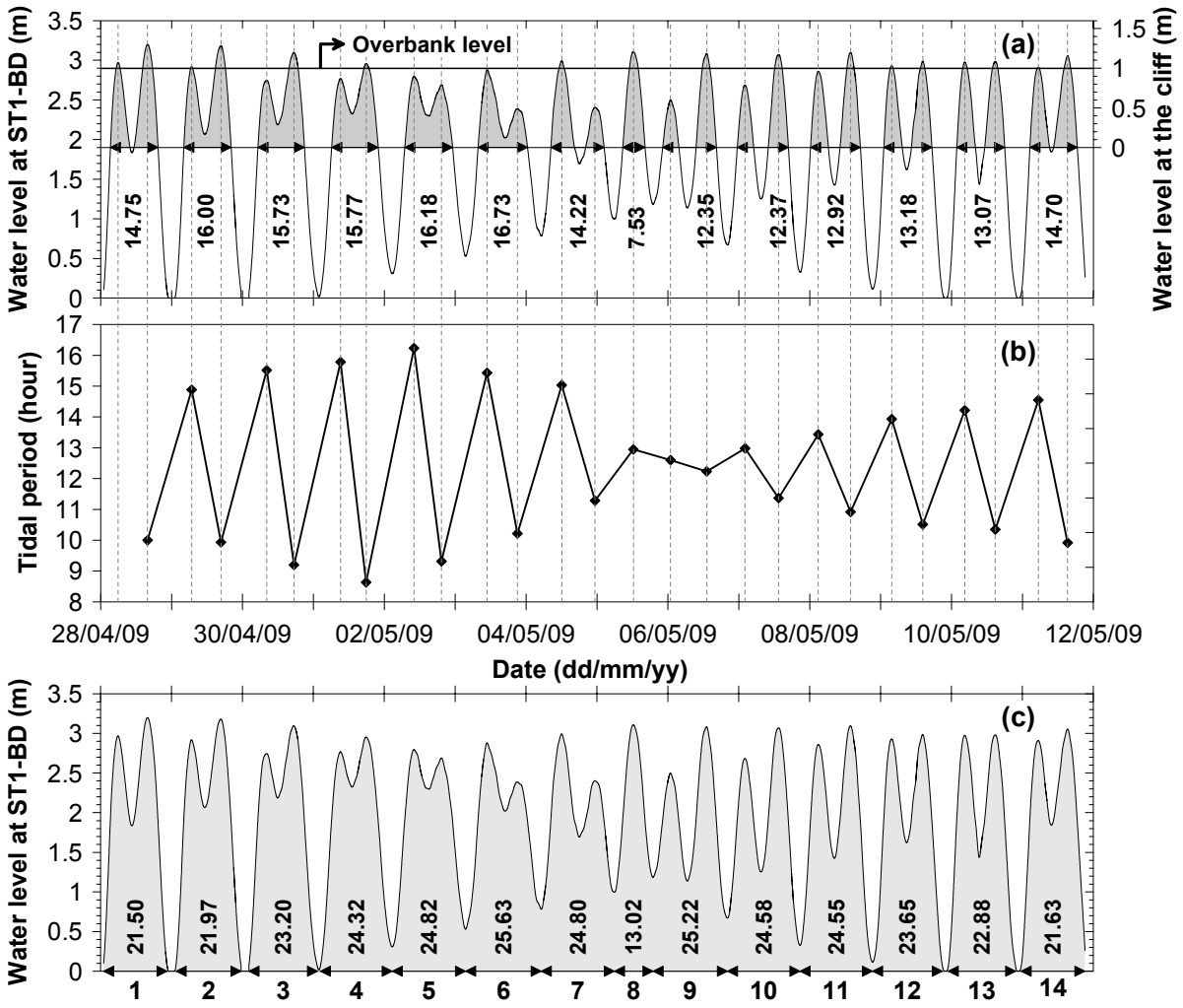

Figure 6.36. Time series plots of water level (a) and tidal period (b) at the tidal flat station (ST1-BD). In Fig. a, the grey part above 1.9 m level is marked as the inundation level at the foot of the mangrove cliff. The bold line at 2.7 m (left axis) is marked for the over bank level (cliff fully inundated). The arrows with the numbers below indicate the duration of inundation (in hours) of the cliff. The zero level on the left axis of Fig. a indicates the water level of the height from station ST1-BD. The tidal periods in Fig. b provide the duration between two consecutive high waters.

Salinity and water temperature

The 14 days dataset of salinity on the tidal flat (ST1-BD) at the Bo De tidal channel mouth shows that the area is fully influenced by marine water. Although the salinities during neap tide are slightly higher compared to those during spring tide (Figure 6.37a, b), the difference

between the highest (32.2 ppt) and lowest (30.3 ppt) salinities is not significant (about 1.9 ppt). On average, the mean salinity is about 31.6 ppt (standard deviation of 0.4).

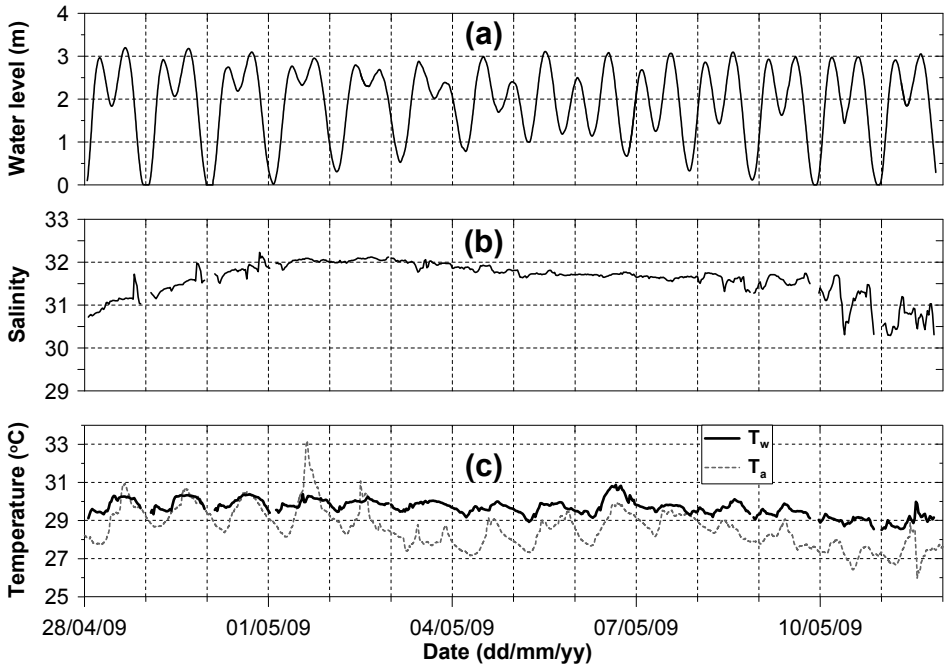

Figure 6.37. (a) Time series plots of water level, (b) salinity, (c) and water temperature and air temperature (T_w and T_a), at the ST1-BD station.

During this period, the water temperature (T_w) ranges between 28.5 and 30.9 °C, with the mean temperature of about 29.7 °C. The T_w fluctuations usually follow air temperature variations rather than tidal variation (Figure 6.37a, c). The variations of water temperature are almost the same as those of the air temperature (T_a). The peaks of high and low T_w usually coincide with the peaks of T_a. However, the water temperatures are mostly higher than the air temperatures.

Waves

During the field campaign, waves occur intensively at the study area. Peaks of wave height (H_s) during the daily tidal cycle mostly exceed 0.4 m and mainly occur in the afternoon during high tides. Wave heights during neap tide are usually higher than during spring tides. Peaks of wave heights at the ST2-BD station are usually higher than the peaks at the ST1-BD station. The maximum significant wave heights at ST2-BD and ST1-BD were about 0.72 and 0.62 m (Figure 6.38a, b). On average during the 14 days period, the mean significant wave heights at ST2-BD and ST1-BD were about 0.35 and 0.29 m.

At ST1-BD, wave heights in the range from 0.2-0.3 m area dominant accounting for about 41.1% of total wave heights (Figure 6.38a5). At ST2-BD, wave heights in the range between 0.3-0.4 m are dominant, accounting for about 40% of total wave heights (Figure 6.38b1).

At ST1-BD, the wave approaches range from SE to S, with SSE as the dominant direction (Figure 6.38a2, a3, a4). The distribution of wave energy according to wave direction shows that 98.9% of the wave energies are transferred to the coast by waves approaching from SE to S directions. Waves approaching from SSE transfer about 51.2% of the total energy to the coastline (Figure 6.39a). Wave periods range from 3 - 9 s, with the dominant period of 7-second, accounting for about 28.8% (Figure 6.39c). The distribution of wave energies related to wave period shows that the 4-secod and 7-second periods content about 50% of the total wave energies (Figure 6.39b). Longer wave periods (>= 7 seconds) were measured during two days (4-5 May 2009), during neap tide (Figure 6.39c). These waves coincide with the *Chan-hom* tropical storm that influenced this area (see also Figure 6.35).

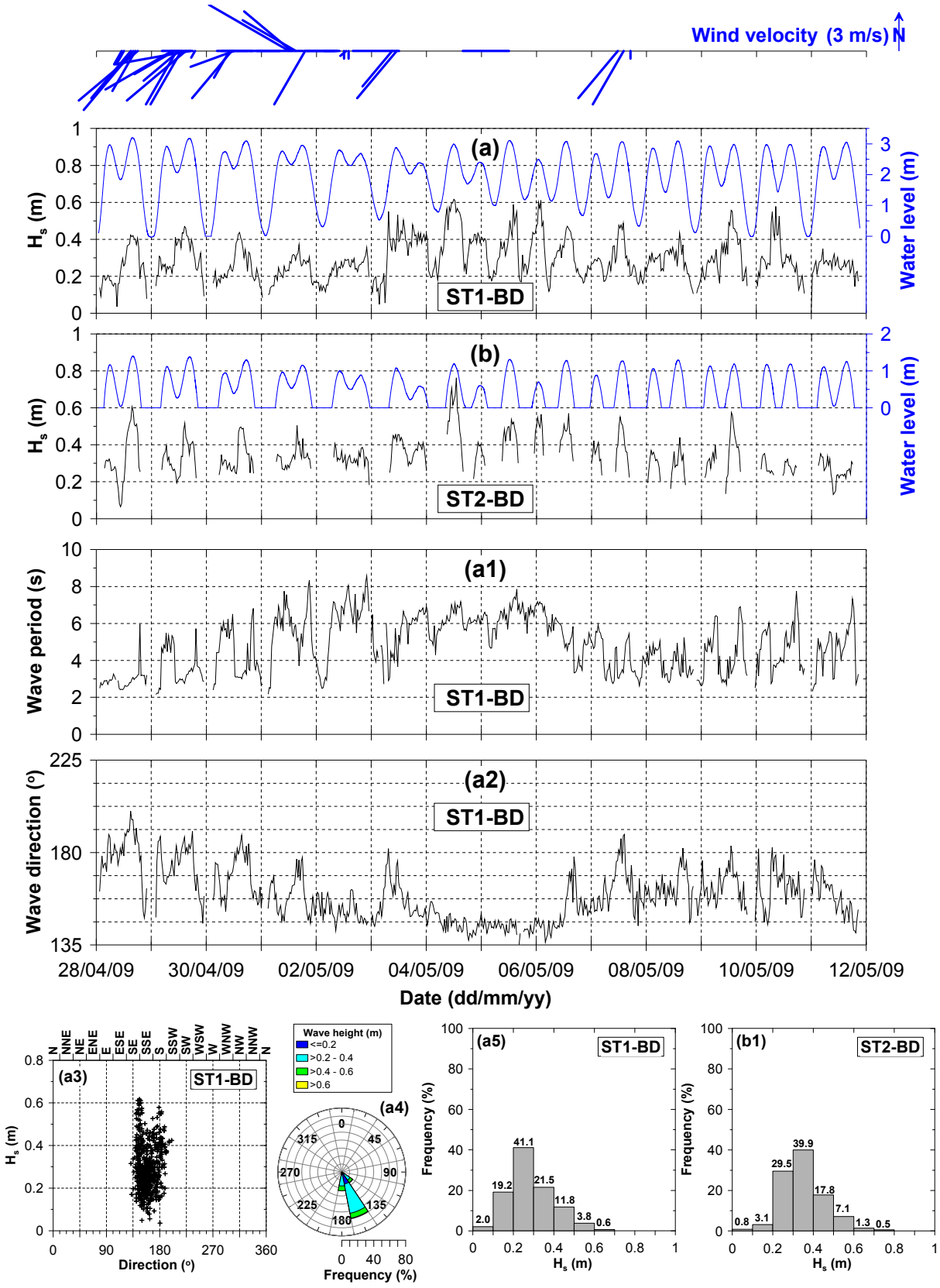

Figure 6.38. Graphs of incident wave and tidal influenceon the mangrove cliff including vector plot of wind velocities. Figures a, b are time series plots of significant wave height (H_s) including water level at the ST1-BD and ST2-BD stations. Fig. a1, a2 are time series plots of mean wave period and mean wave direction at ST1-BD; Figure a3, a4, a5 are the diagram of H_s versus wave direction, directional distribution of H_s, frequency distribution of H_s at ST1-BD, respectively. Fig. b1 is frequency distribution of H_s at ST2-BD.

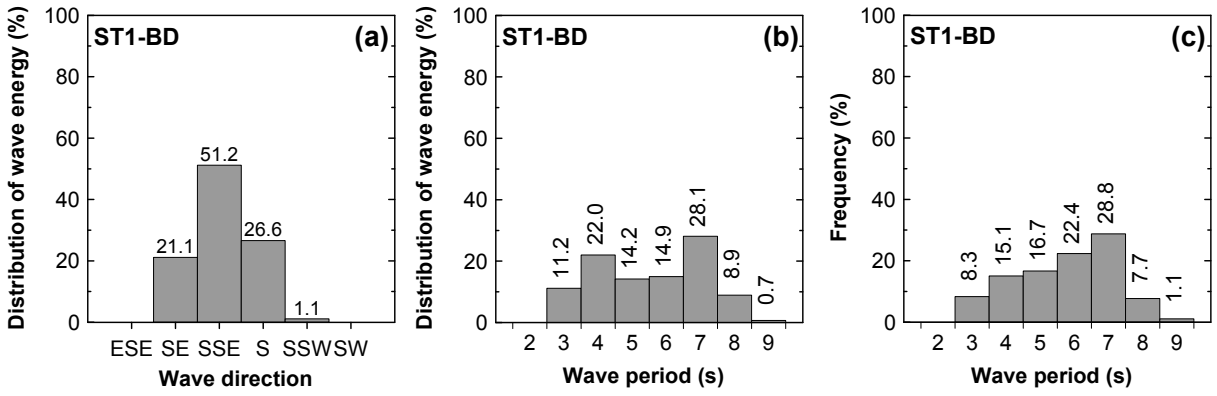

Figure 6.39. Wave characteristics at the ST1-BD station. (a) Directional distribution of wave energy; (b) Distribution of wave energy by mean wave period; (c) Frequency distribution of mean wave period.

Current

The current velocities at station ST1-BD strongly show the asymmetry between ebb and flood currents (Figure 6.40). The direction of flood current is mainly NNE. Conversely, the ebb current directions are usually from SSW to SW (Figure 6.40, c). The peaks of flood current are higher compared to peaks of ebb current speeds. Particularly, higher peaks of flood current prevail at those times when the ranges of tide (from higher low water to high water are small (Figure 6.40a, b). The maximum flood current speed (0.6 m/s) is about 3 times higher than the maximum ebb current speed (0.19 m/s). On average during the 14 days, the mean flood speed (0.19 m/s) is 3.6 times higher than the mean ebb speed (0.05 m/s).

During 14 days, current velocities smaller than 0.1 m/s are predominantly, accounting for about 58.1% of the time (Figure 6.40d). Velocities ranging between 0.5-0.6 m/s seldom occur, accounting for only about 1.3% all measured data.

The strong asymmetry of the current can be explained by wave influence. waves mostly approach from SSE, therefore, they enhanced the flood current speeds and reduced the ebb current speeds.

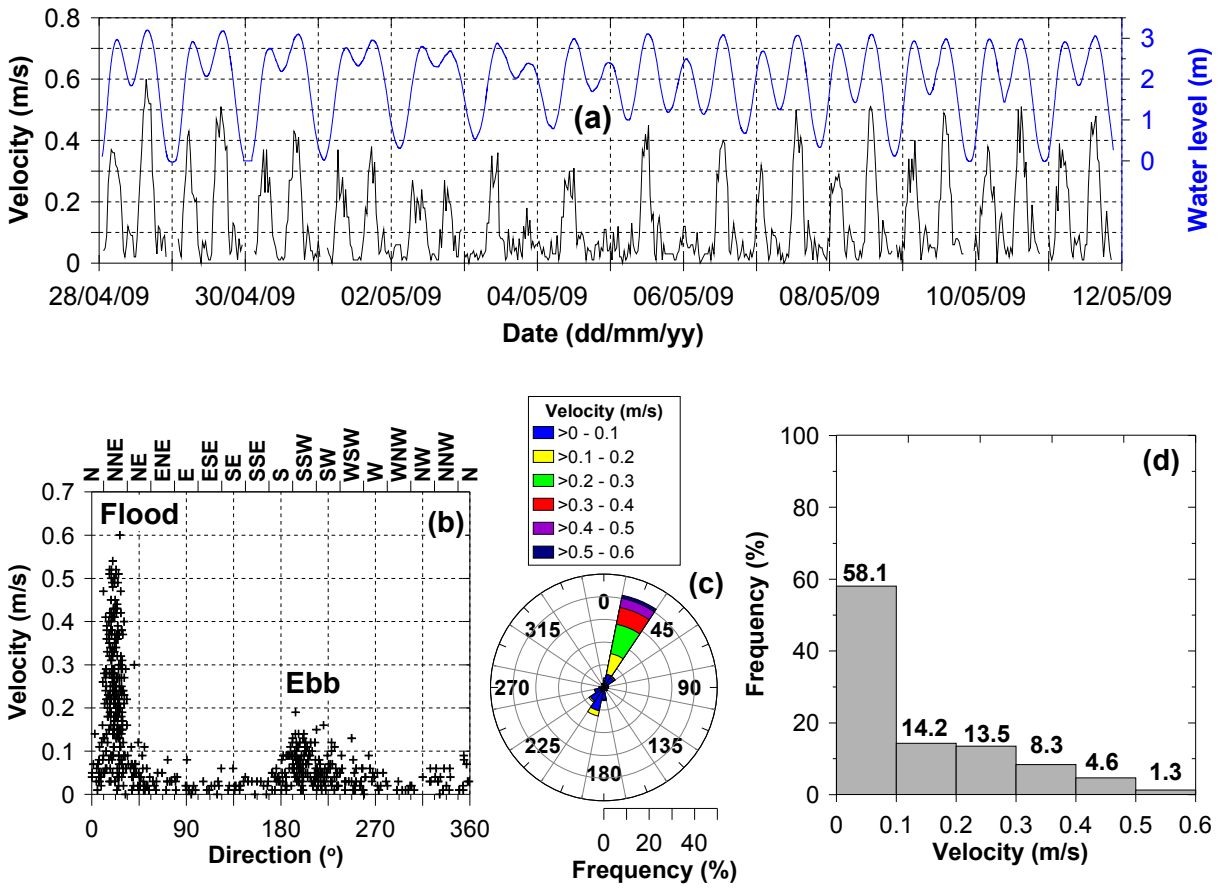

Figure 6.40. Graphs showing water level and current velocity at the tidal flat station (ST1-BD). Fig. a presents a time series plot of current velocity including water level. Fig. b, c, d are diagrams of current velocities versus directions, directional distribution of current velocity, and frequency distribution of current velocity.

Suspended matter

At ST1-BD, most of the highest of concentration of suspended sediment (SSC) occurs during ebb tide when the tidal ranges are small (Figure 6.41c). During the rising tide, the SSC values are small.

During the 14 day period, maximum and minimum values of SSC were about 0.861 and 0.058 g/l. The mean SSC was about 0.223 g/l (standard deviation of 0.1). However, SSC values higher than 0.8 g/l occurred only one time, on 28 April 2009 at 8:00 am. The SSC values are mainly in the range from 0.1-0.4 g/l (accounting for about 90% of measured values during 14 days), where the range from 0.1-0.2 g/l is most dominant (account for about 45.5%) (Figure 6.42).

Although the flood currents are much faster than the ebb current, the SSC values of the flood tides are very small compared to those of ebb tide (Figure 6.41a, b, c). The peaks of SSC neither follow immediately the actions of high waves nor high current speeds. These peaks mainly occur around the end of the ebb phase stage after the striking of high waves.

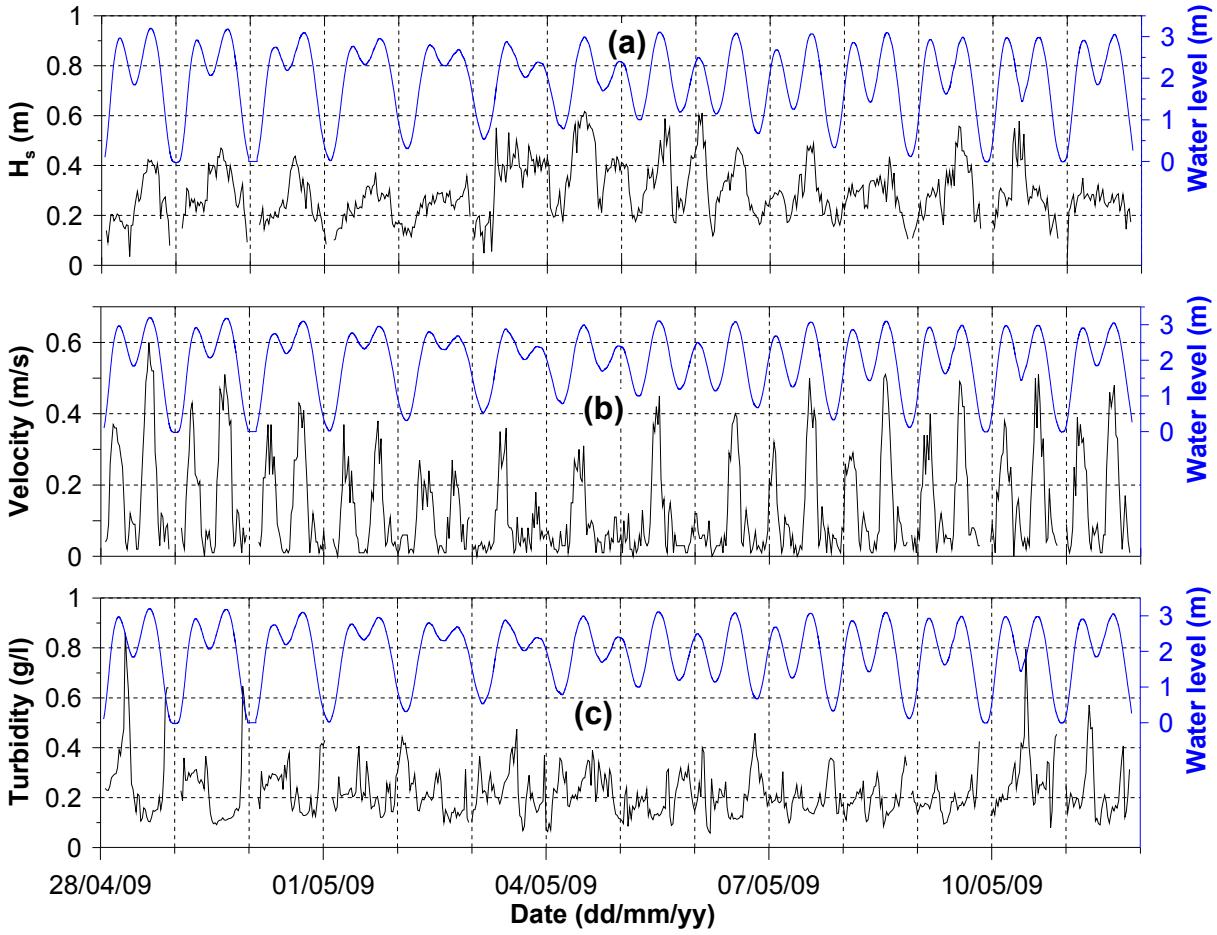

Figure 6.41. Time series of significant wave height (a), current velocity (b), and suspended sediment concentration (c) including the water level at the ST1-BD station.

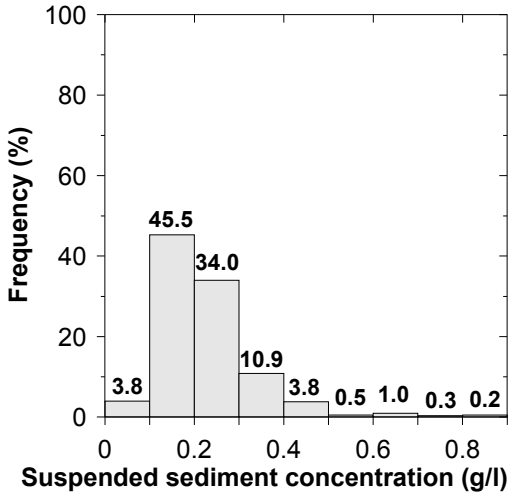

Figure 6.42. Frequency distribution of suspended sediment concentration.

6.3.5.2. Short-term mangrove cliff retreat and affecting factors

The subchapter provides data about the tidal and wave influence acting on the cliff. Along the mangrove cliff, there are 13 repeated cliff retreat measurements during about 332 hours (~ 13.8 days) from 27 April at 23:00 to 11 May 2009 at 19:00.

During the measurement period, no cliff retreat occurred for about 33.6% of the time. The maximum retreat is about 47.0 cm. The mean retreat for the whole period is about 2.5 cm, with a standard deviation of about 6.0. These values (Table 6.11) show that the cliff retreat is relatively high and non-uniform in time and space.

The mean cliff retreat values (MR, Table 6.11) from all measurements in Bo De vary from 0.9 to 8.2 cm, and 2.5 cm on average. The mean retreat rates (MRR, Table 6.11) vary from about 0.86 to 3.83 cm/day, with 2.38 cm/day on average. The linear cliff retreat trend shows that the retreat rate is about 2.51 cm/day (Table 6.11, Figure 6.43)

Table 6.11. Short-term mangrove cliff retreat in Bo De including 13 repeated measurements during the whole period from 27 April 2009 at 23:00 to 08 May 2009 at 19:00.

	Periods of dataset (in 2009)												
Period name	1	2	3	4	5	6	7	8	9	10	11	12	13
From dd/mm	27/04	28/04	29/04	30/04	02/05	03/05	04/05	05/05	06/05	07/05	08/05	09/05	10/05
hh	23	22	23	23	00	06	05	07	06	08	09	19	19
To dd/mm	28/04	29/04	30/04	02/05	03/05	04/05	05/05	06/05	07/05	08/05	09/05	10/05	11/05
hh	22	23	23	00	06	05	07	06	08	09	19	19	19
Period (day)	0.96	1.04	1.00	1.04	1.25	0.96	1.08	0.96	1.08	1.04	1.42	1.00	1.00
Profile name	Mean cliff retreat from 3 stations at a profile (cm)												
1	1.9	4.1	7.9	3.5	1.6	7.7	4.2	2.4	3.5	3.6	8.8	8.1	4.7
2	10.7	3.2	3.8	2.5	6.9	3.7	0.3	1.1	0.0	0.2	1.2	3.1	0.1
3	3.2	4.1	4.5	2.4	3.8	5.7	12.4	0.8	1.5	2.9	1.7	0.8	3.4
4	0.9	0.6	0.7	0.5	0.0	0.5	0.2	0.0	0.2	0.3	1.1	1.4	0.5
5	1.4	1.1	0.8	0.2	0.3	0.1	0.2	0.0	0.1	0.2	0.4	0.4	0.4
6	0.8	3.5	1.3	5.3	1.9	13.6	6.8	0.0	0.0	0.0	0.3	0.2	0.0
7	0.3	0.0	0.0	0.0	0.3	0.0	0.3	0.0	2.7	0.0	3.8	0.3	0.3
8	1.3	1.4	0.2	0.3	0.2	2.0	0.8	0.4	0.1	0.0	0.9	0.4	0.0
9	0.5	1.7	1.8	0.2	0.4	2.8	47.0	27.2	2.6	1.3	6.2	0.6	1.0
10	0.6	0.5	0.8	0.0	0.4	0.5	10.1	2.8	4.0	0.4	3.2	0.3	0.0
	Mean cliff retreat (cm) (from 30 stations)												
MR	2.2	2.0	2.2	1.5	1.6	3.7	8.2	3.5	1.5	0.9	2.8	1.6	1.0
CMR	2.2	4.2	6.3	7.8	9.4	13.1	21.3	24.8	26.3	27.2	29.9	31.5	32.5
MRR (cm/day)	2.25	1.94	2.17	1.44	1.26	3.83	7.61	3.63	1.36	0.86	1.95	1.57	1.04

MR: Mean Retreat (mean cliff retreat from 30 stations at 10 profiles); CMR: cumulative MR; MRR: Mean Retreat Rate.

Mean cliff retreat and mean cliff retreat rate for all dataset are about 2.38 cm and 2.51 cm/day, respectively.

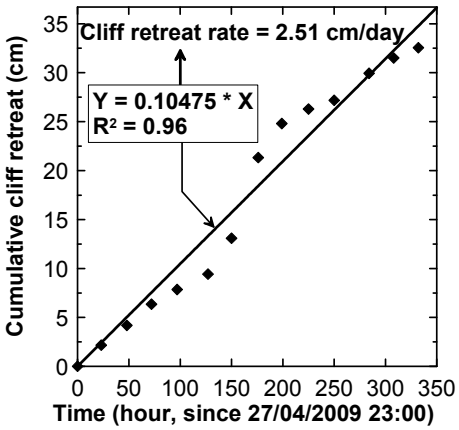

Figure 6.43. Cumulative cliff retreats and linear trend based on the 13 mean cliff retreat values during the period from April 2009 at 23:00 to 08 May 2009 at 19:00.

Thirteen mean cliff retreats together with the inundation of the cliff and total wave energy inputs at the ST1-BD and ST2-BD stations are shown in Figure 6.44. These data show that the cliff retreat during neap tide is higher than during spring tide. However, the retreat relates mainly to high wave energy inputs than to the duration of inundation. Peaks of cliff retreat coincide with peaks of wave energy (Figure 6.44b).

During neap tide, the highest retreat value is 8.2 cm simultaneously with the highest total wave energy input of 4,932 $J.m^{-2}$ at ST1-BD and 3,979 $J.m^{-2}$ at ST2-BD. The lowest retreat amounts 0.89 cm corresponding with the lowest total wave energy input (about 2,132 and 2,481 $J.m^{-2}$ at ST1-BD and ST2-BD). The highest cliff retreat and total wave energy input occurred from 4 to 6 May 2009 during neap tide. At this time, the area was influenced by the Chan-hom tropical depression/storm (Figure 6.35).

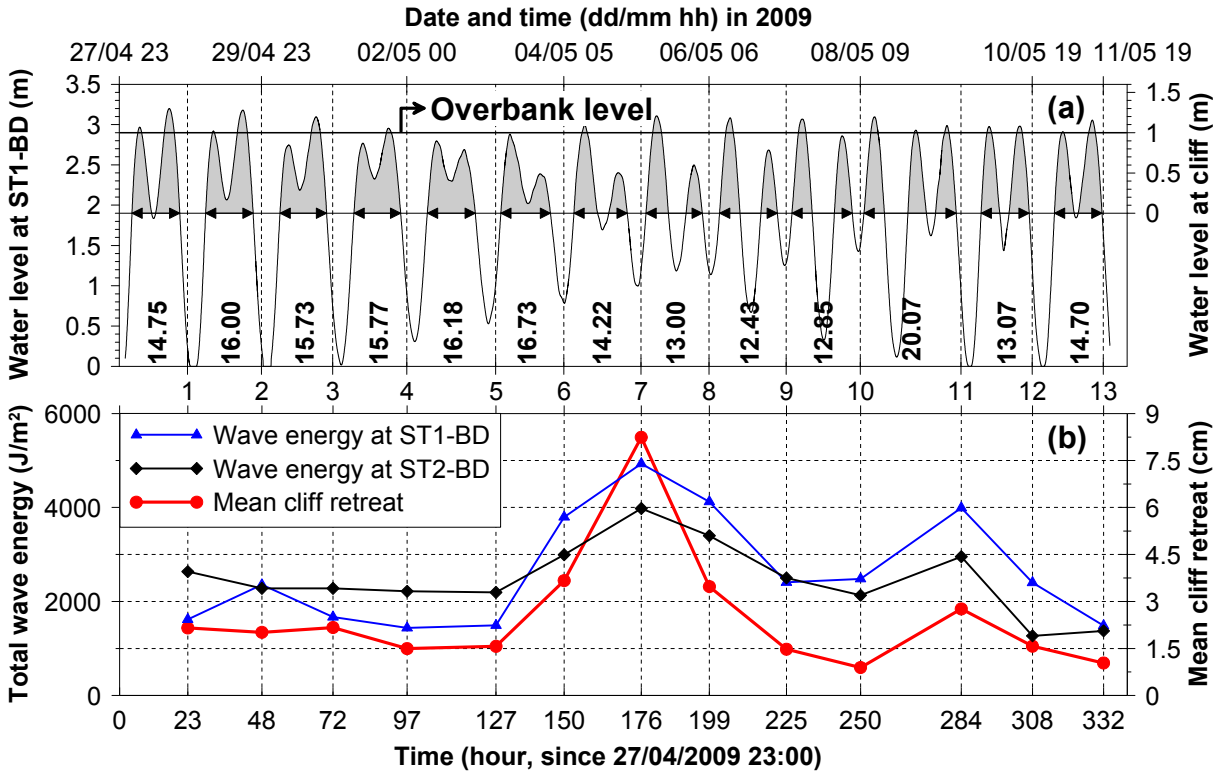

Figure 6.44. (a) Water level at the ST1-BD station and cliff inundation (grey area), numbers below the grey area indicate the durations of inundation (in hours). (b) Mean cliff retreat and wave energy at the ST1-BD and ST2-BD stations. The mean cliff erosion is the arithmetic mean of the cliff retreat at 30 stations.

Mechanism of mangrove cliff retreat in Bo De:

Thirteen measurements of the cliff retreat during 14 days in Bo De show that the cliff retreat belongs to only "surface erosion type" (Figure 6.45). "Notch and slope failure "erosions types were not observed at this study site. The cliff heights in Bo De are relatively small where the mean height is about 0.7 m. Moreover, the cliff's soil is characterized by consolidated sediment with a predominant amount (>90%) of mud. These clues might explain the unique surface erosion type (no creation of "notch erosion").

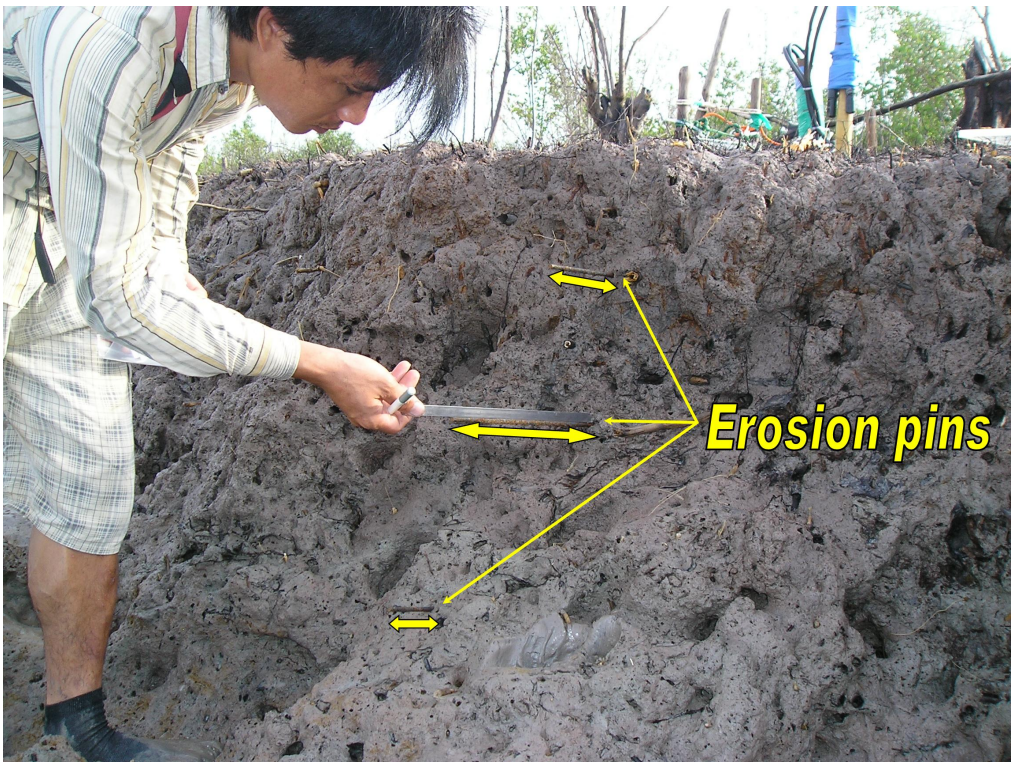

Figure 6.45. Type of erosion- Surface erosion- of the mangrove cliff in Bo De.

Topographical change on the tidal flat

The topography of transect about 110 m in front of the cliff, which was measured two times in 14 days, shows that the bed on this transect is slightly eroded (Figure 6.46). The tidal flat is eroding. Due to the erosion, there are many scour holes in this area. During the 14-day experiment, no sedimentation was observed on the tidal flat in front of the cliff.

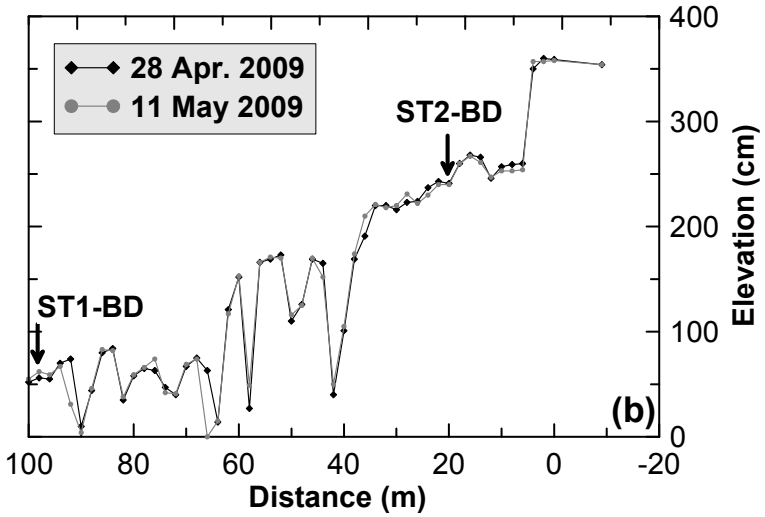

Figure 6.46. Topographical changes on the tidal flat in Bo De.

6.4. Comparison of meteorological hydrological geographical conditions between Can Gio and Bo De

Although both study sites are situated in the mangrove coasts of southern Vietnam with a distance between two sites of about 350 km. Both sites are different from each other many aspects:

- The mean annual rainfall for a 5-year period (2004-2008) at Ca Mau (2290 mm) (about 45 km north of Bo De) is about 2 times higher than that at Can Gio (1180 mm) (Figure 4.6).
- The environment in Bo De is mostly influenced by marine water with almost no fresh water discharge from the Bo De tidal channel or any other tributaries, while the Can Gio site is located at the river mouth of the Dong Nai - Sai Gon rivers system. The measured salinities during about 14 days in summer at the sites in Can Gio and Bo De show that Can Gio is influenced by fresh water, Bo De is not (Section 6.2, Figure 6.17b; Section 6.3.3, Figure 6.37b). The mean salinity in Bo De (31.6 ppt) is about 1.3 times higher than that in Can Gio (24.2 ppt).
- The morphology in front of the cliff in Bo De is complicated compared to Can Gio. The tidal flat in Bo De is built up by old mangrove soil, with many scour holes due to erosion. The gradient of the tidal flat is 2.1%. The surface of the tidal flat in Can Gio is smooth with a gradient of 0.4% (Figure 5.1a2, b2).
- The mean cliff height at Can Gio (about 1.8 m) is about 2.6 times higher than the mean height in at Bo De (0.7 m). On the top of the cliff in Can Gio, there are densely distributed, young living mangrove trees, representing mixed type of mangrove forest. The height of trees is about 2-3 m. The root systems of the mangrove trees are distributed from the top of the cliff with their cables penetrating down to app. 90 cm into the cliff soil. On top of the cliff at Bo De truncated mangrove stumps are existing. However, a small amount of mangrove roots can still be seen on the cliff surface.
- The grain size analyses of the sediment of the mangrove cliffs and the shear strength measurements on the cliff surface in Can Gio and Bo De show that the cliff's sediment in Bo De is more consolidated compared to Can Gio. The grain size distributions of the cliff's sediment in Can Gio are mainly characterized as bimodal type, with the first mode in the range from medium to coarse silt and the second mode in the range from very fine to fine sand (Section 6.2.3, Figure 6.14). The grain sizes of the cliff's sediment in Bo De are mainly characterized as unimodal, compose of fine to medium silt (Section 6.3.2, Figure 6.34). On average, the mud contents are about 78% for Can Gio and 93.5% for Bo De. The mean shear strength of the cliff soil

in Bo De is 0.1923 kg/cm^2 (standard deviation, SD = 0.0594), which is about 1.5 times higher than in Can Gio (0.1273 kg/cm^2, SD = 0.0421) (Table 6.7, Table 6.10)

The tidal regimes at both sites are the same, mixed tides, mainly semidiurnal. The tidal ranges are almost as strong as the range at Vung Tau. At Can Gio on the Nga Bay river mouth, the maximum and mean tidal ranges are 24 and 23 cm, respectively higher than at Vung Tau (Section 6.1.2, Figure 6.5b, Table 6.5). The maximum and mean tidal ranges at Bo De are almost the same as that at Vung Tau (Section 6.1.3, Figure 6.5c, Table 6.5). Can Gio and Bo De are both influenced by the monsoon as well as strong seasonal water level fluctuations. Higher inundations together with onshore-wind directions in winter might generate high waves approaching more or less directly to the coasts. In summer, the inundations are low compared to the winter. Wind from SW during summer mostly generates less waves than the NE monsoon during winter.

7. DISCUSSIONS

7.1. Seasonal water level variations and their influences on inundation

Based on data of a 19 years period (1991 – 2009) from seven tide gauge stations along the eastern coast of the Mekong Delta (Vung Tau, Vam Kinh, Binh Dai, An Thuan, Ben Trai, My Thanh, and Ganh Hao, for locations see Figure 5.4), mean sea level variations were elaborated and analyzed. It can be shown that except at Vung Tau, a relative sea level rise occurs with rates of about 6.0 mm/year up to 13.1 mm/year with an average of 9.6mm/year (Chapter 6.1.1.4, Figure 6.4). As Vung Tau is located on a geologically stable basement it is an ideal reference station to assess the relative sea level rise along the east coast of the Mekong Delta as well as to refer the tidal characteristics at those locations, where detailed measurements have been carried-out and long-term tide datasets are not available.

Along the east coast of the Mekong Delta, including the Can Gio - Vung Tau area, the tidal regimes are mixed tide, mainly semi-diurnal (Chapter 6.1, Figure 6.1, Figure 6.5, Table 6.1). However, by combining long-term mean tidal ranges (19-year period) at seven locations with short-term mean tidal ranges at 4 stations, where own measurements have been carried-out (Can Gio, Dong Tranh, Bo De, and Rach Goc; see Figure 5.4), the mean tidal ranges at all eleven near-river mouth locations show that the tidal range variations mostly follow latitudinal changes (Figure 6.2, Figure 6.7). From Binh Dai to higher latitude locations, the tidal ranges are increasing. From Binh Dai to lower latitude positions, the tidal ranges are also increasing until Ganh Hao, but further to southern locations, the tidal ranges are decreasing. Among all these 11 locations, the highest mean tidal range occurs at Ganh Hao (2.826 m), while the lowest tidal range is at Rach Goc (2.135 m). However, from the linear trend of latitudinal changes of the tidal range, the lowest tidal range values are calculated for the tip of the Ca Mau peninsula. These complex tidal range variations indicate that the coastal currents are complex, causing complicated coastal sediment transport processes (Albers and von Lieberman, 2011; Unverricht et al., 2012).

The monthly values of mean higher high water (MHHW), mean high water (MHW), mean sea level (MSL), mean low water (MLW) and mean lower low water (MLLW) from the 19-years dataset show strong seasonal variations. All values are higher for the winter period (NE monsoon) compared to the summer period (SW monsoon). They are highest in November and lowest in June/ July (Table 6.4, Figure 6.3). The differences in heights between highest and lowest values of MHHW and MLLW are about 45 cm and 53 cm on average causing higher inundations during winter compared to the summer.

The highest values of MHHW, MHW, and MSL in November at the long-term stations suggest that highest inundation is mainly controlled by the tide. However, values measured at Vam Kenh, Binh Dai, An Thuan, Ben Trai, and My Thanh are higher than those at Vung Tau and Ganh Hao (Table 6.4) This leads to the assumption that the inundation is additionally influenced by contributions from the fresh water runoff of the Mekong River. The Mekong Delta has the highest inundation in October at the end of the rainy season. The highest fresh water discharge occurs in September at the upstream stations (Chau Doc and Tan Chau), which are located about 200 km inland from the river mouths of the Bassac and other Mekong River branches (Dang, 2007). The propagation time of this discharge peak to downstream location My Thuan, which is located about 100 km inland from the coast and from the upstream station (Tan Chau), is about 7-22 days (Hung et al., 2011). Hence, this peak arrives at the river mouths around November, which matches the measured data from (Albers and von Lieberman, 2011) where the highest peak of fresh water discharge in the Soc Trang province was measured end of October. The influence of the fresh water discharge can be observed to about 10 km inner the river mouth in late November (Wolanski et al., 1996).

Higher inundation in winter is also influenced by the monsoon. During summer, southwesterly wind dominates, pushing the water mass offshore, which reduces inundation by tides. During winter, easterly to northeasterly winds are controlling the wind regime, pushing the water mass onshore and increase the water levels. The semiannual or seasonal water level variations can as well be caused by changes in the wide-scale ocean circulation, air pressure, fresh water runoff, etc (Lisitzin and Pattullo, 1961; Lisitzin, 1974; Kjerfve, 1990; Mazda and Kamiyama, 2007), but these effects have not been analyzed for this study area due to the lack of necessary data. Higher water levels in winter and lower water levels in summer are not related to seasonal variations of air pressure, as the air pressure during summer is lower than during winter (Figure 4.6a)

During the year, from November, the water level decreases until reaching the lowest level during summer in June/July, then it rises again. Although the mean tidal range (MTR) during the wet season is slightly higher than during the dry season, the difference between highest MTR and lowest MTR is not significant, only about 0.23 m on average (Figure 6.3h). Tidal current velocities of both ebb and flood tides are strongly correlated to durations of ebb and flood rather than tidal ranges (Chapter 6.2.3.2, Figure 6.9). A dataset of tidal current and water level, which were measured in June at the mouth of the Dong Tranh River (DT-WL, see Figure 5.4, Figure 5.5) shows that there are no differences in maximum velocities during highest tidal range period in June (lowest tidal inundation) and during lowest tidal range period in November (highest tidal inundation).

The Mekong Delta is sinking because of relative sea level rise (Syvitski et al., 2009). The mean annual sea level values obtained from the analyses of a 19 years dataset from different stations along the east coast of the Mekong Delta illustrates clearly the sinking trend, supporting the conclusion of Syvitski et al. (2009). For all long-term tide gauge stations, a relative sea level rise for the east coast of the Mekong Delta could be determined (Figure 6.4). Although, besides the general statement of global sea level rise (Solomon et al., 2007) published data are sparse for this region to assess all reasons for this trend of relative sea level rise. Sand mining in the lower basin of the Mekong Rivers and dam construction for hydro-electricity power plans in the upstream of the Mekong River (Pham, 2010) are causing reduced sediment supply to the coast (Kummu and Varis, 2006; Seto and Fragkias, 2007). Extraction of ground water for household, aquaculture, and particularly for shrimp farming ponds might be the main reasons causing a relative sea level rise as it is described for many areas in delta regions (Crossland et al., 2005; Nguyen, 2007a; Overeem and Syvitski, 2009). Over-pumping ground water is especially popular in the Ca Mau area, where most of the freshwater from the ground is used not only for household purposes but also for shrimp farms in particular, which consumes large amounts of ground water.

7.2. Main driving forces on mangrove cliff retreat

This discussion is based on two datasets, short-term mangrove cliff retreat correlated with tide and wave energy inputs in Can Gio and Bo De and long-term measurements on the cliff retreat in Can Gio, which were carried-out for a period of about 1 year covering the rainy- and dry season.

Both environments differ in terms of rainfall, fresh water discharge, morphology, mangrove tree distribution, cliff heigh, and physical properties of the soil building up the cliff, but are almost influenced by the same intensity of the monsoon and the tides (Chapter 6.4). Furthermore, both sites used to be accumulating areas in former times. At the Can Gio site, old dead mangrove stump are seen at about 80 cm below the current mangrove surface. An old mangrove surface layer, which is located about 1 m below the recent surface, is also found at Bo De (Figure 4.1). Unfortunately, for both areas, there is only limited knowledge about the accumulating stages (Schwarzer et al., 2007) as well as the beginning of the erosional phases.

The short-term mangrove cliff retreat in Can Gio, together with hydrodynamic inputs (e.g. waves and tidal inundation) shows that the cliff retreat is related to both long duration of inundation and wave energy input. Surprisingly, the cliff is retreating under low wave energy input but long duration of inundation during neap tide. Higher wave energy input during spring tide does not force the cliff to retreat immediately (Figure 6.1). This dataset

demonstrates clearly that the tide plays the most important role in cliff retreat, while wave energy input is the second main factor influencing the retreat. Increasing cliff retreats during longer periods of tidal inundation suggest that a cliff retreat will be faster if high waves are associated with long periods of tidal inundation.

The short-term mangrove cliff retreat in Bo De, together with tide and wave energy inputs show that here the cliff retreat is mostly related to wave energy input. Higher cliff retreat occurs during stronger wave energy release at the cliff. Due to the exposure to high waves during most of the time of the measurements, the direct influence of the tide (or inundation) on the cliff retreat might be masked by high waves; hence, it may be not seen apparently. However, the cliff retreat during neap tide, when the cliff is inundated for a longer period, is higher than during spring tide, when cliff inundation happens only for a short time (Figure 6.44). As the lower low water levels are also higher during neap tide compared to spring tide, waves can affect the cliff even during those periods when the water level is maintained at higher levels for a longer duration.

During the short term field campaign in Can Gio, waves mostly attacked perpendicular to the cliff, and high waves occurred around high tide (Figure 6.18a, c, Figure 6.19a). These waves have been mainly wind induced with a predominant period of 5 seconds (Figure 6.19b). Those waves are not induced by the summer monsoon (SW monsoon), which blows in offshore direction; they are generated regularly by onshore breezes, which are generated due to temperature difference between the land and the ocean. During summer, high tides usually occur during the day. As the water temperatures are lower than the air temperatures at high tides (Figure 6.17a, c), the onshore breezes are formed. When the wind of the SW monsoon is weak, the onshore breeze controls the wind regime.

During the short term measuring period in Bo De during summer, the wave periods scatter in the range from 3-8 seconds, where the 4- and 7-second periods are more dominant compared to other periods. Waves of 4- and 7-second periods transfer most of the energy to the coast (Figure 6.39). The wind regime during this period is mainly controlled by the SW wind monsoon (see Figure 6.38). An onshore breeze was not observed. The condition to form that wind did not exist because the water temperature was mostly higher than the air temperature (Figure 6.37). During the measuring period, the area was also influenced by the tropical depression/storm Chan-hom 2009 (Figure 6.35). Its impact on generating strong swell waves is indicated by the predominant 7-second wave period. During this period, when the swell waves, generated by the Chan-hom storm arrived at the coast, the sea state was very calm and waves generated by the SW monsoon were not observed. Generally, the SW wind generates a wave attack to the cliff, as the configuration of the coast is mostly striking west-east. Such wind waves, which have a period of around 3-5 seconds, contribute to about

47.4% of the total wave energy input during the period of the 14-days measurements (Figure 6.39b).

The results about the wind- and depression/storm induced waves show that during low wave energy input in summer, three types of waves, which attack more or less directly the cliff shorelines and cause cliff retreat. They are caused by a) onshore breezes (found in Can Gio), b) SW monsoon, and (c) tropical depression/storm, which occurred in Bo De. The knowledge about those different wave energy inputs help to explain the reason for cliff retreats during low energy season in summer at both sites.

While the area in Bo De is purely influenced by natural waves of natural origin, the site in Can Gio is also influenced by ship-induced waves, which are known to cause sediment re-deposition (Rapaglia et al., 2011) and coastal erosion (Kask et al., 2003; Houser, 2010). The study site in Can Gio is located near the main navigation channel where large ships enter to sail to the harbors of Ho Chi Minh City. Ship-induced waves were observed at the study site in Can Gio during several field campaigns, but unfortunately, they were not recorded by the instruments during the field surveys. As this measurement would have required a different sampling strategy with a much higher sampling rate, which would have consumed too much energy from the batteries. Therefore, the influence of the ship-induced wave was observed, but cannot be quantified.

The results above imply that tide and wave actions principally cause mangrove cliff erosion, where tides play the most dominant role, while waves are a secondary factor causing cliff retreat. The tide causes the recession directly (for the case of the mangrove cliff in Can Gio) and when the water levels are high enough so that waves can have an impact on the shoreline, this will accelerate the cliff retreat.

7.3. Role of seasonal variations of the inundation and monsoon in mangrove cliff retreat

In Can Gio, the retreat trend from the short-term dataset (about 13 days), shows that the retreat rate is about 0.36 cm/day (Figure 6.23), while the mean long-term retreat rate, which is calculated from the dataset of the 1 year measurement, is about 1.31 cm/day (Figure 6.27c). The value for the retreat rate from the long-term dataset is about 3.6 times higher than that from the short-term dataset. This difference can be explained by seasonal variations of tidal and wave energies. Annual water level fluctuations at Vung Tau tide gauge station show that the values of mean higher high water (MHHW) and mean lower low water (MLLW) are lowest in summer (in June-July) and highest in winter (in November) (Figure 6.3 6.3, Table 6.4). Hence, the inundation during winter is higher than during summer.

Additionally, the area is also influenced by the monsoon. The wind directions in winter (northeast monsoon) are ranging from NE to E, with predominant easterly wind. Conversely, during summer (SW monsoon) the wind from the SW direction is dominant (Figure 4.5). These reversed wind directions suggest that wind induced waves during the winter are stronger and more direct to the cliff than during the summer. Consequently, the cliff retreat during winter is faster than during summer.

The short-term period of the cliff retreat measurements in Bo De was carried-out in summer, during low tide and low wave energy conditions. However, it is assumed that higher wave energy inputs in winter might result in a stronger cliff retreat. Therefore, an estimation of annual cliff retreat in Bo De should result in higher values than the retreat value 2.51 cm/day, which is retrieved from the 14-day experiment in summer. Additionally, the Mekong Delta coast is experiencing a relative rise of mean sea level with the mean rate for the entire area of about 9.6 mm/year (Chapter 6.1.2.4, Figure 6.4). When the sea level is rising, inundation increases and coastal retreat might be enhanced.

As discussed above, the annual cliff retreat rate in Bo De is about 9.2 m/year (2.51 cm/day), while the annual retreat in Can Gio is about 4.8 m/year (1.31 cm/day). These values show that the cliff retreat rate in Bo De is about 2 times higher than in Can Gio. As both sites are mostly influenced by the same strong tidal energy, it is suggested that at Bo De the wave energy is higher compared to Can Gio.

Tropical storms/depressions seldom occur in the entire study area (Table 4.1, Table 4.2, Figure 4.8), although they usually appear in November-December. This period coincides with the time of highest inundation. From modeled results (Le et al., 2007), it is known that storm surge associated with flooding from the Mekong Rivers can cause the coast of the Mekong Delta to be inundated by up to 0.6-0.8 m. Therefore, the influence of the tropical storms/depressions on coastal erosion will be stronger.

7.4. Role of tidal current regime in the retreat of mangrove cliff shoreline

Coastal currents, especially the current asymmetry is one of cause of coastal erosion due to of its exporting character by a resultant one-way sediment transport direction (Mazda et al., 2002; Winterwerp et al., 2005). No sedimentation was found on the tidal flats, in front of the eroding cliff shorelines in Can Gio and Bo De. The tidal flows at the river mouths in both investigation areas (Can Gio and Bo De) are dominated by ebb currents and ebb dominated sediment transport. This asymmetry of the tidal currents prevents sedimentation processes and is one reason why both sites are continuously retreating.

Even if the mangrove cliff in Can Gio retreats about 4.79 m/year (1.31 cm/day, Figure 6.27) the topography on the tidal flat in front of the cliff is relatively stable. No change was observed for a period of seven month (Figure 6.29). This stable morphology indicates that the sediment resulting from cliff erosion is transported offshore or alongshore without leaving remnants and supporting the sediment budget of the tidal flats. These results might be explained as well by the asymmetry of the flow regime rather than by the indication from the asymmetry in suspended sediment concentration (SSC) between the ebb- and flood period. Data of tidal currents and SSCs on the tidal flat, at ST1-CG station, show that the ebb current durations and ebb current speeds are longer and higher than those occurring during flood tide (Figure 6.11, Figure 6.20); the SSC during ebb phase is not significantly higher than during the flood phase (Figure 6.22). Because the materials of the surface sediment of the tidal flat are mainly composed of fine to medium silt and fine sand (Figure 6.15), they can be re-suspended easily by the waves and tidal currents, thus, recognizing the difference in SSC between ebb and flood tides is blurred. Moreover, at the main channel of the Nga Bay river mouth in front of the tidal flat (MS1-CG station, see Figure 4.1b), the speeds and durations in ebb phases are also faster and longer than those in flood phases (Figure 6.11). Hence, these tidal flow asymmetries cause the export of sediment and prevent the accumulation of the eroded cliff material as well as the sediment discharge from the river or from marine origin.

In Bo De, during 14 days, the average cliff retreat is 32.5 cm (Table 6.11). The accumulation on the tidal flat in front of the cliff is not observed, even the topography on the tidal flat is slightly eroded (Chapter 6.3.6, Figure 6.46). The reason for this removal sediment out of the study site cannot be explained by the predominant of flood current on the tidal flat, as this flood dominant might be caused by strong waves (Chapter 6.3.3, Figure 6.38, Figure 6.39). The asymmetry of SSCs between ebb tide and flood tide might help to explain this situation. During rising tide, the SSCs are almost smaller compared to those during falling tide (Chapter 6.3.3, Figure 6.41). The lower SSCs in flood tides suggest that the marine water does not supply sediment to the coast and the consolidated bed sediment on the tidal flat (Figure 6.34c) is not reworked by strong waves or currents. The origin of higher SSCs in ebb phases, after strong wave attacks, might be expected from the eroded cliff. Additionally, the tidal currents at the main channel around the tidal flat are fast (with velocities of up to 1.1 m/s at near the bottom) and ebb dominant (Figure 6.31, Figure 6.32). Therefore, the eroded sediment is moved out of the area by this tidal current asymmetry.

During a synodic month, asymmetry of tidal current does not appear every time because of water level fluctuation situations. The water level fluctuations or the tidal ranges variations between two consecutive spring tides are different (Chapter 6.1, Figure 6.1). Data on current velocity during November at the Dong Tranh river mouth station in Can Gio (DT-WL station, Figure 5.4), which captured two consecutive spring tides, shows that the current velocities of

the higher spring tide are higher than those of the lower spring tide, especially for the peaks of velocity. Additionally, the asymmetry of tidal currents only occurs about 5-6 days during the higher spring tide around the highest range of tide (Chapter 6.2.2, Figure 6.9). This information suggests that an asymmetry of sediment transport due to the asymmetry of tidal current only happens a few days each month during higher spring tide. The tidal currents in Can Gio and Bo De were only collected during higher spring tide periods. The longer-term of the current velocities at the Dong Tranh river mouth suggest that the occurrence of the asymmetries of tidal currents in Can Gio and Bo De are similar to Dong Tranh. This means that the asymmetries of sediment transport directions due to the tidal flow asymmetries at two these river mouths only occur a few days each month during higher spring tide. Consequence of this short time in asymmetry of tidal flow at a river mouth is a good proposal for current measurements to find whether there is an asymmetry of currents or erosion/sedimentation in an estuary. To assess asymmetry of tidal current in a river mouth, duration of current measurements should last for at least a full synodic month (Kjerfve, 1979) or for a fortnight period during higher spring tide.

In summary, at three river mouths, two in Can Gio (the Dong Tranh and Nga Bay river mouths) and one in Bo De (the Bo De tidal river mouth), there exists tidal flow asymmetries. At Dong Tranh, the flood current is dominant (Figure 6.9), whereas at Nga Bay and Bo De, ebb currents are dominant (Figure 6.10, Figure 6.20, Figure 6.31, Figure 6.32). Along the Dong Tranh River, the natural mangroves are propagating northeasterly, which indicates the area is accumulating (Tuan et al., 2002), except at a small area in Nang Hai creek, close to west side of the Dong Tranh river mouth (Vo, 2006). Own observation and field data about flood dominant current regime at the Dong Tranh river mouth confirm the observation of Tuan and his colleagues. In contrast to the depositional trend along the Dong Tranh River, erosions are occurring at both Nga Bay and Bo De tidal channel mouths. The topographies on the tidal flats at both sites are neither built up higher by the sediment supply from the river or marine waters nor from the eroded mangrove cliff. These tidal flow asymmetries and their consequences might be a key answer for explaining why the mangrove cliff shorelines are retreating continuously at these sites.

The above evidence helps for understanding the driving hydrodynamic processes affecting mangrove cliff retreat as well as for assessing their role in controlling the retreat. Besides the important role of tide and wave, the asymmetry of tidal flow is the third major factor controlling the cliff retreat because of its exporting sediment trend, which quite matches to the study of Mazda et al. (Mazda et al., 2002)

7.5. Role of cliff's soil property in speed of retreat

The consolidation of the cliff soil in Bo De is higher than in Can Gio (Chapter 6.4). The shear strength of cliff soil in Bo De (0.1923 kg/cm^2) is about 1.5 times higher than in Can Gio (0.1273). A retreat of 1 cm mangrove cliff needs wave energy inputs of about 857 J/m^2 in Can Gio and about 1105 J/m^2 in Bo De. To retreat mangrove cliff, the necessary wave energy input in Bo De is about 1.3 times higher than Can Gio. Additionally, the cliff in Can Gio also retreats under low wave input but higher duration of inundation. These clues suggest that, for the less-consolidated soil likely Can Gio, the tide (with support from small waves (Winterwerp et al., 2005)) can cause the cliff retreat directly by the inundation, whereas the tide apparently does not affect the high-consolidated cliff shoreline in Bo De. This clue suggests that the cliff soil property plays a role in reducing the speed of cliff erosion. Higher consolidated sediment of mangrove shoreline can reduce speed of erosion.

7.6. Mechanism of cliff retreat and the role of mangroves in coastal erosion

There are three kinds of mangrove cliff retreat including 'surface erosion', 'Notched erosion', and 'slope failure' along the shoreline in Can Gio and Bo De (Chapter 6.2.7, Chapter 6.3.5.2).

'Surface erosion' is a typical kind of cliff erosion, where the cliff is eroded uniformly from the top to the bottom. This erosion type mainly occurs at locations without mangrove trees or less densely trees on top. Lower cliff heights can also support surface erosion. For example, in the Bo De area cliff heights exceed not more than 1m. However, the most important influence factor is the low abundance of mangrove trees, which stabilize the cliff.

'Notched (or scouring) erosion' occur at locations where the mangrove trees are living densely on top of the cliff. Especially, the root system is well developed from top until the middle part of the cliff. There, the roots can stabilize the mangrove soil and make this part less vulnerable to tide and waves. As a result, the lower part is eroded faster than the upper part. It leads to a notch at the bottom of the cliff (Figure 6.28b). This erosion type prevail the cliff retreat in Can Gio.

Coops et al. (1996) present that the root system of salt-marsh vegetation do not always protect the cliff from erosion. There, the movement of the roots due to wave action releases the sediment from the cliff. It demonstrates how roots can affect the resistance of cliff sediments in an opposite way. This study did not clearly observe the effect of mangrove root movement to the mangrove cliff erosion. However, difference in the compositions of the cliff soils can influence this effect.

In the King Sound coastline, Australia, Semeniuk (1980) identified that the cliff erosion is mainly caused by scouring due to strong tidal currents. The importance of wave action is minor. In Can Gio, the cliff erosion is largely affected by both tide and wave actions. However, the tidal inundation is the most important factor for cliff erosion rather than the tidal currents. Maximum tidal current in front of the cliff does not exceed 0.16 m/s. Waves have a small influence due to its low energy input (Figure 6.24).

'Slope failure' is a consequence of the notched erosion. Therefore, scours destabilize the cliff above and lead to slope failures. As a result, blocks of mangrove soil can collapse from the cliff. This erosion type can be found only at the site in Can Gio.

This study shows clearly that mangroves reduce coastal erosion. The mangrove root support the mangrove soil consolidation and attenuate currents and waves not in the area of the cliff, but during the inundation in the mangrove forest (Furukawa et al., 1997; Mazda et al., 1997; Mazda et al., 2006; Vo and Massel, 2006).

7.7. Other possible parameters influencing on the cliff retreat

There are as well other parameters, which might influence the cliff retreat. In comparison to the influence of waves and tides, they are neglected in this study. However, they should be mentioned here.

Ground water fluctuation and biological activities by amphibic organisms has been observed by Perillo et al. (2005) in marsh sediments and Nordhaus et al. (2009) in Mangroves. The influence of these two factors could be observed in the field as well. On the cliff surface, there are many holes or burrows, which are mainly created by sea crabs. Partly they have their origin by the mangrove root systems. When the cliff is inundated, it captures the water, which is discharges to the surrounding areas during low tide, especially at lower low waters. This ground water leaves the cliff via such holes when the cliff is exposed. The speed of the out-flowing water is usually stronger during spring tide, when the tidal ranges are high, the water level fluctuations are fast, and the ebb durations are long. This ground water discharge might cause some small erosion or weaken the consolidated mangrove cliff soil. Moreover, such holes can enhance the erosion by water-turbulence when waves are hitting the cliff during the period of inundation.

During the rainy season, the area often experiences heavy rain showers during only a short period. Water runoff from those rains might also affect the cliff retreat, especially if the heavy rain occurs at times when the cliff is completely exposed. However, this impact is difficult to measure. During the short term measuring campaigns in Can Gio and Bo De, there

were just a few light rain-showers. Therefore, the rain-induced cliff retreat could not be estimated.

Irregularity in space of mangrove cliff retreat is a characteristics phenomenon, which was observed in King Sound, Australia (Semeniuk, 1980) but as well as in Can Gio and Bo De. It usually originates from the complex configurations of the mangrove cliff shorelines and the distributions of mangroves on top. It is expected that the complexities in the configuration of the mangrove shorelines and the distributions of mangrove trees might influence the enhancing/reducing cliff retreat rate. These rates are difficult to evaluate, however.

7.8. Evaluating future coastal erosion in the study area

No doubt, negative human impacts on the study coasts are increasing alarmingly. Clearing mangroves for urban, aquaculture (Tong et al., 2004) wood etc are adversely pressing on the coasts. Sand mining and dam construction upstream are other possible sources that are causing a lack of sediment supply to the coast. Disadvantageous conditions in tidal flow asymmetry are preventing the accumulation at both study sites in Can Gio and Bo De. Moreover, increasing relative sea level rise at the Mekong Delta coast, which causes wide ranging inundation (Figure 6.4) (Solomon et al., 2007; Syvitski et al., 2009) combined with global warming effects are causing the coast to be exposed to unfavorable situations like increasing tidal energy. Furthermore, tropical storms have occurred more often during the last 20 years (from 1991-2010) compared to previous times (from 1945 to 1991, Chapter 3.2, Figure 4.1, Figure 4.2, Figure 4.8). These signs do not indicate the coastal retreats in Can Gio and Bo De are decelerating. Conversely, the erosions will tend to increase in future, especially in Bo De. It might be stated that the entire east coast in South Vietnam is facing a serious problem, the erosion.

7.9. Summary

So far, the above assessments and discussions have very clearly demonstrated the processes controlling the retreat of mangrove dominated coasts. Three important hydrodynamic factors controlling the mangrove-cliff retreat include:

(1) duration of tidal inundation, which is mainly a result of water level change due to the tides,
(2) wave, and
(3) tidal current asymmetry have been discussed above.

In addition, this study also emphasizes the role of the soil composition of mangrove cliffs, which has an influence of the shoreline retreat. Mangrove shoreline retreat or erosion

phenomenon in mangrove swamp is unequal in time and space as described in several studies (e.g. Semeniuk, 1980, 1981; Blasco and Aizpuru, 2002; Thampanya et al., 2006)). Both datasets of mangrove cliff retreat, obtained in Can Gio and Bo De, support the observations from Semeniuk (1980). Moreover, the datasets of short- and long-term cliff retreat in Can Gio, together with the short-term dataset in Bo De illustrate clearly this non-uniformity. The difference of cliff retreat rates vary from location to location and depend on the configuration of the cliff shoreline, the distribution of mangrove vegetation and soil properties (e.g. shear strength and grain size distribution). The cliff retreat rates change in both, short-term and long-term time scales, because of variations in tide and wave energy inputs. Within a fortnight cycle, the cliff retreat rate during neap tide is usually higher than during spring tide; within the year, the retreat rate during winter is higher than during summer. Long-term cliff retreat in mangrove coasts is related to the asymmetry of current flow as Mazda et al. (Mazda et al., 2002)pointed out. This study results agree with the work Mazda et al. (2002). Both eroding sites in Can Gio and Bo De have asymmetries in tidal current, where ebb currents are faster.

Additionally, previous studies and this study show, that shorelines in mangrove swamps have been retreated or changed almost any time and any place. These results demonstrate clearly, that mangrove vegetations reduce speed of coastal erosion. The studies of salt-marsh cliff erosions by Coops et al. (1996) and Feagin et al. (2009) showed that the vegetations in the salt-marsh support coastal erosion due to wave action. These observations in different salt-marshes lead to state that vegetation in salt-marsh included mangrove swamps can not fully prevent coastal erosion, but it slows down the erosion.

The two short-term datasets of mangrove shoreline retreat in two different sites show undoubtedly, that mangrove shoreline retreat is very sensitive to the inundation. This evidence further strengthens the recognition that mangroves are being threatened by the adverse effects of local and global sea level rises, which cause higher inundation, associated with climate change, which increases intensity and frequency of storms.

8. CONCLUSIONS

The east coast in South Vietnam (from Vung Tau to Ca Mau) is strongly affected by a mixed tide, mainly semi-diurnal with tidal range up to 4.08 m. The tidal range variations along this coast are complex and follow latitudinal changes. The highest and lowest mean tidal ranges are at Ganh Hao (2.826 m) and Rach Goc (2.175m), respectively.

The study area is strongly influenced by seasonal variation in tidal levels. The water levels and inundations during winter are higher compared to those during summer. The highest water level and inundation occur in November, whereas the lowest ones happen in June/ July. Based on the 19-year hourly water level datasets at seven coastal locations, the differences in mean higher high water (MHHW) between two seasons are about from 38 to 51 cm, and 45 cm on average.

This study shows the mechanism of the mangrove cliffs retreat as well as proved how the hydrological factors force the recession. There are three kinds of mangrove cliff retreat including 'surface erosion', 'notched (or scoured) erosion', and 'slope failure erosion'.

The mangrove cliff shorelines are retreating by three major hydrological factors including tide (or the inundation due to the tide), wave, and tidal flow asymmetry. Among these three impact factors, the tide plays a key role in the mangrove cliff retreat because the tide can cause the cliff retreat directly by the inundation. The wave needs the tide guide to act to the cliff and higher wave energy input causes higher cliff retreat, hence the wave is the second significant factor accelerating the cliff recession. As results of the tidal flow asymmetries, at both areas in Can Gio and Bo De, ebb currents are faster than flood currents, the tidal flat in front of the shorelines are not built up higher by the sediment from eroded shorelines or sediment supply from river or marine origins. These tidal flow asymmetries prevent the accumulation process therefore it is considered the third important factor maintaining the recession process.

Mangrove cliff shoreline retreat phenomenon is non-uniform in space and time and site specific due to complex configuration of the shoreline and distribution of mangrove trees, differences in water level variations and wave energy inputs, and soil compositions.

Mangrove cliff retreat rates vary in fortnight (neap-spring tidal cycle) and annual time scales. Due to longer inundation duration and higher tidal level, neap tides have a stronger influence on erosion than spring tides. Higher tide and wave energies situations in winter have stronger impacts on the cliff retreat.

For the less-consolidated sediment mangrove shoreline, inundation duration has to be taken into account in assessing the erosion because the mangrove shoreline is eroded directly during higher inundation, perhaps with triggering by very small wave height.

The retreat rates of the cliff shorelines in Can Gio and Bo De are estimated about 4.7 and 9.6 m/year, respectively.

Although mangroves can reduce the erosion rate due to their binding sediment from the root systems, they do not always prevent the coastal recession. The mangrove shorelines have retreated under normal conditions, even weak wave action conditions, which are always present in the areas at any time.

The restoration of coastal mangrove forests is not only necessary to mitigate coastal erosion problem as well as the others harmful effects, but also to diversity the ecosystem. However, finding suitable places or methods for rehabilitating the mangroves will have to be studied carefully. At least, both sites in Can Gio and Bo De are not appropriate places for mangroves development because the accumulation process does not exist in these places.

References

Albers, T., and von Lieberman, N., 2011. Current and erosion modelling survey, 72 pp.

Allen, J.R.L., 1989. Evolution of salt-marsh cliffs in muddy and sandy systems: A qualitative comparison of British West-Coast estuaries. Earth Surface Processes and Landforms, v. 14 (1), p. 85-92.

Allen, J.R.L., and French, P.W., 1989. An apparatus for sequentially sampling unconsolidated cohesive sediments exposed on salt-marsh and river cliffs. Sedimentary Geology, v. 61 (1-2), p. 151-154.

Alongi, D.M., 2002. Present state and future of the world's mangrove forests. Environmental Conservation, v. 29 (03), p. 331-349.

Alongi, D.M., 2008. Mangrove forests: Resilience, protection from tsunamis, and responses to global climate change. Estuarine, Coastal and Shelf Science, v. 76 (1), p. 1-13.

Alongi, D.M., Dixon, P., Johnston, D.J., Van Tien, D., and Thanh Xuan, T., 1999. Pelagic processes in extensive shrimp ponds of the Mekong delta, Vietnam. Aquaculture, v. 175 (1-2), p. 121-141.

bin Hassan, K., 1993. The changing mangrove shorelines in Kuala Kurau, Peninsular Malaysia. Sedimentary Geology, v. 83 (3–4), p. 187-197.

Blasco, F., and Aizpuru, M., 2002. Mangroves along the coastal stretch of the Bay of Bengal: Present status. Indian Journal of Marine Sciences, v. 31 (1), p. 9-20.

Blott, S.J., and Pye, K., 2001. GRADISTAT: a grain size distribution and statistics package for the analysis of unconsolidated sediments. Earth Surface Processes and Landforms, v. 26 (11), p. 1237-1248.

Carter, C.H., and Guy Jr, D.E., 1988. Coastal erosion: Processes, timing and magnitudes at the bluff toe. Marine Geology, v. 84 (1-2), p. 1-17.

Carter, J., 1959. Mangrove Succession and Coastal Change in South-West Malaya. Transactions and Papers (Institute of British Geographers), No. 26, p. 79-88.

Clifford, A.K., and Gary, W.S., 1973. Nodal tidal cycle of 18.6 Yr.: Its importance in sea-level curves of the east coast of the United States and its value in explaining long-term sea-level changes. Geology, v. 1, p. 141-144.

Coops, H., Geilen, N., Verheij, H.J., Boeters, R., and van der Velde, G., 1996. Interactions between waves, bank erosion and emergent vegetation: an experimental study in a wave tank. Aquatic Botany, v. 53 (3–4), p. 187-198.

Crossland, C.J., Kremer, H.H., Lindeboom, H.J., Crossland, M.J.I., and Le Tissier, M.D.A. (Eds.), 2005. Coastal Fluxes in the Anthropocene. Springer-Verlag Berlin Heidelberg, 232 pp.

Dahdouh-Guebas, F., Jayatissa, L.P., Di Nitto, D., Bosire, J.O., Lo Seen, D., and Koedam, N., 2005. How effective were mangroves as a defence against the recent tsunami? Current Biology, v. 15 (12), p. R443-R447.

Dang, T.A., 2007. Research on the hydrological regime of Hau River belong to An Giang Province. Master thesis (in Vietnamese: Nghiên cứu chế độ thủy văn sông Hậu đoạn chảy qua thành phố Long Xuyên tỉnh An Giang), University of Science, Ho Chi Minh City, Vietnam.

Davidson-Arnott, R.G.D., van Proosdij, D., Ollerhead, J., and Schostak, L., 2002. Hydrodynamics and sedimentation in salt marshes: examples from a macrotidal marsh, Bay of Fundy. Geomorphology, v. 48 (1-3), p. 209-231.

Defant, A., 1960. Physical oceanography, v. 2. Pergamon Press, 598 pp.

Duke, N.C., Meynecke, J.-O., Dittmann, S., Ellison, A.M., Anger, K., Berger, U., Cannicci, S., Diele, K., Ewel, K.C., Field, C.D., Koedam, N., Lee, S.Y., Marchand, C., Nordhaus, I., and Dahdouh-Guebas, F., 2007. A World Without Mangroves? Science, v. 317 (5834), p. 41-42.

Eijkelkamp, 2005. Operating Instructions.

Ellison, J.C., 1993. Mangrove Retreat with Rising Sea-level, Bermuda. Estuarine, Coastal and Shelf Science, v. 37 (1), p. 75-87.

Ellison, J.C., 1999. Impacts of Sediment Burial on Mangroves. Marine Pollution Bulletin, v. 37 (8-12), p. 420-426.

Emanuel, K., 1987. The dependence of hurricane intensity on climate. Nature, v. 326 (2), p. 483-485.

Emanuel, K., 2005. Increasing destructiveness of tropical cyclones over the past 30 years. Nature, v. 436 (7051), p. 686-688.

Emery, K.O., and Kuhn, G.G., 1982. Sea cliffs: Their processes, profiles, and classification. Geological Society of America Bulletin, v. 93 (7), p. 644-654.

FAO, 1993. Mangrove for production and protection. A changing resource system: Case study in Can Gio District, Southern Vietnam. Food and Agriculture Organization of the United Nations Forestry. Regional Wood Energy Development Programme in Asia. Bankok, Thailand.

FAO, 2007. The world's mangrove 1980-2005. Food and Agriculture Organization of the United Nations Forestry Paper 153. Rome, Italy.

Feagin, R.A., Lozada-Bernard, S.M., Ravens, T.M., Möller, I., Yeager, K.M., and Baird, A.H., 2009. Does vegetation prevent wave erosion of salt marsh edges? Proceedings of the National Academy of Sciences, v. 106 (25), p. 10109-10113.

Foreman, M.G.G., 2004. Manual for tidal heights analysis and prediction. Pacific Marine Science Report 77-10.

Furukawa, K., and Wolanski, E., 1996. Sedimentation in Mangrove Forests. Mangroves and Salt Marshes, v. 1 (1), p. 3-10.

Furukawa, K., Wolanski, E., and Mueller, H., 1997. Currents and Sediment Transport in Mangrove Forests. Estuarine, Coastal and Shelf Science, v. 44 (3), p. 301-310.

Gagliano, S.M., and McIntire, W.G., 1968. Reports on the Mekong River Delta. Coastal Studies Institute, Louisiana State University. Technical Report No. 57, 143pp.

Gilman, E.L., Ellison, J., Duke, N.C., and Field, C., 2008. Threats to mangroves from climate change and adaptation options: A review. Aquatic Botany, v. 89 (2), p. 237-250.

Gilman, E.L., Ellison, J., Jungblut, V., Lavieren, H.V., Wilson, L., Areki, F., Brighouse, G., Bungitak, J., Henry, M., Kilman, M., Matthews, E., Jr., I.S., Teariki-Ruatu, N., Tukia, S., and Yuknavage, K., 2006. Adapting to Pacific Island mangrove responses to sea level rise and climate change. Climate Research, v. 32 (3), p. 161-176.

Giri, C., Ochieng, E., Tieszen, L.L., Zhu, Z., Singh, A., Loveland, T., Masek, J., and Duke, N., 2011. Status and distribution of mangrove forests of the world using earth observation satellite data. Global Ecology and Biogeography, v. 20 (1), p. 154-159.

Hoang, V.H., and Nguyen, H.N., 2006. Results on study about wave field of Dong Nai- Saigon estuaries and suggestion of sea bank and river mouths protection methods. Proceedings in Vietnam-Japan Estuary Workshop, Hanoi, Vietnam.

Hong, P.N., and San, H.T., 1993. Mangrove of Vietnam. IUCN, Bankok, Thailand.

Hooke, J.M., 1979. An analysis of the processes of river bank erosion. Journal of Hydrology, v. 42 (1–2), p. 39-62.

Houser, C., 2010. Relative importance of vessel-generated and wind waves to salt marsh erosion in a restricted fetch environment. Journal of Coastal Research, v. 26 (2), p. 230-240.

Hung, N.N., Delgado, J.M., Tri, V.K., Hung, L.M., Merz, B., Bárdossy, A., and Apel, H., 2011. Floodplain hydrology of the Mekong Delta, Vietnam. Hydrological Processes.

Huynh, T.M.H., and Nguyen, H.A., 2003. Geoinformatics in environment monitoring and land-use planning for the wetland - Case study of Cangio - Hochiminh City-South Vietnam. Environmental Informatics Archives, v. 1, p. 447-457.

Kask, J., Talpas, A., Kask, A., and Schwarzer, K., 2003. Geological setting of areas endangered by waves generated by fast ferries in Tallinn Bay. Proceedings of the Estonian Academy of Sciences, Engineering, v. 9 (3), p. 185-185.

Kathiresan, K., and Bingham, B.L., 2001. Biology of mangroves and mangrove Ecosystems, Advances in Marine Biology, Volume Volume 40. Academic Press, p. 81-251.

Kathiresan, K., and Rajendran, N., 2005. Coastal mangrove forests mitigated tsunami. Estuarine, Coastal and Shelf Science, v. 65 (3), p. 601-606.

Kjerfve, B., 1979. Measurement and analysis of water current, temperature, salinity, and density. In: Dyer, K.R. (Ed.), Hydrography and sedimentation in estuaries. Cambridge University Press, p. 186-216.

Kjerfve, B., 1990. Manual for investigation of hydrological processes in mangrove ecosystems. UNESCO/UNDP, New Delhi, India, 79 pp.

Komar, P.D., 1976. Beach processes and sedimentation. Prentice Hall, Inc. Englewood Cliffs, New Jersey, 426 pp.

Kummu, M., and Varis, O., 2006. Sediment-related impacts due to upstream reservoir trapping, the Lower Mekong River. Geomorphology, v. 85 (3-4), p. 275-293.

Le, T.V.H., Nguyen, H.N., Wolanski, E., Tran, T.C., and Haruyama, S., 2007. The combined impact on the flooding in Vietnam's Mekong River delta of local man-made structures, sea level rise, and dams upstream in the river catchment. Estuarine, Coastal and Shelf Science, v. 71 (1-2), p. 110-116.

Lisitzin, E., 1974. Sea-level changes. Elsevier Oceanography Series 8. Elsevier Scientific Publishing Company, Amsterdam - Oxford - New York, 286 pp.

Lisitzin, E., and Pattullo, J.G., 1961. The Principal Factors Influencing the Seasonal Oscillation of Sea Level. J. Geophys. Res., v. 66 (3), p. 845-852.

Massel, S.R., and Brinkman, R.M., 1998. On the determination of directional wave spectra for practical applications. Applied Ocean Research, v. 20 (6), p. 357-374.

Mazda, Y., and Kamiyama, K., 2007. Tidal deformation and inundation characteristics within mangrove swamps. In: Mazda, Y., Wolanski E., and Ridd P.V. (Eds.), The role of physical processes in mangrove environments. TETERRAPUB, Tokyo, p. 156-167.

Mazda, Y., Magi, M., Ikeda, Y., Kurokawa, T., and Asano, T., 2006. Wave reduction in a mangrove forest dominated by Sonneratia sp. Wetlands Ecology and Management, v. 14 (4), p. 365-378.

Mazda, Y., Magi, M., Nanao, H., Kogo, M., Miyagi, T., Kanazawa, N., and Kobashi, D., 2002. Coastal erosion due to long-term human impact on mangrove forests. Wetlands Ecology and Management, v. 10 (1), p. 1-9.

Mazda, Y., Wolanski, E., King, B., Sase, A., Ohtsuka, D., and Magi, M., 1997. Drag force due to vegetation in mangrove swamps. Mangroves and Salt Marshes, v. 1 (3), p. 193-199.

Mikhailov, V., and Arakelyants, A., 2010. Specific features of hydrological and morphological processes in the mouth area of the Mekong River. Water Resources, v. 37 (3), p. 253-267.

MONRE, 2009. Climate change, sea level rise scenarios for Vietnam. Ministry of Natural Resources and Environment (MONRE), Vietnam, 34 p.

NAS, 1974. The effects of herbicides in South Vietnam. Part A: Summary and conclusions. The Committee on the Effects of Herbicides in Vietnam, National Research Council. National Academy of Sciences, Washington, D.C.

Nguyen, H.N., 2007a. Flooding in Mekong River Delta, Vietnam. Human Development Report 2007/2008.

Nguyen, M.H., and Duong, C.D., 2006. Coupled circulation, wave modeling in the Dinh An estuary for studying of the navigational access channel migration. Proceedings in Vietnam-Japan Estuary Workshop, Hanoi, Vietnam.

Nguyen, Q.T., 2007b. Research on the hydrodynamic and environmental regimes of the East Sea in southeast Vietnam. Master thesis (in Vietnamese: Nghiên cứu chế độ động lực và môi trường vùng biển đông nam bộ), Vietnam National University, Hanoi-College of Science, Vietnam.

Nguyen, V.L., Ta, T.K.O., and Tateishi, M., 2000. Late Holocene depositional environments and coastal evolution of the Mekong River Delta, Southern Vietnam. Journal of Asian Earth Sciences, v. 18 (4), p. 427-439.

NOAA, 2000. Tide and current glossary. Silver Spring, Maryland, 34 pp.

NOAA, 2003. Computational techniques for tidal datums handbook. Silver Spring, Maryland, 113 pp.

Nordhaus, I., Diele, K., and Wolff, M., 2009. Activity patterns, feeding and burrowing behaviour of the crab Ucides cordatus (Ucididae) in a high intertidal mangrove forest in North Brazil. Journal of Experimental Marine Biology and Ecology, v. 374 (2), p. 104-112.

Overeem, I., and Syvitski, J.P.M., 2009. Dynamics and Vulnerability of Delta Systems. LOICZ Reports & Studies No. 35. GKSS Research Center, Geesthacht, 54 pages.

Pawlowicz, R., Beardsley, B., and Lentz, S., 2002. Classical tidal harmonic analysis including error estimates in MATLAB using T_TIDE. Computers & Geosciences, v. 28 (8), p. 929-937.

Perillo, G.E., Minkoff, D., and Piccolo, M.C., 2005. Novel mechanism of stream formation in coastal wetlands by crab–fish–groundwater interaction. Geo-Marine Letters, v. 25 (4), p. 214-220.

Pham, H.G., 2010. Dams and hydropower development in Vietnam. The international Journal on Hydropower and Dams, v. 17 (3), p. 48-52.

Proske, U., Hanebuth, T.J.J., Behling, H., Van Lap Nguyen, Thi Kim Oanh Ta, and Bui Phat Diem, 2010. The palaeoenvironmental development of the northeastern Vietnamese Mekong River Delta since the mid Holocene. The Holocene, v. 20 (8), p. 1257-1268.

Rapaglia, J., Zaggia, L., Ricklefs, K., Gelinas, M., and Bokuniewicz, H., 2011. Characteristics of ships' depression waves and associated sediment resuspension in Venice Lagoon, Italy. Journal of Marine Systems, v. 85 (1–2), p. 45-56.

Ross, P., 1974. The effects of herbicides in South Vietnam. Part B: The effects of herbicides on the mangrove of South Vietnam. National Academy of Sciences - National Research Council, Washington, D.C, 33p.

Russel, D.R., 2004. Theoretical analysis of narrow-band surface wave magnitudes. Air Force Technical Applications Center.

Schwarzer, K., Czerniak, P., and Le, X.T., 2007. Short term rediposition rates versus long term deposition rates in a mangrove forest, Can Gio, Saigon River mouth, Southern Vietnam Quatenary International, v. 167/168, p. 372-372.

Seapoint Sensors Inc., 2000. Seapoint Turbidity Meter user manual.

Semeniuk, V., 1980. Mangrove zonation along an eroding coastline in King Sound, north-western Australia. Journal of Ecology, v. 68 (3), p. 789-812.

Semeniuk, V., 1981. Long-term erosion of the tidal flats King Sound, north western Australia. Marine Geology, v. 43 (1-2), p. 21-48.

Seto, K.C., and Fragkias, M., 2007. Mangrove conversion and aquaculture development in Vietnam: A remote sensing-based approach for evaluating the Ramsar Convention on Wetlands. Global Environmental Change, v. 17 (3-4), p. 486-500.

Shaw, P.-T., and Chao, S.-Y., 1994. Surface circulation in the South China Sea. Deep Sea Research Part I: Oceanographic Research Papers, v. 41 (11–12), p. 1663-1683.

Smith, T.J., III, Robblee, M.B., Wanless, H.R., and Doyle, T.W., 1994. Mangroves, Hurricanes, and Lightning Strikes. BioScience, v. 44, No. 4, p. 256-262.

Solomon, S., D., Qin, M.M., Chen, Z., Marquis, M., Averyt, K.B., Tignor, M., and Miller, H.L., 2007. Climate Change 2007: The Physical Science Basis, Contribution of Working Group I to the Fourth Assessment Report of the IPCC. Cambridge University Press, Cambridge, United Kingdom and New York, NY, USA, 1009 pp.

Spalding, M.D., Blasco, E., and Field, C., 1997. World mangrove Atlas. The International Society for Mangrove Ecosystems, Okinawa, Japan, 178 pp.

Sterr, V.H., 1989. Der Abbruch von Steilkuesten in der suedwestlichen Kieler Bucht - unterspezieller Beruecksichtigung des Januarsturmes 1987. Die Kueste.

Syvitski, J.P.M., Kettner, A.J., Overeem, I., Hutton, E.W.H., Hannon, M.T., Brakenridge, G.R., Day, J., Vorosmarty, C., Saito, Y., Giosan, L., and Nicholls, R.J., 2009. Sinking deltas due to human activities. Nature Geosci, v. 2 (10), p. 681-686.

Ta, T.K.O., Nguyen, V.L., Tateishi, M., Kobayashi, I., and Saito, Y., 2005. Holocene delta evolution and depositional models of the Mekong River Delta, Southern Vietnam. River deltas - concepts, models, and examples, SEPM Special Publication, no 83 (2005), p. 453–466.

Ta, T.K.O., Nguyen, V.L., Tateishi, M., Kobayashi, I., Saito, Y., and Nakamura, T., 2002a. Sediment facies and Late Holocene progradation of the Mekong River Delta in Bentre Province, southern Vietnam: an example of evolution from a tide-dominated to a tide- and wave-dominated delta. Sedimentary Geology, v. 152 (3-4), p. 313-325.

Ta, T.K.O., Nguyen, V.L., Tateishi, M., Kobayashi, I., Tanabe, S., and Saito, Y., 2002b. Holocene delta evolution and sediment discharge of the Mekong River, southern Vietnam. Quaternary Science Reviews, v. 21 (16-17), p. 1807-1819.

Tamura, T., Horaguchi, K., Saito, Y., Nguyen, V.L., Tateishi, M., Ta, T.K.O., Nanayama, F., and Watanabe, K., 2010. Monsoon-influenced variations in morphology and sediment of a mesotidal beach on the Mekong River delta coast. Geomorphology, v. 116 (1-2), p. 11-23.

Tamura, T., Saito, Y., Sieng, S., Ben, B., Kong, M., Sim, I., Choup, S., and Akiba, F., 2009. Initiation of the Mekong River delta at 8 ka: evidence from the sedimentary succession in the Cambodian lowland. Quaternary Science Reviews, v. 28 (3–4), p. 327-344.

Thampanya, U., Vermaat, J.E., Sinsakul, S., and Panapitukkul, N., 2006. Coastal erosion and mangrove progradation of Southern Thailand. Estuarine, Coastal and Shelf Science, v. 68 (1-2), p. 75-85.

Thu, P.M., and Populus, J., 2007. Status and changes of mangrove forest in Mekong Delta: Case study in Tra Vinh, Vietnam. Estuarine, Coastal and Shelf Science, v. 71 (1-2), p. 98-109.

Tong, P.H.S., Auda, Y., Populus, J., Aizpuru, M., Habshi, A.A., and Blasco, F., 2004. Assessment from space of mangroves evolution in the Mekong Delta, in relation to extensive shrimp farming. International Journal of Remote Sensing, v. 25 (21), p. 4795-4812.

Tran, D.T., Saito, Y., Dinh, V.H., Nguyen, V.L., Ta, T.K.O., and Tateishi, M., 2004. Regimes of human and climate impacts on coastal changes in Vietnam. Regional Environmental Change, v. 4 (1), p. 49-62.

Tuan, L.D., Oannh, T.T.K., Thanh, C.V., and Quy, N.D., 2002. Can Gio Mangrove Biosphere Reserve. Agriculture Publisher, Ho Chi Minh City, Vietnam, 311 pp.

Unverricht, D., Nguyen, C.T., Heinrich, C., Szczuciński, W., Lahajnar, N., and Stattegger, K., 2012. Suspended sediment dynamics during the inter-monsoon season in the subaqueous Mekong Delta and adjacent shelf, southern Vietnam. Journal of Asian Earth Sciences (0).

van Loon, A.F., Dijksma, R., and van Mensvoort, M.E.F., 2007. Hydrological classification in mangrove areas: A case study in Can Gio, Vietnam. Aquatic Botany, v. 87 (1), p. 80-82.

Vo, L.H.P., 2006. Surface waves propagation in mangrove forest and induced suspended sediment concentration. Doctoral thesis, Institute of Oceanology Polish Academy of Sciences, Sopot, Poland, 191pp.

Vo, L.H.P., and Massel, S.R., 2006. Experiments on wave motion and suspended sediment concentration at Nang Hai, Can Gio mangrove forest, Southern Vietnam. Oceanology v. 48 (1), p. 23-40.

Walsh, J.P., and Nittrouer, C.A., 2004. Mangrove-bank sedimentation in a mesotidal environment with large sediment supply, Gulf of Papua. Marine Geology, v. 208 (2–4), p. 225-248.

Winterwerp, J.C., Borst, W.G., and de Vries, M.B., 2005. Pilot study on the erosion and rehabilitation of a mangrove mud coast. Journal of Coastal Research, p. 223-230.

Woodroffe, C.D., 1990. The impact of sea-level rise on mangrove shorelines. Progress in Physical Geography, v. 14 (4), p. 483-520.

Woodroffe, C.D., 1992. Mangrove sediments and geomorphology. In: Robertson, A.I., and Alongi D.M. (Eds.), Tropical Mangrove Ecosystems-Coastal and Estuarine Studies. American Geophysical Union, p. 7-41.

Woodroffe, C.D., 1995. Response of tide-dominated mangrove shorelines in Northern Australia to anticipated sea-level rise. Earth Surface Processes and Landforms, v. 20 (1), p. 65-85.

Wyrtki, K., 1961. Physical oceanography of the Southeast Asian waters. In: NAGA Report, vol. 2. Scripps Institution of Oceanography, University of California, La Jolla, California, 195pp.

Xue, Z., Liu, J.P., DeMaster, D., Van Nguyen, L., and Ta, T.K.O., 2010. Late Holocene Evolution of the Mekong Subaqueous Delta, Southern Vietnam. Marine Geology, v. 269 (1-2), p. 46-60.

Yanagisawa, H., Koshimura, S., Goto, K., Miyagi, T., Imamura, F., Ruangrassamee, A., and Tanavud, C., 2009. The reduction effects of mangrove forest on a tsunami based on field surveys at Pakarang Cape, Thailand and numerical analysis. Estuarine, Coastal and Shelf Science, v. 81 (1), p. 27-37.